Shape Memory Alloy Design by Machine Learning for Biomedical and High-Temperature Applications

by

Alireza Nazarahari

A Dissertation Submitted to the
Graduate School of Sciences and Engineering
in Partial Fulfillment of the Requirements for
the Degree of

Master of Science

in

Materials Science and Engineering

KOÇ
ÜNİVERSİTESİ

January 14, 2021

Shape Memory Alloy Design by Machine Learning for Biomedical and High-Temperature Applications

Koç University

Graduate School of Sciences and Engineering

This is to certify that I have examined this copy of a master's thesis by

Alireza Nazarahari

and have found that it is complete and satisfactory in all respects,
and that any and all revisions required by the final
examining committee have been made.

Committee Members:

_____

Prof. Demircan Canadinç (Advisor)

_____

Prof. Murat Sözer

_____

Assist. Prof. Sıdıka Mine Toker

Date: _____

Dedicated to my family.

ABSTRACT

Shape Memory Alloy Design by Machine Learning for Biomedical and High-Temperature Applications

Alireza Nazarahari

Master of Science in Material Science and Engineering

January 14, 2021

Shape memory alloys (SMAs) are of great importance due to their extensive usage in biomedical applications, aerospace engineering, or robotics. In recent years, although there has been a considerable amount of research to achieve optimum compositions of SMAs for these applications, due to the high experimental costs, the demand for alloys with optimum properties has not been met for many applications yet.

In this research, using the predictive power of artificial intelligence and machine learning, a systematic approach to predict the optimum composition of the SMAs was proposed to address two problems related to the binary NiTi and NiTi-based SMAs. In particular, in chapter two, the optimum chemical composition was proposed to minimize the Ni ion release in the binary NiTi SMA. The method to do so was to gather a database from the existing literature and using it to train a special algorithm that provides the information for predicting the desired compositions. In chapter three, using the same approach, two models were developed to predict the phase transformation temperatures and thermal hysteresis of multi-component NiTi-based SMAs. These models were used to predict the optimum alloy with the highest Phase transformation temperatures with the least possible thermal hysteresis.

ÖZETÇE

Yüksek Lisans Tez Başlığı
Alireza Nazarahari
Malzeme Bilimi ve Mühendisliği, Yüksek Lisans
14 Ocak 2021

Şekil hafızalı alaşımlar (shape memory alloys – SMA) biyomedikal, uzay mühendisliği ya da robotik alanlarındaki geniş kapsamlı kullanımlarından dolayı büyük öneme sahiptir. Son yıllarda bu uygulamalar için optimum kompozisyona sahip SMA'yı bulabilmek adına önemli miktarda araştırma yapılmasına rağmen; yüksek deney maliyetlerinden dolayı, optimum kompozisyona sahip alaşımlara olan ihtiyaç hala karşılanamamıştır. Bu çalışmada yapay zekâ ve makine öğrenmesinin tahmin gücünü kullanarak, ikili NiTi ve NiTi bazlı şekil hafızalı alaşımlarla ilgili iki problemi çözmek adına optimum kompozisyona sahip şekil hafızalı alaşım kompozisyonu öngörmek için sistematik bir yaklaşım sunulmuştur. Özellikle ikinci bölümde, minimum Ni salınımı ve optimum kimyasal kompozisyona sahip ikili bir NiTi SMA kompozisyonu ileri sürülmüştür. Bunu yapmak için kullanılan metod şu şekildedir: hali hazırda var olan literatürden bir veri tabanı oluşturulmuş ve istenilen kompozisyonu tahmin etmek için gerekli bilgiye sahip olan bu veri tabanı özel bir algoritmayı eğitmek için kullanılmıştır. Üçüncü bölümde, çok bileşenli NiTi bazlı şekil hafızalı alaşımların faz değişim sıcaklığı ve termal histerezisini tahmin edebilmek için aynı yaklaşım kullanılarak iki model geliştirilmiştir. Bu modeller, en yüksek faz değişim sıcaklığına ve en düşük termal histerezise sahip optimum alaşımı tahmin edebilmek için kullanılmıştır.

AKNOWLEDGEMENTS

Firstly, I would like to show my gratitude to Dr. Demircan Canadinç, my advisor, for the opportunity to join his group and for his constant support throughout my study. In the last 1.5 years of my M.Sc., there was not a single moment that I regret selecting him as my advisor and I am grateful for his support and friendliness.

Besides my advisor, I would like to thank the thesis committee members, Dr. Murat Sözer, and Dr. S. Mine Toker, for their participation and valuable comments on my thesis which has helped to improve it.

I was very lucky to join the AMG group, not only because of the scientific aspects but also of the great atmosphere which endorsed friendship and collaboration rather than toxic competitions. Firstly, I should thank Ibrahim Burkay Tuğluca for his support and friendliness and also for all the discussions that we had which gave me new insights toward the world. Secondly, I should thank Aysel Aysu Çatal for her friendly attitude in conjunction with her frankness and sincerity. I should Also thank Şeyma Gürel Saydam for her support and collaboration before and after her graduation.

In addition, I should thank my friends who were there for me whenever I needed them. The first person that I want to thank is Maryam Hedayat, a real friend who has supported me in all the ups and downs that I face in the last three years. The second person whom I should thank is Yağmur Ersoy who helped me in the hard times that I faced at Koç University. Besides, I want to thank Shabnam Fadaei, Hüseyin Küçükkeçeci for their help, support, and companionship.

TABLE OF CONTENTS

LIST OF TABLES

LIST OF FIGURES

ABBREVIATIONS

AI	Artificial Intelligence
ADAM	Adaptive Moment Estimation
ANN	Artificial Neural Network
AS	Artificial Saliva
A_s	Austenite Start
CNN	Convolutional Neural Network
FFNN	Feed-Forward Neural Network
HEA	High Entropy Alloy
ICP-MS	Inductively Coupled Plasma Mass Spectrometry
ML	Machine Learning
MSE	Mean Squared Error
MIS	Minimally Invasive Surgeries
MLFFNN	Multilayer Feed-Forward Neural Network
MLP	Multilayer Preceptrons
OWSME	One-Way Shape Memory Effect
PTT	Phase Transformation Temperature
PE	Pseudo Elasticity
ReLU	Rectified Linear Unit
RNN	Recurrent Neural Networks
SMA	Shape Memory Alloy
SME	Shape Memory Effect
TH	Thermal Hysteresis
TWSME	Two-Way Shape Memory Effect

Chapter 1:
INTRODUCTION

1.1 Motivation and background

1.1.1 Artificial intelligence

Humankind has dreamt about building machines and devices that can function intelligently on their own for a long time. A wish that did not come true until the invention of computers and the development of logical and mathematical basis of artificial intelligence [1]. Artificial intelligence (AI), Also known as computational intelligence, is the study of various intelligent agents that can individually think, decide and take actions that are appropriate for a specific condition [2]. The initial expectation of the scientific society was to create machines that are as intelligent as humans. The efforts to meet this expectation resulted in the development of useful machines in many applications such as autonomous flight technologies which have successfully replaced a considerable amount of the pilots' workload during commercial flights [3].

However, nowadays this expectation has grown and created the demand for machines that can function more efficiently than a human operator and resulted in various inventions such as sorting devices that organize hundreds of mails in a brief time to send them to different destinations [4,5], or weather forecasting models with higher accuracy than earlier ones [6]. In addition, numerous novel applications have been created by the introduction of AI algorithms, that are now part of our daily lives and previously were not available due to constraints in human abilities. An example of these applications can be the use of big data (millions of instances) in algorithms that suggest certain products such as music, books, etc. to the users based on their preferences. Another example is, the novel approach in science that the underlying relationships of the complex problems are determined via AI algorithms, the relationships that might not be easy to grasp by the human mind which can include market analysis or scientific relationships of different parameters [7–12].

The aforementioned examples of AI applications in various fields are telltale signs of the advantages that the implementation of AI can result if used properly. These

benefits can range from reducing the costs, risks, or biases induced by humans in different roles. In addition, AI can lift the restrictions of humans' abilities in processing a large amount of information or the unprecedented relations of different parameters. However, to achieve these benefits, it is necessary to understand various kinds of AI methods and their abilities and restrictions.

1.1.2 Machine learning

Despite being presumed as synonyms by many, AI and machine learning (ML) are not equal terms. ML is a subset of AI in which a machine observes an amount of data to build a model on it, then uses this model to predict new and unseen conditions. In this definition, a machine "learns" while by observing new cases, its performance and correct prediction increases [2,13,14]. The practical motivation behind machine learning is that the person who designs a computer program cannot predict all the possible conditions that a program would face, therefore in case of a new and unprecedented condition, the machine is going to fail completely. More importantly, in many incidents, the designers of the machines are not aware of the real answer to the problems, therefore they need the machine to find out the answers based on the relations inherited in the data [2]. Considering these motivations and problems that they can address, the development of ML algorithms has gained great value within the last decades. However, to implement these algorithms, it is necessary to know the basis of their functionality.

In summary, ML algorithms use both computer programming and statistics knowledge to train a model on an already available dataset known as "training dataset" while a performance criterion optimizes the performance of the model to fit the training dataset. Subsequently, the model's performance in predicting new instances is evaluated using another performance criterion on a new dataset called "test dataset". Thus, if a model has sufficient performance in both of these criteria, it would be considered as a successful model [13,14]. Generally, ML models can be divided into two main groups of supervised and unsupervised learning. In supervised learning, data instances including inputs, labeled with output information are taught to the model and the model's performance and accuracy are evaluated using output data. On the contrary, in unsupervised learning, the training data does not include outputs and the model will find the underlying relations and patterns of the input on its own. In another approach, the

type of output data is considered for categorizing the ML models. Therefore, ML models are divided into classification and regression models. In the group of classification models, the output of the dataset shows different groups or categories that the input data belongs to, and the model tries to learn how the input information relates to these categories. On the other hand, in regression problems, the model tries to predict actual values of the output data rather than the category, therefore predicting continuous values for the output [13]. In both of these categories of models, the use of statistical methods in conjunction with computer programming has given the ML models the ability to tackle linear and non-linear problems that might be governing different physical phenomena, making them a powerful tool to solve different physical problems that might be highly expensive to address by conventional computational methods [13,14]. The potential of ML methods in solving computationally expensive problems, in addition to the possibility of designing machines that can work individually in unprecedented conditions, has led to the development of various ML methods to address different problems. Out of many available ML methods, artificial neural networks have been selected in this work due to their power of modeling complex problems.

1.1.3 Artificial Neural Networks

One of the fastest-growing ML methods from the beginning of the millennia is artificial neural networks (ANNs) which due to their abilities of general approximation has opened a new window in the use of ML methods in real-life applications.

History of neural network

The idea of artificial neural networks initiated at the year of 1943 by the efforts to model functions of the human mind's neurons as simple electrical circuits which were successful to lay the basis for further studies [15]. Later works published in the 1950s supported the previous approach and presented the fact that if two neurons fire at the same time, the connection between them would be enhanced [16]. As the motivation behind these works was to imitate the power of the human mind, ANNs were put to simulations done by early computers to assess their possible abilities. These efforts failed initially; however by the late 1950s promising results were achieved in some applications such as an adaptive filter for canceling echo on telephone lines. The early promising results in addition to the expectations brought by the name of neural networks caused unjust demands from projects working on ANNs, which due to the

technological limits of the time, for instance limited computational power, caused the project goals to be unfulfilled which severely decreased fundings, therefore, hindering the growth of neural networks by 1970s. Fortunately, the era of stagnation for neural networks was ended by the technological rivalry of the United States and Japan in the 1980s, causing the new developments in neural networks. These developments were accelerated by the fact that the computational power of the computers was improved by that time and more successful applications of ANNs brought attentions back to ANNs [2,17]. However, it was not until the use of parallel computational power of graphics processing units (GPUs) in ML methods that facilitated the efficient training of several layers of neurons in a network, therefore giving the chance to address complex problems that demand deeper networks for modeling.

Deep learning

In order to define the concept of deep learning, it is necessary to understand the basis of deep and shallow networks. Generally, in every network, each node is known as a unit and they work as a group of nodes in a layer that takes the input values as their weighted sum from their predecessor and uses a linear or nonlinear function to calculate the output of that layer. Subsequently, these outputs will be used as the input for the next layer and this process would repeat until the last layer which gives the final output of the network. In the case of shallow networks, the path of the calculation is short, since the input values pass through only one layer and the output of it would be the final result of the network. This process is visualized using graph representations in Figure 1.1. On the contrary, the calculation path for the deep networks, also known as neural networks, are longer. A schematic for such networks is shown in Figure 1.2 indicating that when the input data is imported to deep networks, the calculation path that the data goes through consists of several calculation steps, thus it is called a deep network, and the learning process achieved through deep networks are called deep learning [18]. Considering the fact that both deep networks and neural networks are used interchangeably, the term of neural networks was used in this work since it is commonly utilized by the scientific society.

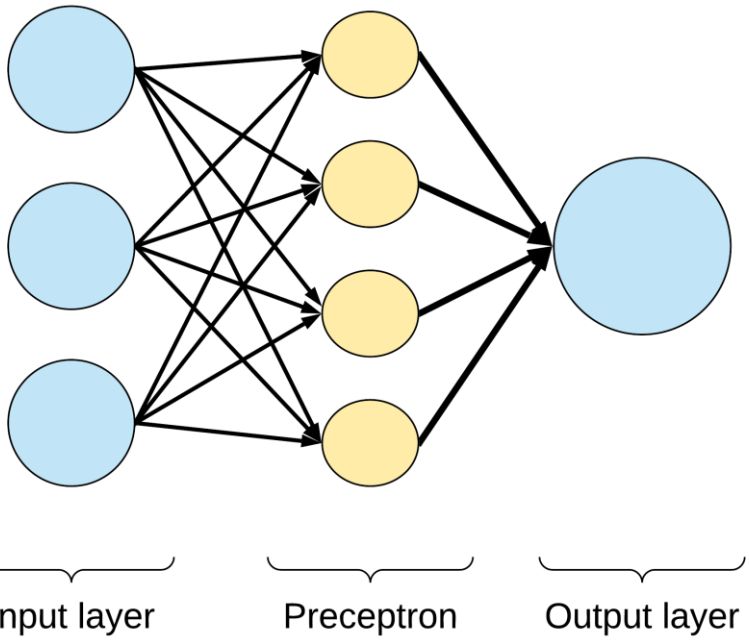

Figure 1.1.Schematic of a shallow network.

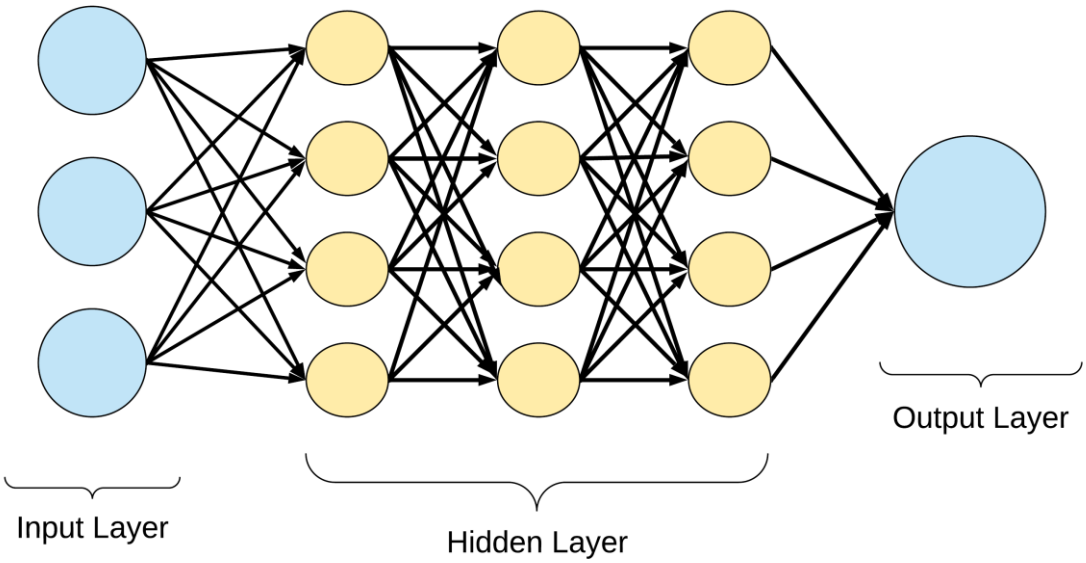

Figure 1.2 Schematic of a deep network.

To further understand the functionality of the ANNs, it is necessary to shed light on the calculation process and the mathematical basis of the ANNs. To do so, a training dataset is defined that consists of the input data which is presented as a matrix of $X =$

$\begin{bmatrix} X_1 \\ X_2 \\ \dots \\ X_n \end{bmatrix}$ and the output data of Y $= \begin{bmatrix} Y_1 \\ Y_2 \\ \dots \\ Y_n \end{bmatrix}$. In the neural networks, the input data goes through mathematical processes by the weights related to neurons of each layer represented as $\theta^j = \begin{bmatrix} \theta_1 \\ \theta_2 \\ \dots \\ \theta_m \end{bmatrix}$ for layer j. To make the demonstration of this mathematical process easier, let us consider a network with 2 hidden layers. The calculations would start by matrix multiplication of neuron weights to the input data which is shown as followed:

$$Z^{(1)} = \theta^1 X \qquad (1.1)$$

The $Z^{(1)}$ will be imported to the "activation function" of the hidden layer which works as a threshold limit and pass on the vector $a^{(1)}$ to the next layer as an input. This process will continue if the number of hidden layers is more than one. In the case of the assumed network, after the second layer, the $a^{(3)}$ vector, which is the output of the last hidden layer, known as hypothesis function shown by $h_\theta(X)$, is passed to the "Cost function" to evaluate the model's performance by comparing the $a^{(3)}$ vector to the Y vector and report it by a performance criterion.

So far, the model has proposed a prediction based on the initial weights of the hidden layers; however, these weights are predefined, and as a result, the prediction made by them will not be able to fit the data properly; therefore, an adjustment in these weights is necessary for a functional model. The most common solution to this problem is the "Backpropagation" technique which uses the gradient of cost function with respect to the parameters of the network which affect the cost, to find the path of local minima for the cost of the model. In particular, by applying the chain rule, the relative formula for each parameter affecting the cost is found for the previous layer. Subsequently in an iterative manner, similar parameters are found for each previous layer. Finally, using the acquired values, the effect of changing each neuron's weight is found and is utilized to adjust the weights accordingly [19]. The introduction of the Backpropagation was able to alleviate the problem of high computational cost of finding the minimum cost for the model, however, the performance of Backpropagation is highly dependent on the functions and architecture of the model, making them an important part of developing an ANN model. Therefore, in the following, each of these functions is briefly explained:

Activation function

The activation function is the nonlinear part of the calculation that thresholds the input values in a nonlinear fashion. There are various activation functions that have been used in ANNs, each of them having advantages and disadvantages:

1. Sigmoid function

Sigmoid or logistic activation function have been used in ANNs with various modifications for a long time as a nonlinear function with real inputs with properties such as differentiability, positive derivatives and smoothness in some degrees. The function itself is defined as:

$$f(x) = \left(\frac{1}{(1+\exp(-x))}\right) \qquad (1.2)$$

The advantage of sigmoid function is that it is easy to understand. However, the disadvantages of this function vary from having non-zero centered output which causes problems in Backpropagation, slow convergence, gradient saturation and damping sharp gradients [20].

2. Tanh

Tanh activation function is the hyperbolic tangent function that is commonly used in natural language processing and speech recognition machines. This function follows the formula of:

$$f(x) = \frac{(e^{X}-e^{-X})}{(e^{X}+e^{-X})} \qquad (1.3)$$

Tanh function is preferred to the sigmoid function due to the fact that it is a zero centered, thus helping the Backpropagation process to converge easier. On the other hand, it suffers from "vanishing gradient" which sigmoid function is also suffering from. The vanishing gradient creates "dead neurons" in the network, meaning that some of the neuron weights are rarely used in the learning process, thus, limiting the learning ability of the model. With this limitation, development of new activation functions was highly demanded for creating better performing models with less computational effort.

3. ReLU

Rectified linear unit (ReLU) is one of the most common activation functions that is in use in many state-of-the-art applications today. This function has addressed the downsides of sigmoid and Tanh functions in the vanishing gradient by rectifying the negative input values to 0. The formula of the function is which shows the method of thresholding is:

$$f(x) = \max(0, x) = \begin{Bmatrix} x_i, if\ x_i \geq 0 \\ 0, if\ x_i < 0 \end{Bmatrix} \quad (1.4)$$

One major advantage of the ReLU is that it does not use exponentials or divisions in computation, therefore it is reducing the computational effort of the learning. On the other hand, ReLU has greater tendency to overfit the data comparing to the sigmoid function, demanding more attention to the learning process.

4. Soft plus

Soft plus is the smooth version of ReLU function that can prevent the gradient vanishing as well as increasing the convergence speed. The formula calculating this function is:

$$f(x) = \log(1 + e^x) \quad (1.5)$$

The main application of this function is statistical analyses, in which it can converge faster than the sigmoid or ReLU functions. However, due to the use of exponentials in the calculations, it has a higher computational cost [21].

Cost function

Generally, in ML methods, cost functions (Also known as loss function) are the tool for evaluating the models' performance by creating a performance criterion and calculating the amount of error using the difference between the predicted values of the model and the output value of the dataset according to the formula defined by the performance criterion. The cost functions are usually selected based on the model's application and the data used for the learning process [13,18]. The two functions that are common today are mean squared error (MSE) for regression and Cross entropy function for classification problems.

1. Mean squared error

Mean squared error (MSE) is a well-known function that calculates the average over squared differences of the predicted and actual values. The mathematical presentation of it is shown as the following formula:

$$MSE = \frac{1}{n} \sum_{i=1}^{n} (Y_i - \widehat{Y}_i)^2 \quad (1.6)$$

This cost function is mainly used in regression problems in which models try to predict continuous values as their output which means that the higher cost represents predictions values with higher difference from the output value. The calculated cost values or the errors are always positive, starting from zero. MSE has the ability to deal

with outliers in a dataset, preventing the model from predicting the outliers with significant error [22].

2. Cross-entropy

The cross-entropy cost function, also known as the logarithmic cost or the logistic cost function, is a commonly used cost function in classification applications in which the model predicts the class that an instance belongs to. Therefore, it is necessary to use methods that evaluate the correct distribution. The formula for this function is:

$$H(p,q) = -E_p[\log q] \qquad (1.7)$$

In which the cross-entropy of the distribution q with respect to the distribution of p for a specific set is calculated. The cross-entropy function logarithmically ranges between zero and one, in which zero is for perfect prediction and one is for extremely large errors [23].

Artificial Neural Networks Architecture

The architecture of the neural networks plays a significant role on the performance of the model for their specific application both in convergence speed and the prediction power since the architecture defines the flow of data through the network which eventually calculates the results. Therefore, various architectures for ANNs are developed to address different problems but the most common three of them are as followed:

1- Multilayer Feed-forward Neural Networks

Feed-forward neural networks (FFNN) also known as perceptrons are one of the earliest NN architectures that have been developed which in the case of networks with several hidden layers are known as Multilayer Feed-forward neural networks (MLFFNNs) or Multilayer preceptrons (MLPs). The most important feature of these networks is that the flow of data in these networks are only in one direction, from the input to the output layer, and the neurons of each layer are constructed in a way that there is not a backward or recurrent path for the data [24]. In Figure 1.2 this architecture is illustrated.

This architecture has the widest range of applications and can be helpful in the case of statistical analysis or forecasting problems. However, there are shortcomings such as overfitting problems or high computational cost in case of a large amount of data (e.g. image processing). The downsides of the MLFFNNs has resulted in the development of other architectures for more specific applications [13,18].

2- Convolutional neural networks

Considering the drawbacks of MLFFNNs in image processing applications, a distinct type of neural network named Convolutional neural networks (CNNs) were devised to address these issues as well as improving the performance of the models for image processing applications. In these networks, a complicated input such as a picture is divided into several parts, and subsequently, each part is separately fed through the network during the learning process. In addition, the more important feature of these networks is that the neurons in the layers are convolutional and unlike MLFFNNs, they are only connected to the nearby neurons. Therefore, during the learning process, they only have effects on the neurons close to them. In addition to these two features, as the data moves deeper in the network, its size shrinks due to the pooling layers that collect only important details and set aside the irrelevant information, increasing the model's performance in picking up distinct features from the images [25]. A representative scheme of the CNNs is shown in Figure 1.3.

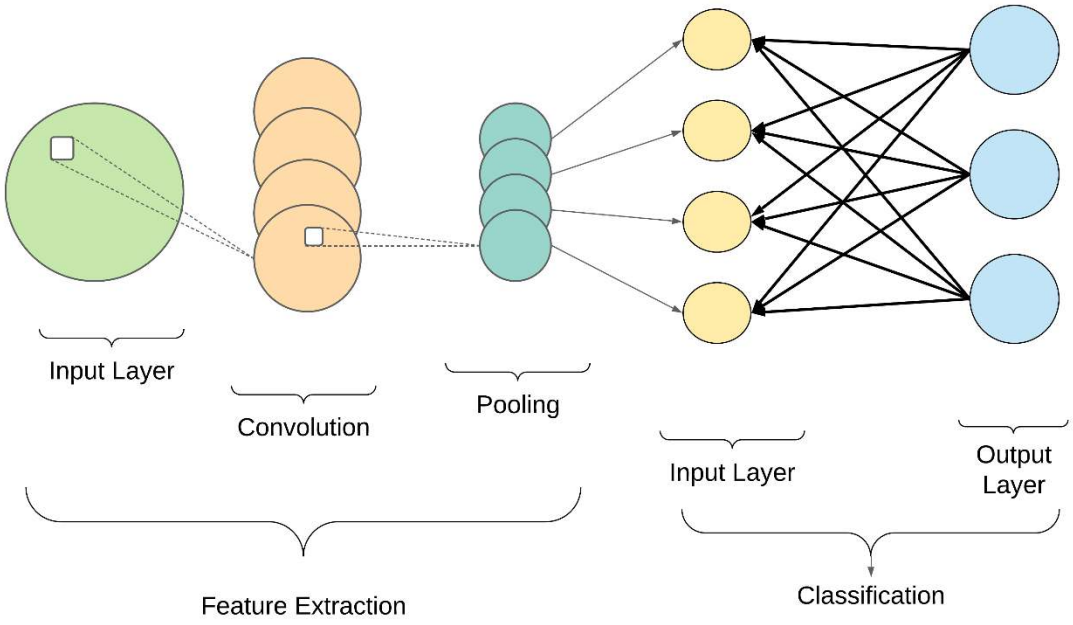

Figure 1.3 Schematic of an ANN with Convolutional Neural Network (CNN) architecture.

3- Recurrent neural networks

The MLFFNNs and CNNs are able to address problems in which training and prediction are based on a defined individual input. However, In the case of applications that the sequential prediction is needed such as word suggestion, the model falls

between the area of supervised and unsupervised learning. Thus, a new NN architecture was invented for this purpose recurrent neural networks (RNNs). In the RNNs, the neurons can be connected through the passes and through time, therefore giving the ability to compute highly complex problems that consist of nuggets of information that each of them demanded a separate program to models such as word processing and natural language translation [26]. An example of this architecture is depicted in Figure 1.4, showing the different flow of information compared to the MLFFNNs and CNNs.

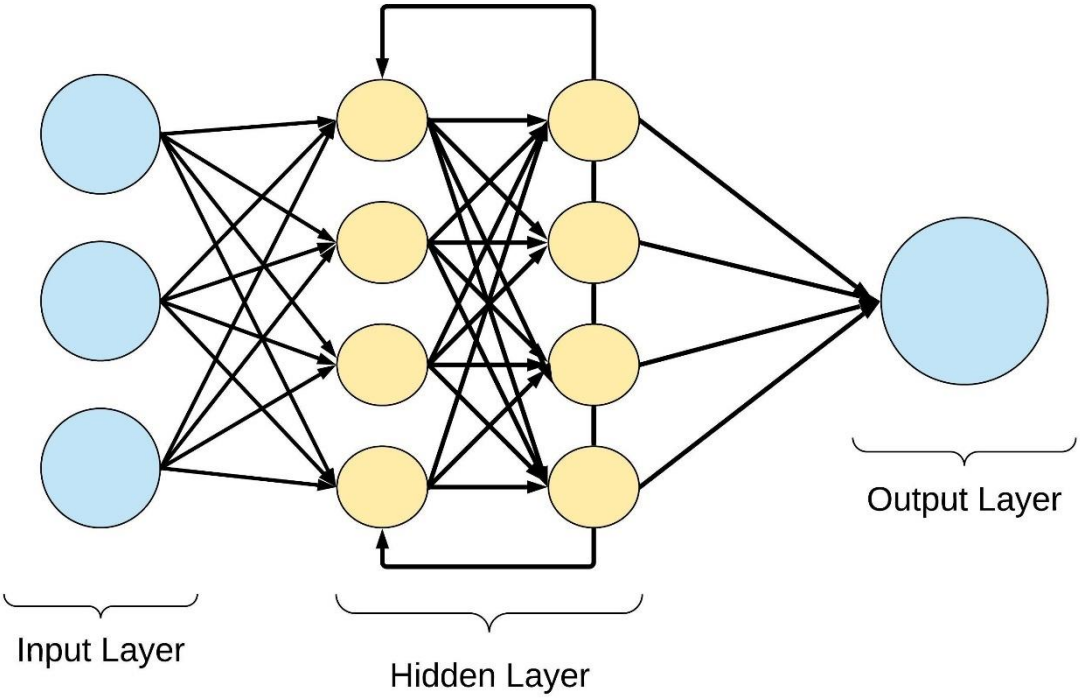

Figure 1.4 Schematic of an ANN with Recurrent Neural Network (RNN) architecture.

Neural network frameworks

Programming an efficient computational framework to undertake ML tasks demands a considerable amount of specialized knowledge in the field of computer science. Therefore, to facilitate the use of ML methods and particularly neural networks for the users, various ML and NN frameworks have been developed by the experts of the field. Two of the widely used frameworks that are specialized for NN applications are:

1- TensorFlow

This artificial intelligence platform is developed by the Google under Google brain project with the aim of democratizing AI and expanding its use to ordinary users by

providing an open-source library for neural networks. The underlying programming languages of this platform are C++ and Python, however, it is available for use on Python, Java, and many other platforms [27]. One of the main advantages of this TensorFlow is that there are numerous documentation and guidelines available as well as a large active community of users that can provide solutions in case of facing problems. Moreover, by the introduction of TensorFlow 2.0, several new libraries were added to this framework such as Keras which simplifies the process of coding for ordinary users. However, one disadvantage that they have is that in terms of speed in the case of big data, it performs slower than the other frameworks.

2- PyTorch

As the successor of the Torch library, PyTorch has been developed by Facebook to be an open-source library for ML methods to be mainly used in python or C++. This framework has found its place in many large projects such as twitter and salesforce due to its ability in tensor computation and tape-based automatic differentiation which help the NN models to be developed in the shortest time. In addition to the speed of training, this framework uses a simple and transparent method for the development of NN architectures, making it an easy framework to develop models [28]. However, the user community of this platform is smaller than TensorFlow's community at this moment.

1.2 NiTi shape memory alloys

1.2.1 Shape Memory Effect

Shape memory effect (SME) as a phenomenon was initially found in a gold cadmium alloy in 1951 as the “rubber-like” behavior in metals. However, it was not until the invention of Nitinol (Nickel Titanium made by Naval Ordinance laboratory) that SME gained attention from the scientific society which resulted in numerous studies and categorization of the SME into three main groups of One-way shape memory effect (OWSME), Two-way shape memory effect (TWSME) and pseudo elasticity (PE). These categories represent the behavior of the shape memory alloys (SMAs) in case of a change in the temperature or applied mechanical load, which is due to the different mechanisms of austenite-to-martensite phase transformation that induce SME in these alloys [29]. In the case of OWSME, the alloy is initially produced with the austenite phase and then by applying mechanical deformation, the martensite phase is induced in the structure through detwinning. Consequently, by removing the stress and increasing the temperature of the alloy to higher than the Austenite start (A_s) temperature, the martensite phase goes through a reverse phase transformation to austenite phase with the initial orientation, therefore inducing the load to reverse the mechanical deformation. This process which is shown in Figure 1.5 is single-use and by the time that all the martensite phase is transformed back to austenite, the mechanically deformed shape cannot be achieved unless an external load is applied again. On contrary, the TWSME is able to transform between these two phases only using thermal energy if a proper training process is done on the component. To be more precise, the training process includes adding micro stresses which cause bias in the nucleation and growth of martensite. Therefore, in a path similar to Figure 1.6, it is possible to reverse the transforming of austenite to martensite with the use of thermal energy. In contrast to the OWSME and TWSME, the PE is a different phenomenon in which the alloy gains the ability to get highly deformed without failure and subsequently, return to its original shape in a similar manner to elastic materials. This property is acquired through a reversible deformation mechanism called twinning in which due to lower energies required for this mechanism, it happens before the slip and prevents the slip mechanism to induce permanent deformation to the material [30–32]. The stress-strain curve related

to PE behavior is illustrated in Figure 1.7 showing the extraordinary behavior of alloys with PE properties.

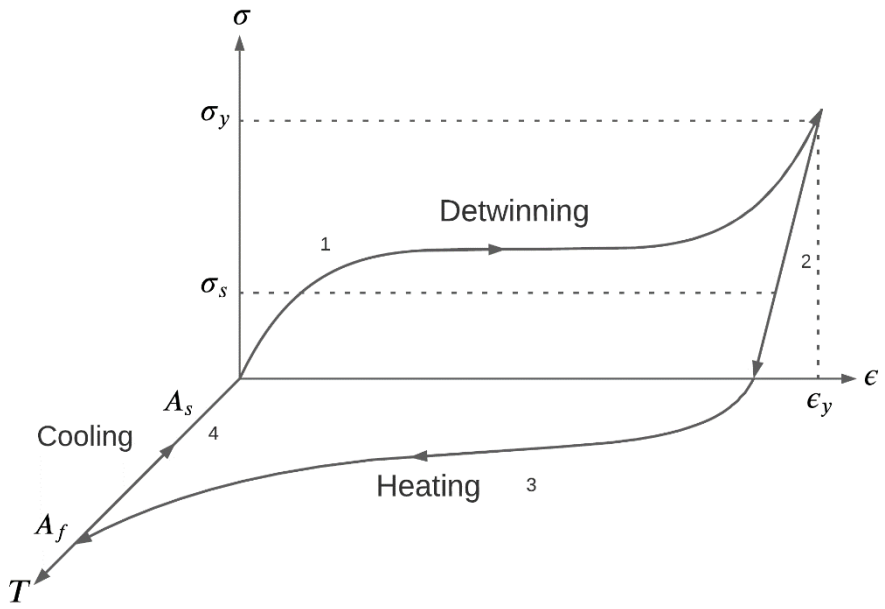

Figure 1.5 Schematic for a stress-strain-temperature diagram showing the SME behavior in SMAs. In this diagram, the external stress is applied to the alloy in stage 1 passing the elastic stress (σ_s) reaching to the yield stress (σ_y), resulting in mechanical deformation through detwinning and elastic deformation up to the yield strain (ϵ_y). As the load is removed in stage 2, the material loses the strain of the elastic deformation. In stage 3, as the temperature increases to the austenite finish, the deformation resulted from detwinning is reversed by the martensite-to-austenite temperature. In stage 4, the temperature of the material is decreased to below Austenite start, returning the material to its initial austenite phase [29] .

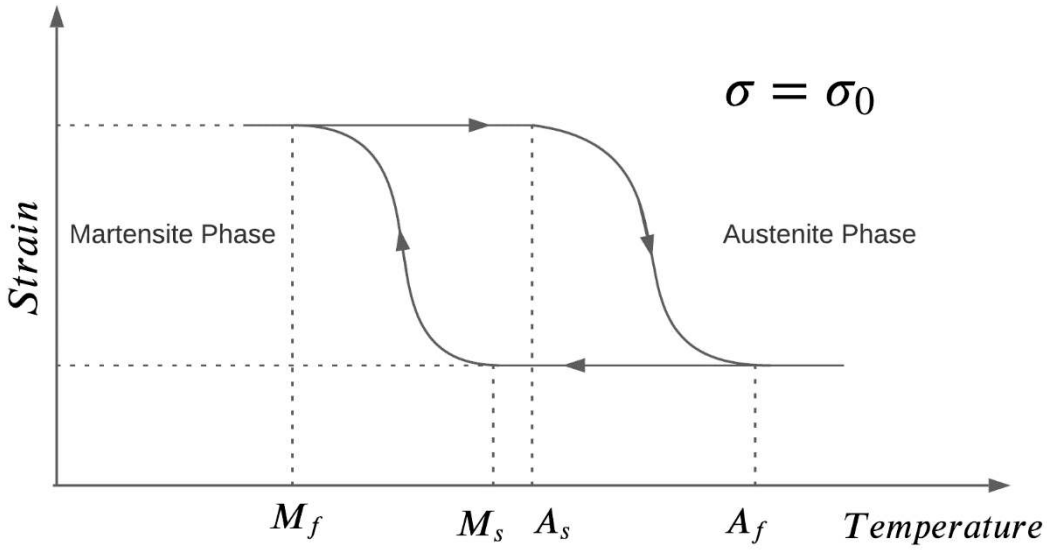

Figure 1.6 Strain-temperature curve represents the TWSME for the SMAs in constant applied stress. In this curve, as the temperature of a deformed sample increases to above As temperature, the martensite to austenite phase transformation occurs, decreasing the induced strain in the material. This change ends as the temperature passes the

A_f. Subsequently, by decreasing the temperature to below M_s, the material experiences the reverse phase transformation which induces strain to the material. This transformation finishes as the temperature falls below M_f.

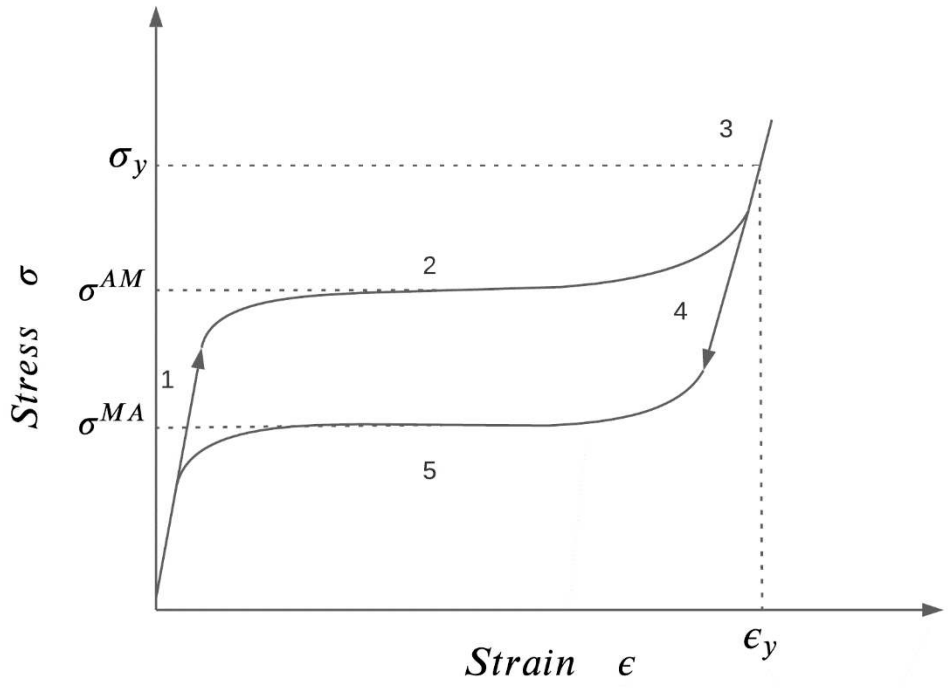

Figure 1.7 Stress-strain curve representing the PE behavior of SMAs. In this curve, stage 1 represents the elastic deformation of austenite as the stress increases. By further increase of the stress to σ^{AM}, the austenite transforms to single-variant martensite that is shown in stage 2. Subsequently, As the stress increases during stage 3, single-variant martensite undergoes elastic deformation. The elastic deformation ends as the yield stress of the material is reached. During stage 4, by the decrease of the stress down to theσ^{MA} , the elastic strain is recovered and is continued by the martensite to austenite transformation in stage 5.

The aforementioned transformations play a significant role in the possible applications of the SMAs. Therefore, understanding the underlying parameters of these transformations are highly valuable for both scientists and engineers designing components using SMAs. Various studies have investigated the effects of such parameters [33–35]. Within the studied parameters, chemical composition has been shown to be one of the most important factors which define the phase transformation temperatures (PTTs) of SMAs. It is proved that not only the elements existing in an alloy has substantial effect on the phase transformation temperatures of the alloy, but also the slightest change in the ratio of the elements can result in several degrees change in the PTTs [11,36]. Thus, it can be concluded that in any study to design a component using SMAs, the chemical composition should be considered as a primary factor.

1.2.2 Binary NiTi Shape Memory Alloys

From the already known chemical composition of alloys which present SMEs, the most common system is the Nickel Titanium based alloys. This system in the case of NiTi binary with close to equimolar composition owns PTTs below 100°C which has made it a reasonable choice for low-temperature applications such as actuators or sensors which mainly use the TWSME as the mechanism for their work. However, the most important application of the binary NiTi is the biomedical applications that mainly use the OWSME or PE properties of the SMAs in conjunction with the reasonably good corrosion resistance of the NiTi alloys comparing to the conventional alloys. Several examples for the use of Binary NiTi in these applications are mentioned in the following:

- Orthodontic archwires

The introduction of SMAs to be used as orthodontic archwires had a substantial effect on the ability to remodel the patients' teeth due to the fact that the NiTi wires gave better control over the applied forces that function to move the desired teeth to their correct position. In particular, using the conventional alloys (e.g. stainless steels), if the applied forces were lower than what it was aimed to be, the remodeling process would not occur. On the other hand, if excessive forces were applied, it could cause bone absorption, which can be an undesirable side effect to the patient. This problem was solved by the replacement of NiTi archwires since the forces applied by the SME have a more homogeneous distribution. In addition, the NiTi archwires reduced the need for retightening to keep the necessary forces since it gains its load from the SME and not externally applied loads [37,38].

- Medical staples

Medical staples are devices used in sealing procedures of tissues, blood vessels, or other body parts that need force to be kept sealed during or after surgery. These staples which can be made of both absorbable or non-absorbable materials offer faster implementation comparing to sutures, as well as other possible applications [29]. In the case of NiTi staples, they are mainly used as compression staples to set the broken bones in place by compressing them consequently, enhancing the healing process. Specifically, staples are kept in temperatures lower than human body temperature in the martensitic phase, then by planting them into the human body, their temperature would

increase above the A_s temperature, causing the phase transformation to start which implies a uniform compression on the attached bones [40].

- Stents in cardiovascular applications

Atherosclerosis is a common cardiovascular issue that is caused by adhesion and build-up of substances such as fat inside blood vessels which hinders or even prevents the flow of blood inside the vessel [31]. Several approaches exist to address this issue including bypassing the closed vessel or Endarterectomy which are invasive solutions for this issue, demanding a complex surgery to conduct. A less invasive alternative to these methods for the cases of localized lesions is dilatation. In this method, using a delivering vessel, a cold SMA stent made of NiTi is sent to the spot where Atherosclerosis has occurred. Subsequently, the stent enlarges due to body temperature to the desired size, preventing any damage to the vessel due to excessive stress [38,42].

- Surgical instruments for minimally invasive surgeries

During conventional surgeries, it is necessary to apply several cuts and incisions to give the surgeon access to the location and organs that were aimed for the surgery. These incisions, apart from being painful to the patient after the surgery, can cause various complexities during the healing process such as inflammation or prolonged healing process. Therefore, it would be ideal to minimize the incisions caused during surgeries. To address this demand, minimally invasive surgeries (MIS) has been devised. In these surgeries, using several small incisions, MIS devices are inserted into the body acting as the surgeon's hand performing the surgeries inside the body without exposing the internal organs. This method has several merits to conventional methods such as minimizing the need for general anesthesia, minimizing the healing time. However, it is highly technology and skill dependent. Thus, the invention of new devices or improvements over the previous designs can highly affect the surgeon's performance during the operation [43].

Considering the existing demand for superior MIS devices, NiTi SMAs were used to improve the designs already in use as well as the invention of new devices for the MIS applications. In particular, these devices used PE of SMAs to perform tasks that were possible to do by conventional alloys. As an example, curved surgical instruments (e.g. curved blades) are sent inside the body in compressed shape using small incisions just for the transferring tubes. Subsequently, they are taken out of their vessels to perform the desired task [44].

Challenges facing NiTi alloys use in biomedical applications

The most important property of materials to be used in biomedical applications is their biocompatibility, meaning that they should not cause damage to the tissues around the component or the other organs of the human body. Therefore, while designing any component for biomedical applications, it is important to take the biocompatibility as an important factor besides mechanical or functional properties [45]. In particular, Since most of the implant materials are made of metallic alloys, it is necessary to consider the corrosion behavior of these alloys due to the fact that the living body contains highly corrosive fluids which not only can cause corrosion of the implant and release of metallic ions to the body but also they can induce cracks and weak points which leads to mechanical failure [46,47]. Therefore, numerous studies investigated the response of metallic alloy systems in corrosive conditions simulating the human body to understand the biocompatibility of various metallic alloys.

Several alloy systems have been proposed to be used in implant materials due to their superior biocompatibility comparing to the conventional structural alloys, such as low carbon steels and aluminum alloys. The most common families of such alloys include stainless steel family, Co-Cr alloys, and Titanium alloys [48]. Within these alloys, the NiTi family gained considerable attention due to their SME properties which can be useful for various device designs. The NiTi alloys include Titanium which is known as a biocompatible element [49], however they also include Nickel which can cause various issues inside the human body. In particular, metallic Nickel is considered toxic and can cause severe issues in the case of inhalation or digestion. However, these issues are mainly related to the people who are in constant exposure to the high amount of nickel, such as miners or factory workers. [50]. In daily life, the exposure is constrained to lower amounts of Ni, mainly through imitating jewelry or implants which contain Ni within their constituents. Several studies have investigated the effect of Ni in such cases and they have shown that an excessive amount of Ni which is in the form of Ni ion can cause issues ranging from allergy showing itself as rash or blisters to decreased fertility or even cancer [51,52]. Therefore, one can conclude that in order to use NiTi alloys and exploit their SME properties, it is necessary to consider the Ni ion release as an important factor to investigate the biocompatibility of NiTi alloys.

Considering the mentioned importance of ion release, numerous studies investigated the Ni ion release from NiTi alloys in different simulating corrosive media to represent the ion release response in various body positions [53–58]. In the case of

orthodontic application, artificial saliva (AS) is considered as an effective solution imitating the conditions of the human oral cavity [59]. Therefore, a significant number of studies used Ni ion release in AS to investigate the biocompatibility of NiTi in orthodontic applications. In particular, several studies focused on using static immersion experiments to study the biocompatibility and surface properties of NiTi archwires [60–63], while others used electrochemical tests in AS as the method of experimentation [64]. These studies signified the effect of various parameters such as chemical composition, surface quality of the samples and pH of the corrosive media while emphasizing the fact that these parameters do not follow a simple relationship with the ion release, therefore demanding a systematic approach to deal with the Ni ion release issue for the NiTi alloys.

1.2.3 NiTi Based multicomponent alloys

One of the key factors of designing a component that utilizes the SME to function is the PTTs of the material since it would determine the temperature range that the component is able to function. In the case of binary NiTi alloys, the PTTs are below 100°C which limits the functionality of these alloys to low temperatures [65]. However, many possible applications for the SMAs demand higher PTTs to function such as components working close to engines or components related to fuel systems in the aerospace industry [66]. Thus, various studies focused on approaches to increase the PTTs of NiTi alloys. In one approach, the increase of PTTs was achieved through changing training parameters for the samples. However, this method needs a considerable amount of experimental work since the training parameter's relationships are highly complex and more importantly, there is a limit to this increase due to the intrinsic effect of chemical composition [21]. Therefore, in another approach, the effect of the addition of various alloying elements to the composition and its effect on the PTTs were investigated and it was shown that the addition of elements such as Pd, Pt, Au and, Hf can increase the PTTs of the alloys while the addition of Fe, Co, Cr, and V will decrease the PTTs of the respective alloy [56]. One might conclude that by the addition of elements that increase the PTTs of the alloys, the problem of using SMAs in high temperatures is solved. However, it has been shown that the addition of such elements will increase the Thermal hysteresis (TH) of these alloys, meaning that the temperature difference between the A_F and M_f of these alloys increase and would result

in loss of functionality of the device in high temperature. In particular, since the temperature difference increases, the component will need more time to lose or gain energy to reach the respective PTT, therefore, it cannot be used in components that demand fast response [66,68]. The lost or gained energy during martensitic transformation can be measured using differential scanning calorimetry as depicted in Figure 1.8 which can be helpful to find the PTTs of SMAs.

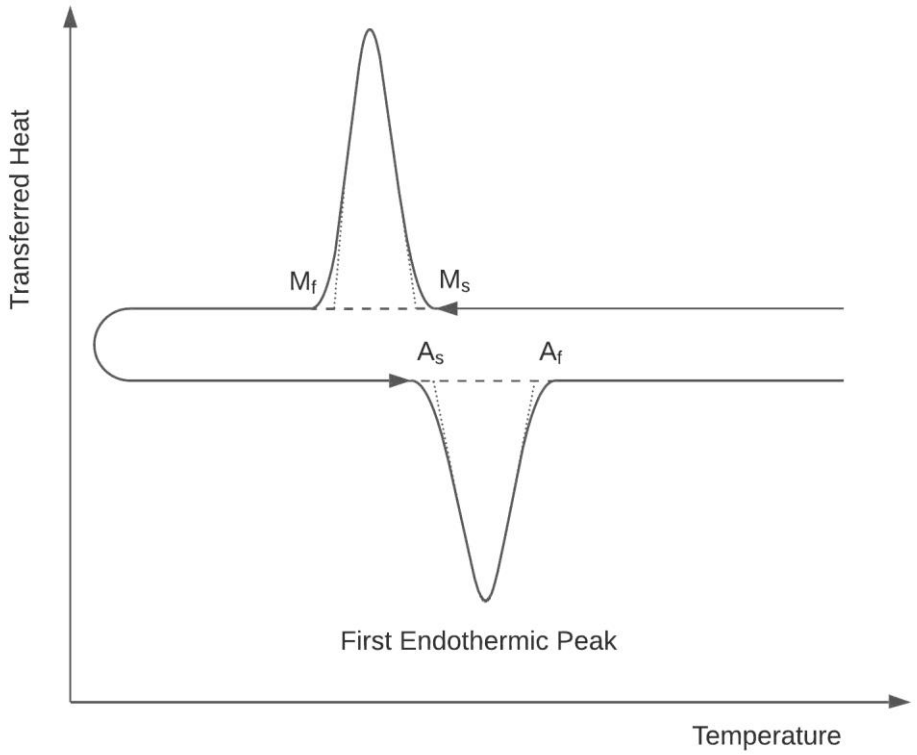

Figure 1.8 Transferred heat diagram with respect to the temperature represents the thermal energy lost or gained during martensite to austenite transformation.

In response to the demand for alloys with lower TH, several studies focused on decreasing the TH of these alloys by addition of alloying elements and it has been shown that elements such as Fe and Cu can decrease the TH of these alloys. Therefore, it can be concluded that in order to achieve high PTTs while keeping the TH as low as possible, it is necessary to consider various alloying elements. However, considering the sensitivity of PTTs to variations in chemical composition and the possible alloying elements, overwhelming number of experiments should be done to achieve an optimum chemical composition.

1.3 Objective

The current study has focused on exploiting the abilities of AI in understanding the underlying relationship of natural phenomena to enhance and ease the experimental works in the field of metallurgy. In the second chapter, the aim is to use the AI-based methods to minimize the experimental work to find the chemical composition of NiTi SMAs with the least amount of Ni ion release to achieve the most biocompatible chemical composition of NiTi that can be used in orthodontic archwire applications. In particular, using the already published literature available online, a training dataset is collected and by implementing an ANN algorithm on the dataset, a predictive model is developed. Using this model, the range of chemical composition in which the NiTi shows desirable SMAs is surveyed and the most biocompatible range was predicted. Consequently, using immersion testing, the results of these predictions were validated. In the third chapter, using the same approach, two datasets were collected to optimize PTTs and the TH of NiTi based SMAs with the addition of Cu, Fe, and Pd. Subsequently, two separate models were developed to predict an indicative value for the PTTs and the TH value individually. To decide on the optimum chemical composition for both PTTs and TH, the desirability approach was chosen to calculate a desirability score for each prediction. Finally, the optimum chemical composition was selected based on the highest desirability score to be used for further investigations.

1.4 References

[1] P. David, M. Alan, R. Goebel, Computational Intelligence: A Logical Approach, First edit, Oxford university press, 1998.

[2] S. Russell, P. Norvig, Artificial Intelligence: A Modern Approach, 4th Editio, Pearson, 2020.

[3] S. Tang, V. Kumar, Autonomous Flight, Annu. Rev. Control. Robot. Auton. Syst. 1 (2018) 29–52. https://doi.org/10.1146/annurev-control-060117-105149.

[4] J. M. Pippin, F. W. worth, D. E. Redford, O. K. Kechel, G. R. Mondie, G. A. Isaacs, Apparatus and method for mail sorting, 2006.

[5] M. Tamada, Mail sorting apparatus, 1984.

[6] S.S. Baboo, I.K. Shereef, An Efficient Weather Forecasting System using

Artificial Neural Network, Int. J. Environ. Sci. Dev. (2010) 321–326. https://doi.org/10.7763/ijesd.2010.v1.63.

[7] A. Porshnev, I. Redkin, A. Shevchenko, Machine learning in prediction of stock market indicators based on historical data and data from twitter sentiment analysis, in: Proc. - IEEE 13th Int. Conf. Data Min. Work. ICDMW 2013, IEEE Computer Society, 2013: pp. 440–444. https://doi.org/10.1109/ICDMW.2013.111.

[8] A. Sharma, D. Bhuriya, U. Singh, Survey of stock market prediction using machine learning approach, in: Proc. Int. Conf. Electron. Commun. Aerosp. Technol. ICECA 2017, Institute of Electrical and Electronics Engineers Inc., 2017: pp. 506–509. https://doi.org/10.1109/ICECA.2017.8212715.

[9] Y. Yang, D. Xue, R. Yuan, Y. Zhou, T. Lookman, X. Ding, X. Ren, J. Sun, Doping effects of point defects in shape memory alloys, Acta Mater. 176 (2019) 177–188. https://doi.org/10.1016/j.actamat.2019.06.031.

[10] N. Islam, W. Huang, H.L. Zhuang, Machine learning for phase selection in multi-principal element alloys, Comput. Mater. Sci. 150 (2018) 230–235. https://doi.org/10.1016/j.commatsci.2018.04.003.

[11] D. Xue, D. Xue, R. Yuan, Y. Zhou, P. V. Balachandran, X. Ding, J. Sun, T. Lookman, An informatics approach to transformation temperatures of NiTi-based shape memory alloys, Acta Mater. 125 (2017) 532–541. https://doi.org/10.1016/j.actamat.2016.12.009.

[12] A. Solomou, G. Zhao, S. Boluki, J.K. Joy, X. Qian, I. Karaman, R. Arróyave, D.C. Lagoudas, Multi-objective Bayesian materials discovery: Application on the discovery of precipitation strengthened NiTi shape memory alloys through micromechanical modeling, Mater. Des. 160 (2018) 810–827. https://doi.org/10.1016/J.MATDES.2018.10.014.

[13] E. Alpaydin, Introduction to machine learning, MIT Press Ltd, 2020.

[14] K.P. Murphy, Machine learning: a probabilistic perspective, MIT press, 2012.

[15] W.S. McCulloch, W. Pitts, A logical calculus of the ideas immanent in nervous activity, Bull. Math. Biophys. 5 (1943) 115–133. https://doi.org/10.1007/BF02478259.

[16] D.O. Hebb, The Organization of Behavior: A Neuropsychological Theory, Taylor & Francis, 2005. https://books.google.com.tr/books?id=ddB4AgAAQBAJ.

[17] P. McCorduck, Machines Who Think: A Personal Inquiry into the History and

Prospects of Artificial Intelligence, AK Peters Ltd, 2004.

[18] I. Goodfellow, Y. Bengio, A. Courville, Deep Learning, MIT press, 2016. http://www.deeplearningbook.org.

[19] R. HECHT-NIELSEN, Theory of the Backpropagation Neural Network, in: Neural Networks Percept., Elsevier, 1992: pp. 65–93. https://doi.org/10.1016/b978-0-12-741252-8.50010-8.

[20] C. Enyinna Nwankpa, W. Ijomah, A. Gachagan, S. Marshall, Activation Functions: Comparison of Trends in Practice and Research for Deep Learning, n.d.

[21] A. Nazarahari, D. Canadinc, Prediction of the NiTi shape memory alloy composition with the best corrosion resistance for dental applications utilizing artificial intelligence, Mater. Chem. Phys. 258 (2020) 123974. https://doi.org/10.1016/j.matchemphys.2020.123974.

[22] S. Theodoridis, Mean-Square Error Linear Estimation, Elsevier, 2015. https://doi.org/10.1016/b978-0-12-801522-3.00004-5.

[23] P.T. De Boer, D.P. Kroese, S. Mannor, R.Y. Rubinstein, A tutorial on the cross-entropy method, Ann. Oper. Res. 134 (2005) 19–67. https://doi.org/10.1007/s10479-005-5724-z.

[24] D. Svozil, V. Kvasnička, J. Pospíchal, Introduction to multi-layer feed-forward neural networks, in: Chemom. Intell. Lab. Syst., Elsevier, 1997: pp. 43–62. https://doi.org/10.1016/S0169-7439(97)00061-0.

[25] S. Albawi, T.A. Mohammed, S. Al-Zawi, Understanding of a convolutional neural network, in: Proc. 2017 Int. Conf. Eng. Technol. ICET 2017, Institute of Electrical and Electronics Engineers Inc., 2018: pp. 1–6. https://doi.org/10.1109/ICEngTechnol.2017.8308186.

[26] L. Medsker, D.L. Jain, B. Raton London New York Washington, Recurrent Neural Networks Design and Applications, 2001.

[27] M. Abadi, A. Agarwal, P. Barham, E. Brevdo, Z. Chen, C. Citro, G.S. Corrado, A. Davis, J. Dean, M. Devin, S. Ghemawat, I. Goodfellow, A. Harp, G. Irving, M. Isard, Y. Jia, R. Jozefowicz, L. Kaiser, M. Kudlur, J. Levenberg, D. Mane, R. Monga, S. Moore, D. Murray, C. Olah, M. Schuster, J. Shlens, B. Steiner, I. Sutskever, K. Talwar, P. Tucker, V. Vanhoucke, V. Vasudevan, F. Viegas, O. Vinyals, P. Warden, M. Wattenberg, M. Wicke, Y. Yu, X. Zheng, M. Rucci, A. Casile, TensorFlow: Large-Scale Machine Learning on Heterogeneous

Distributed Systems, ArXiv Prepr. ArXiv1603.04467. 16 (2016) 121–138. https://doi.org/10.1080/09548980500300507.

[28] A. Jain, A.A. Awan, Q. Anthony, H. Subramoni, D.K.D.K. Panda, Performance Characterization of DNN Training using TensorFlow and PyTorch on Modern Clusters, in: Proc. - IEEE Int. Conf. Clust. Comput. ICCC, Institute of Electrical and Electronics Engineers Inc., 2019. https://doi.org/10.1109/CLUSTER.2019.8891042.

[29] S. Miyazaki, K. Otsuka, Development of Shape Memory Alloys, 1989.

[30] S. Miyazaki, K. Otsuka, Development of shape memory alloys., ISIJ Int. 29 (1989) 353–377. https://doi.org/10.2355/isijinternational.29.353.

[31] J.W. CHRISTIAN, Shape Memory Alloys, in: Theory Transform. Met. Alloy., Elsevier, 2002: pp. 1102–1113. https://doi.org/10.1016/B978-008044019-4/50031-3.

[32] T.W. Duerig, K.N. Melton, Engineering Aspects of Shape Memory Alloys, 1990. https://doi.org/10.1016/c2013-0-04566-5.

[33] X. Wang, J. Yu, J. Liu, L. Chen, Q. Yang, H. Wei, J. Sun, Z. Wang, Z. Zhang, G. Zhao, J. Van Humbeeck, Effect of process parameters on the phase transformation behavior and tensile properties of NiTi shape memory alloys fabricated by selective laser melting, Addit. Manuf. 36 (2020) 101545. https://doi.org/10.1016/j.addma.2020.101545.

[34] T.W. Choon, A.S. Salleh, S. Jamian, M. Ghazali, Phase Transformation Temperatures for Shape Memory Alloy Wire, Undefined. (2007).

[35] M. Kök, H.S.A. Zardawi, I.N. Qader, M. Sait Kanca, The effects of cobalt elements addition on Ti2Ni phases, thermodynamics parameters, crystal structure and transformation temperature of NiTi shape memory alloys, Eur. Phys. J. Plus. 134 (2019) 197. https://doi.org/10.1140/epjp/i2019-12570-9.

[36] C. Velmurugan, V. Senthilkumar, S. Dinesh, D. Arulkirubakaran, Review on phase transformation behavior of NiTi shape memory alloys, Mater. Today Proc. 5 (2018) 14597–14606. https://doi.org/10.1016/J.MATPR.2018.03.051.

[37] J. Jerome, T. Brunson, G. Takeoka, C. Foster, H.B. Moon, E. Grageda, M. Zeichner-David, Celebrex offers a small protection from root resorption associated with orthodontic movement., J. Calif. Dent. Assoc. 33 (2005) 951–9. http://www.ncbi.nlm.nih.gov/pubmed/16454238 (accessed November 29, 2020).

[38] D. Mantovani, Shape memory alloys: Properties and biomedical applications,

JOM. 52 (2000) 36–44. https://doi.org/10.1007/s11837-000-0082-4.

[39] A.L. Tajirian, D.J. Goldberg, A review of sutures and other skin closure materials, J. Cosmet. Laser Ther. 12 (2010) 296–302. https://doi.org/10.3109/14764172.2010.538413.

[40] Staples for bone fixation, 2001. www.sma-inc.com., (accessed November 30, 2020).

[41] P. Libby, P.M. Ridker, A. Maseri, Inflammation and Atherosclerosis, Circulation. 105 (2002) 1135–1143. https://doi.org/10.1161/hc0902.104353.

[42] G. Mani, M.D. Feldman, D. Patel, C.M. Agrawal, Coronary stents: A materials perspective, Biomaterials. 28 (2007) 1689–1710. https://doi.org/10.1016/j.biomaterials.2006.11.042.

[43] B. Jaffray, Minimally invasive surgery, Arch. Dis. Child. 90 (2005) 537–542. https://doi.org/10.1136/adc.2004.062760.

[44] History and Current Situation of Shape Memory Alloys Devices for Minimally Invasive Surgery, (n.d.). https://doi.org/10.2174/1875181401002020024.

[45] J.O. Hollinger, An Introduction to Biomaterials, 2011.

[46] V. Geanta, I. Voiculescu, P. Vizureanu, A. Victor Sandu, High Entropy Alloys for Medical Applications, in: High Entropy Alloy., IntechOpen, 2019: pp. 116–124. https://doi.org/10.5772/intechopen.89318.

[47] S. Ghosh, S. Sanghavi, P. Sancheti, Metallic biomaterial for bone support and replacement, in: Fundam. Biomater. Met., Elsevier, 2018: pp. 139–165. https://doi.org/10.1016/B978-0-08-102205-4.00006-4.

[48] G.M. Keegan, I.D. Learmonth, C.P. Case, Orthopaedic metals and their potential toxicity in the arthroplasty patient. A review of current knowledge and future strategies, J. Bone Jt. Surg. - Ser. B. 89 (2007) 567–573. https://doi.org/10.1302/0301-620X.89B5.18903.

[49] B.D. Ratner, A Perspective on Titanium Biocompatibility, in: Springer, Berlin, Heidelberg, 2001: pp. 1–12. https://doi.org/10.1007/978-3-642-56486-4_1.

[50] D. Schaumlöffel, Nickel species: Analysis and toxic effects, J. Trace Elem. Med. Biol. 26 (2012) 1–6. https://doi.org/10.1016/j.jtemb.2012.01.002.

[51] R. Käkelä, A. Käkelä, H. Hyvärinen, Effects of nickel chloride on reproduction of the rat and possible antagonistic role of selenium, Comp. Biochem. Physiol. - C Pharmacol. Toxicol. Endocrinol. 123 (1999) 27–37. https://doi.org/10.1016/S0742-8413(99)00006-7.

[52] N. Henrik Nielsen, T. Menné, Nickel sensitization and ear piercing in an unselected Danish population, Contact Dermatitis. 29 (1993) 16–21. https://doi.org/10.1111/j.1600-0536.1993.tb04530.x.

[53] A. Charles, P. Gangurde, S. Jacob, S. Jatol-Tekade, R. Senkutvan, V. Vadgaonkar, Evaluation of nickel ion release from various orthodontic arch wires: An in vitro study, J. Int. Soc. Prev. Community Dent. 4 (2014) 12. https://doi.org/10.4103/2231-0762.130921.

[54] A. Milheiro, C. Kleverlaan, J. Muris, A. Feilzer, P. Pallav, Nickel release from orthodontic retention wires - The action of mechanical loading and pH, Dent. Mater. 28 (2012) 548–553. https://doi.org/10.1016/j.dental.2011.12.009.

[55] H.H. Huang, Y.H. Chiu, T.H. Lee, S.C. Wu, H.W. Yang, K.H. Su, C.C. Hsu, Ion release from NiTi orthodontic wires in artificial saliva with various acidities, Biomaterials. 24 (2003) 3585–3592. https://doi.org/10.1016/S0142-9612(03)00188-1.

[56] B. Uzer, O. Birer, D. Canadinc, Investigation of the Dissolution–Reformation Cycle of the Passive Oxide Layer on NiTi Orthodontic Archwires, Shape Mem. Superelasticity. 3 (2017) 264–273. https://doi.org/10.1007/s40830-017-0114-3.

[57] J. Gajapurada, S. Ashtekar, P. Shetty, ..., Ion release from orthodontic brackets in three different mouthwashes and artificial saliva: an in-vitro study, IOSR J Dent …. (2016). https://doi.org/10.9790/0853-1504017685.

[58] A.H. Mirhashemi, S. Jahangiri, M.J. Kharrazifard, Release of nickel and chromium ions from orthodontic wires following the use of teeth whitening mouthwashes, Prog. Orthod. (2018). https://doi.org/10.1186/s40510-018-0203-7.

[59] G.R. Batista, C.R.G. Torres, B. Sener, T. Attin, A. Wiegand, Artificial saliva formulations versus human saliva pretreatment in dental erosion experiments, Caries Res. 50 (2016) 78–86. https://doi.org/10.1159/000443188.

[60] X. Li, J. Wang, E. Han, W. Ke, Influence of fluoride and chloride on corrosion behavior of NiTi orthodontic wires, Acta Biomater. 3 (2007) 807–815. https://doi.org/10.1016/j.actbio.2007.02.002.

[61] H. Hermawan, D. Ramdan, J.R. P. Djuansjah, C. Yu, R. Chen, J.J. Li, J.J. Li, M. Drahansky, M.. Paridah, A. Moradbak, A.. Mohamed, H. abdulwahab taiwo Owolabi, FolaLi, M. Asniza, S.H.. Abdul Khalid, T. Sharma, N. Dohare, M. Kumari, U.K. Singh, A.B. Khan, M.S. Borse, R. Patel, A. Paez, A. Howe, D. Goldschmidt, C. Corporation, J. Coates, F. Reading, Metals for Biomedical

Applications, in: Biomed. Eng. - From Theory to Appl., InTech, 2011: p. 13. https://doi.org/10.5772/19033.

[62] S.F. Kurtoğlu, M.B. Yağcı, A. Uzun, U. Ünal, D. Canadinc, Enhancing biocompatibility of NiTi shape memory alloys by simple NH3 treatments, Appl. Surf. Sci. 525 (2020) 146547. https://doi.org/10.1016/j.apsusc.2020.146547.

[63] S.M. Toker, G. Gerstein, H.J. Maier, D. Canadinc, Effects of microstructural mechanisms on the localized oxidation behavior of NiTi shape memory alloys in simulated body fluid, J. Mater. Sci. 53 (2018) 948–958. https://doi.org/10.1007/s10853-017-1586-4.

[64] M. Arndt, A. Brück, T. Scully, A. Jäger, C. Bourauel, Nickel ion release from orthodontic NiTi wires under simulation of realistic in-situ conditions, J. Mater. Sci. 40 (2005) 3659–3667. https://doi.org/10.1007/s10853-005-0448-7.

[65] D. Canadinc, W. Trehern, J. Ma, I. Karaman, F. Sun, Z. Chaudhry, Ultra-high temperature multi-component shape memory alloys, Scr. Mater. 158 (2019) 83–87. https://doi.org/10.1016/j.scriptamat.2018.08.019.

[66] D.J. Hartl, D.C. Lagoudas, Aerospace applications of shape memory alloys, Proc. Inst. Mech. Eng. Part G J. Aerosp. Eng. 221 (2007) 535–552. https://doi.org/10.1243/09544100JAERO211.

[67] M. Zarinejad, Y. Liu, Dependence of Transformation Temperatures of NiTi-based Shape-Memory Alloys on the Number and Concentration of Valence Electrons, Adv. Funct. Mater. 18 (2008) 2789–2794. https://doi.org/10.1002/adfm.200701423.

[68] E.T.F. Chau, C.M. Friend, D.M. Allen, J. Hora, J.R. Webster, A technical and economic appraisal of shape memory alloys for aerospace applications, Mater. Sci. Eng. A. 438–440 (2006) 589–592. https://doi.org/10.1016/j.msea.2006.02.201.

Chapter 2:

PREDICTION OF THE NITI SHAPE MEMORY ALLOY COMPOSITION WITH THE BEST CORROSION RESISTANCE FOR DENTAL APPLICATIONS UTILIZING ARTIFICIAL INTELLIGENCE

2.1 Introduction

Shape memory alloys (SMAs) of Nickel-Titanium (NiTi), due to their exceptional pseudoelasticity and shape memory effects (SMEs), have found many applications in the fields of cardiovascular surgery, orthopedy, and orthodontics [1–5]. In particular, using the aforementioned properties, the medical device designers have devised tools and designs that minimize the need for open surgeries, resetting, or other manipulations which have caused these devices to be favorable in many applications, replacing conventional materials [6]. In contrast to the advantages of NiTi alloys, they are susceptible to corrosion which will cause the release of Ni ions inside human blood due to their high nickel content triggering short or long-term consequences such as allergic reactions, decreased fertility, or damage to surrounding tissues [7,8].

Understanding the various parameters affecting ion release in NiTi alloys have motivated numerous studies. Particularly, effects of different parameters such as microstructure, loading, geometry, and corrosive media were studied and it was concluded that all these parameters play a significant role in the ion release of the NiTi SMAs [9–13]. Moreover, due to the unavoidable Ni ion release, many researchers have used coating and surface treatments via secondary materials as the method to restrict the Ni ion release [14–21]. The results of these studies have shown a significant decrease of Ni ion release for *in situ* experimental conditions. However, coatings bear intrinsic issues due to the mismatch of hardness and elastic modulus of the coating and the substrate and during service, it might detach and expose the substrate completely. Therefore, although the coating is a viable method to prevent the Ni ion release from the implants, a secondary safety measure that utilizes the chemical composition in which NiTi releases the least amount of Ni ion in a specific body location while still showing the required SME properties would be minimizing the risk of using NiTi implants.

However, the relation of the chemical composition of NiTi and its ion release is complicated and demands further studies [22,23]. To tackle this issue, implementing the analytical simulations or the conventional design of experiment (DOE) is not possible, mainly due to the complex nature of the chemical reactions of Ni ion release and the numerous possible alloy compositions that can be selected to perform experimental work.

An alternative answer to such problems that has gained popularity recently is the machine learning (ML) methods that have the ability to deal with the problems that are not solvable with the conventional trial and error or mathematical methods [24–33]. Using both computer programming and statistical theories, these methods train a model using the "training data" available to them while optimizing a performance criterion which is defined to evaluate the performance of the model using "test dataset" which includes the unseen data that gives the opportunity to predict new and unknown data. In addition, the statistical methods used in ML gives the ability to address linear and non-linear problems that would be computationally expensive [34,35].

The aforementioned abilities of ML can be highly valuable in the field of material science in which the problems facing the researchers are highly complicated and to reveal the underlying relationship, an extensive amount of experimental or computational work is needed which is costly in both financial and timely manner. As an example, one recent study investigated the phase formation of the high entropy alloys (HEAs) with respect to their chemical compositions using ML methods using an already available dataset. This study could construct a model that was able to eliminate incorrect candidates which would need to omit costly experiments and come up with reasonable accuracy to predict the phases and reducing the effort to only validation experiments [27]. In another case, a dataset acquired through experimentation of phase transformation temperatures (PTTs) of NiTi-based SMAs were used to develop a model that predicted the PTTs of such alloys with the aim of searching for a higher temperature PTTs in the respective alloy system which could predict alloys with higher PTTs than the highest of the initial dataset with minimum the amount of experimental work [28]. In another example, the evolution of defect density of metallic samples during plastic deformation was predicted and via data obtained from in-situ X-ray diffraction data, with the aim to understand the effect of defect density on the strength-plastic flow which is not possible to understand via conventional methods. Considering

these and the similar studies using the ML methods, the potential of ML methods in materials science as a supplementary tool to facilitate the research via reducing the experimental cost as well as giving the possibility to understand new information from the experimental studies is obvious.

On a similar note, this study has attempted to establish an Artificial intelligence framework to come up with the best chemical composition of NiTi SMA for orthodontic applications and dental implants in terms of biocompatibility, while omitting the trial-and-error process and confining the experimental efforts to only validation experiments. In particular, using the significant amount of literature available on the ion release behavior of NiTi SMAs in a solution simulating a human oral cavity, known as artificial saliva (AS), a data pool was constructed to be utilized in ML algorithms. To perform this task, a three-stage process was implemented as depicted in Figure 2.1. In the first stage, using the available published literature on the Internet, a dataset consisting of training and test dataset was established. In the second step, a well-known ML method known as the multi-layer feed-forward neural network (MLFFNN) is a powerful tool to create a model for the prediction of Ni ion release. Finally, in the third step, using the predicted optimum values from the model, validation experiments were done by manufacturing the respective alloys and conducting immersion experiments in AS to assess its ion release. The results acquired through this work presented an AI framework in which the best biocompatible composition of NiTi was predicted and the alloy with 51.5% Ni was selected as the optimum composition for orthodontic which stood in good agreement with the clinical findings [36]. All-around, the outcome of this work presented that the use of artificial intelligence can reduce the hassles of experimental works in biomedical problems in which the development of alloys demands an extensive amount of experimental work.

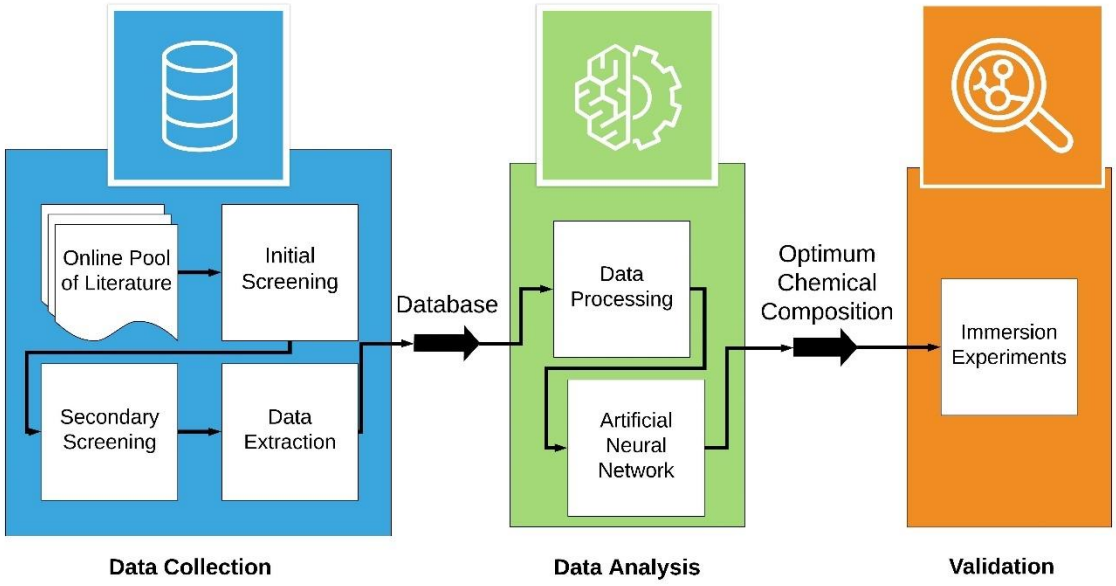

Figure 2.1 Schematic of the adopted procedure to optimize the ion release of NiTi alloy composition.

2.2 Computational Methods

2.2.1 Dataset

Previous studies have shown the use of already published experimental data is an inexpensive and fast way for creating a dataset that can be used as an input for ML algorithms [27]. In this study, the scientific publications on the Ni ion release response of NiTi dental SMAs since the year 2000 have been carefully selected and screened to extract data using Publish and Perish software [37]. To be more specific, two-step screening were used as illustrated in Figure 2.1, which in the first step, patents, non-English, or out of topic publication were screened. The second step, the publications with the criteria that they should solely include the studies which investigated the *in vitro* Ni ion release response of NiTi orthodontic alloys which was acquired through immersion testing in AS solution. Consequently, to extract data instances from these publications for the input of ML algorithms, several features were selected based on their availability in the literature as well as their importance in Ni ion release of the alloys. The aforementioned features were categorized into two groups, the first group containing the feature related to the metallic samples which underwent immersion experiment (Ni, Ti and balancing element in at.%. and surface area of the samples in

cm^2) and the second one related to the experimental conditions of the immersion experiment (including solutions' pH, solutions' amount in ml and experiment time in Hours). For the output of the dataset, Ni ion release in $\frac{\mu g}{cm^2}$ was chosen for easier comparison. As a result, 94 instanced were extracted and included in the dataset [38–42]. *The dataset is included in the appendix of this document.*

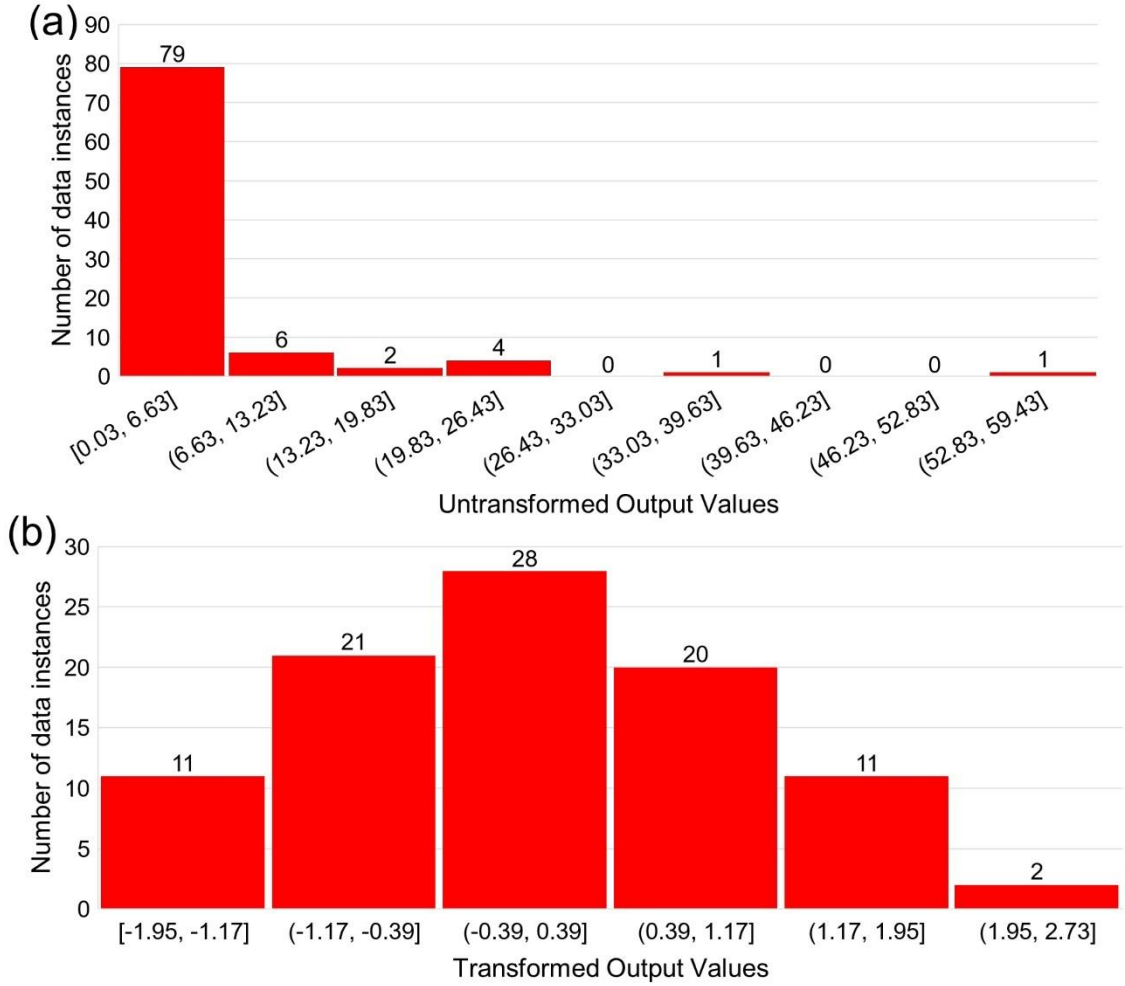

Figure 2.2 (a) Transformed distribution and (b) Untransformed distribution of Output values (Ni ion release)

The distribution of the input as well as the output layer has been examined using histograms and as shown in Figure 2.2 (a) for the output data, and it has been shown that the distribution of the instances is a non-normal distribution which means the data is not evenly distributed around the mean of the respective feature. Previous studies have shown that such distributions using non-normal distribution might deteriorate ML models' accuracy and performance. Therefore, it would be necessary to avoid the use of such distributions [43]. To alleviate this problem, the Yeo-Johnson power transformation function has been used as the tool to reduce the skewness of the data and

transforming it into a near-normality distribution [44]. Specifically, this function uses a continuous function inside a piecewise function, therefore, making continuity possible at the singularity points using the following conditions:

If $\psi^{(k)} = \frac{\partial^k \psi(\lambda,x)}{\partial \lambda^k}$ then, for $k \geq 1$ $\psi^{(k)}$ is continuous in (λ, x) [45]:

$$\psi^{(k)} = \begin{cases} [(x+1)^{\lambda}\{log(x+1)\}^k - k\psi^{(k-1)}]/\lambda & (\lambda \neq 0,\ x \geq 0), \\ \{log(x+1)\}^{k+1}/(k+1) & (\lambda = 2,\ x \geq 0), \\ -[(-x+1)^{2-\lambda}\{-log(-x+1)\}^k - k\psi^{(k-1)}]/(2-\lambda) & (\lambda \neq 0,\ x \geq 0), \\ \{-log(-x+1)\}^{k+1}/(k+1) & (\lambda = 2,\ x \geq 0), \end{cases} \quad (2.1)$$

where λ, is the power parameter.

The result of this transformation for the output values has been shown in the Figure 2.2 (b). It can be seen that the values are now follow a near normality condition which makes the data more desirable for ML implementation.

2.2.2 Artificial Neural Networks

Artificial neural networks (ANNs) Have gained significant popularity within the scientific community as an ML method within the last two decades due to their computational ability to tackle complex problems that contain multiple features [26,27,29,46]. This ability mainly roots in the fact that ANNs were developed to imitate human brain function and use it highly complex, non-linear, and parallel computational power which would result in predicting relationships that are not easily discovered by conventional methods [47,48]. To exploit the abilities of ANNs, various types of ANNs have been developed that can be separated into two groups based on their method of learning which can be supervised or unsupervised learning. In supervised learning, a labeled dataset which contains input and output is used for the learning process, while the model uses the input values for training, the output values are used for evaluating the learning process. On the other hand, in unsupervised learning, the model uses an unlabeled dataset, and it finds the relations whiting the input values by itself. In both types of the learning process, in order to assess the ability of the model to predict new and unseen data, a method called “cross-validation” is used in which the initial dataset is separated into two datasets or “training dataset” and “test dataset”. The training

dataset is used for training the model while the test dataset is only used to evaluate the model performance [49].

One of the most prominent supervised learning algorithms is the multilayer feedforward neural network (MLFFNN) which has proven itself for data prediction and universal approximation [50,51] and due to its abilities was chosen for this work. To be more specific, MLFFNN architectures flow the data from only the input to output layers, which means there is not a recurrent or backward flow of information. This architecture includes one layer working as the input layer which imports the data from the dataset and on output layer which gives out the results of the computational work to be evaluated by comparing the predicted value to the actual value. Between these two layers, several layers of neurons would be placed based on the necessity of the model to achieve the highest performance (The architecture of the model used in this work has been shown in Figure 2.3).

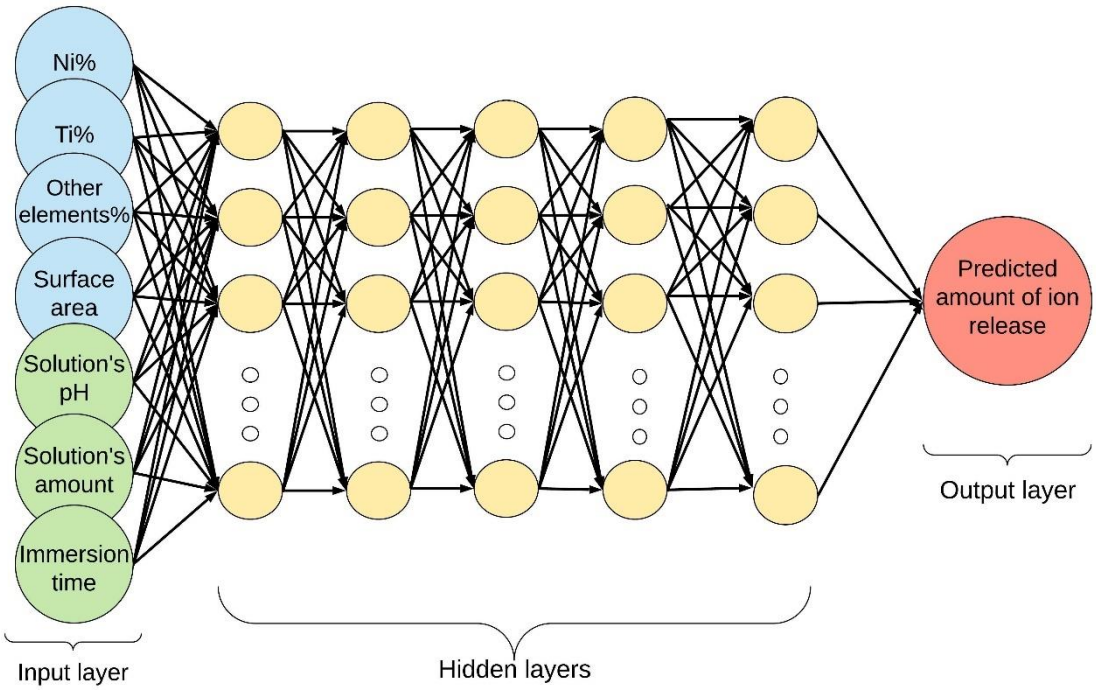

Figure 2.3 MLFFNN architecture implemented in the current work with 5 hidden layer and 35 Neuron in each layer, representing the flow of data in the model.

To elaborate the data processing of the MLFFNN model, it is noteworthy to say that the input data of the training dataset would enter the model as a matrix from the input layer without any change. Subsequently, the data would be passed on to the first hidden layer while going through a linear operation of a matrix holding the weights values of each neuron of the layer. The result of this operation is a matrix which by

addition of a bias value and going through a function called activation function is passed to the next hidden layer. This process is repeated for the next layers until the last hidden layer which calculates the output of the network which is in fact the predicted value by the model. At this stage, the predicted value is compared with the actual value from the output of dataset and its difference is calculated as error by a cost function. The calculated error is used as the criteria for the "back propagation" process in which an optimizer function adjusts the neuron weights to minimize the error of the prediction. In this process, to prevent the model to overfit the training data and keeping its ability to predict unseen data, a regularization function is used for decreasing the model's sensitivity to each instances of the training dataset [52,53].

Considering the effect of the aforementioned functions and the architecture of the network in the performance of the calculations of the model, it is necessary to choose the most suitable functions to be implemented by the MLFFNN model for the specific task. To do so, a recently developed activation function known as rectified linear unit (ReLU) has been selected due to its advantages to the previous activation functions. These advantages include the ability of not saturating the gradient as well as being zero centered [54]. In order to calculate the error, mean squared error (MSE) was used which calculates the error with the following formula:

$$MSE = \frac{1}{n}\sum_{i=1}^{n}(Y_i - \widehat{Y}_i)^2 \qquad (2.2)$$

This function was selected due to its ability of handling regression problems and preventing the prediction of outliers with substantial error[55]. To optimize the cost function, A newly developed optimizer known as "adaptive moment estimation" (Adam) was utilized which has the advantage of not saturating the gradient by using an storing method which saves the exponentially decaying average of the past squared gradients. Moreover, AMSgrad which is an improvement to the Adam optimizer was used to make it less susceptible to the use of downsides of exponential weights which made it harder to converge comparing to the simple stochastic gradient methods [56–58]. To prevent overfitting the data, L2 regularization was used to control the sensitivity of the weights to the instances by using the square L2 norm of the weights which reduces the possibility of overfitting [59].

To put all the aforementioned functions in a framework, TensorFlow 2.0, Which is a popular neural network framework developed by Google was selected due to its

advantages such as being highly versatile and customizable as well as being compatible with useful libraries such as Matplotlib, Keras, Scikit learn and Pandas [44,60–62]. By having a framework ready, it is necessary to decide on the architecture of the model as well as the regularization hyperparameter value which defines the intensity of regularizer function in reducing the weights' sensitivity to the training data. Previous studies has shown that finding these two is only possible through empirical methods [63]. To be more specific, by use of trial and error, different values for the neurons and regularization parameter is used for training the model and the performance of each of these combinations is recorded and finally the combination with the best performance is selected. However, this method would face problem when dealing with the training datasets which do not represent the whole data uniformly, therefore giving the chance to construct a biased model which would perform poorly while predicting. To avoid this issue, while using a randomized dataset for training and testing, a systematic searching method known as K-fold cross validation was utilized to avoid bias issue in addition to improving searching efficiency. In particular, in this method the initial dataset is divided into K number of same sized groups and the model is trained with the combination of architecture and each time on K-1 of these groups and tested via the remaining group. This process is repeated for each of these groups and the performance of the model is recorded. In the final step, the performance criteria are averaged and the value represents the model performance for the architecture and regularizer hyper parameter combination [44]. Figure 2.4 shows the results of 5- and 6-fold cross validation for the MLFFNN model and it can be seen that the model with 5 hidden layers with 35 neurons in each layer and regularization parameter of 0.005 has the best performance with the average MSE of 0.127. It is notable that the maximum number of neurons for each layer has been selected to be 40, due to the high computational cost and negligible improvement that higher number of neurons contained.

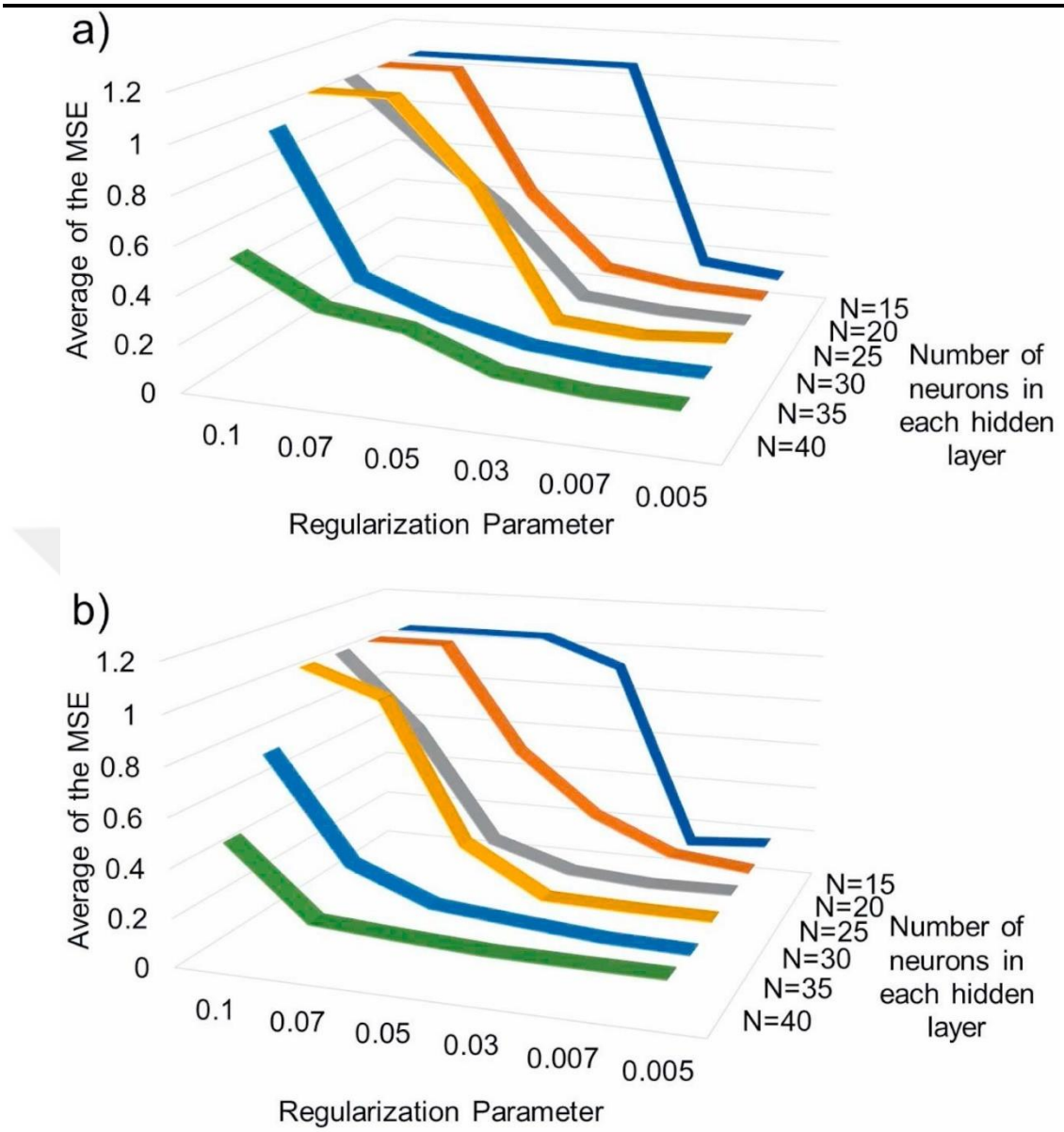

Figure 2.4 (a) Results of 5-fold (b) 6-fold cross validation for different combination of network sizes and regularization parameters representing the average MSE of the model for the respective combination.

2.2.3 Synthetic dataset

To find the optimum chemical composition of NiTi alloys to be used in orthodontic applications in term of ion release, the model's best 5 prediction shown in the Table 2.1 were chosen and the features of them other than the Ni and Ti % were selected to create synthetic datasets with Ni composition ranging from 49 to 55 at.%. with 0.1% intervals balance amount of Ti. The reason to select this range was that the NiTi alloys show SME and pseudo elasticity and the reason to select these 5 instances was the fact that the model has shown its ability to predict the other features with

reasonable accuracy, therefore suggesting the possibility of better prediction in this range for the other compositions. The synthetic datasets created in this step were imported to the MLFFNN model and the ion release value of the instances were predicted by the model.

Table 2.1 Comparison of Ni ion release: predicted vs reported data

Chemical composition of the NiTi alloy, at.%							Ni ion release in $\frac{\mu g}{cm^2}$		
Ni	Ti	Other elements	Wire Surface area (cm^2	Solution's pH	Solution amount (ml)	Time hours	Predicted values in this work	Reported values in the literature	
52.03	47.01	0.96	0.26	5	2	672	3.48	3.60[42]	*Sample 1
50.1	49.9	0	2.41	6.75	100	336	2.69	2.80[40]	*Sample 2
50.05	49.95	0	0.26	2.5	2	336	40.54	38.79[42]	*Sample 3
50.93	49.07	0	0.26	5	2	72	0.59	0.64[42]	*Sample 4
50.05	49.95	0	0.26	5	2	24	1.21	1.32[42]	*Sample 5
50.05	49.95	0	0.26	6.25	2	672	2.80	3.07[42]	
51.95	48.05	0	0.26	3.75	2	24	0.56	0.66[42]	
50.93	49.07	0	0.26	5	2	336	0.98	0.77[42]	
51.95	48.05	0	0.26	3.75	2	168	2.12	1.61[42]	
51.95	48.05	0	0.26	5	2	24	0.25	0.39[42]	

2.3 Results and discussion

2.3.1 Machine Learning Results

The results of model training process have been illustrated in the Figure 2.5 as the learning curves of the MLFFNN model and it can be seen that the model performs well while fitting the training dataset, which is in fact foreseeable due to the fact that the Neural Network models have the ability to fit complex data if they are large enough. However, to evaluate the model's performance in prediction of new and unseen data,

the cross-validation curve has higher importance. For this model it can be understood from the cross-validation curve in Figure 2.5 that the model converges to 0.059 which is a low value for the MSE and shows the ability of the model for predicting new instances. To further elaborate model's performance, the performance diagram of the model has been depicted in the Figure 2.6 which shows both the test and training instances in itself. This diagram consists of two axes, the horizontal axis which is for the transformed actual values of the ion release and the vertical axis for the predicted values from the model. If the point representing the data instance sits on the diagonal line, it represents accurate prediction by the model and the more the distance from this line is, the more is the error of prediction. It can be seen that the data instances, both from training and test dataset, sit in a relatively close distance from the line, showing the ability of the model in predicting the ion release of the instances.

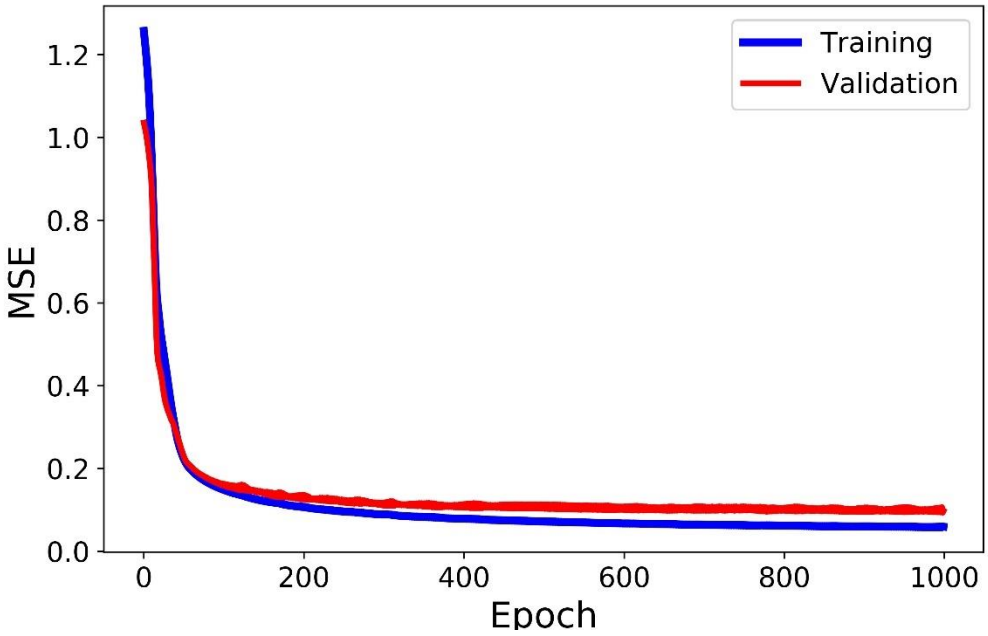

Figure 2.5 Learning curve of the best performing MLFFNN model representing the training and the cross-validation curves for 1000 iterations (Epochs).

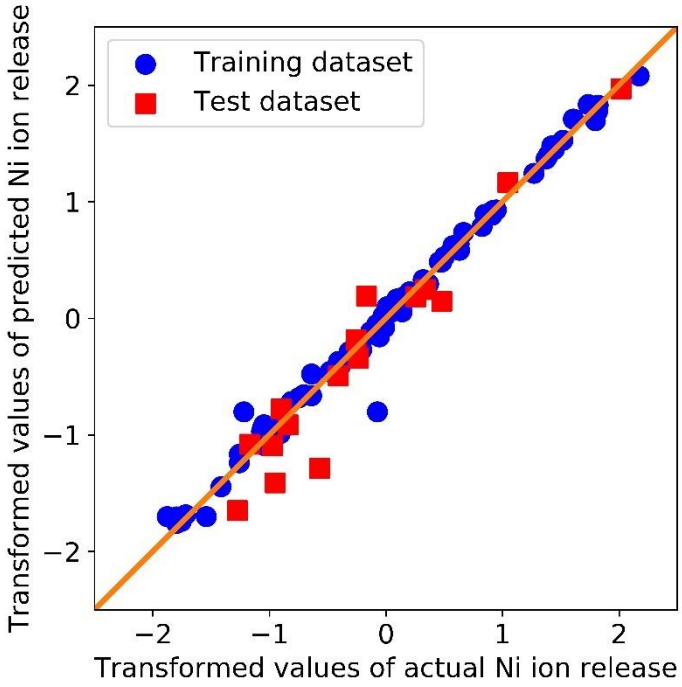

Figure 2.6 Performance diagram of the MLFFNN model representing the predicted vs actual values of transformed Ni ion release reported in literature.

To apply the trained MLFFNN model as the tool for finding the composition of NiTi which releases the least amount of Ni ion release into the oral cavity, synthetic datasets were imported to the model. The results of the predictions of the model for each dataset is presented in the Figure 2.7, in which each dataset is represented by name of "Sample" (from 1 to 5), representing the transformed values of Ni ion release and the Ni content of the alloys in at. %.. Based on the results from Figure 2.7 it can be seen that the ion release within range of 49-50% Ni is higher and faces a local minimum within the range of 50-53.4 at.%. and it would increase afterward concomitant with the increase in the Ni content of the alloy. It is notable that the sample 3 has a different trend in the range of 49-55% Ni and the ion release for this sample does not change significantly. This difference is attributed to the different experimental conditions which each of these samples represent (e.g. the different pH values) which can change the corrosion mechanism and therefore affecting the ion release considerably [12]. In addition, it is known that he formation of passive oxides on the surface of the NiTi SMA affects the ion release of the alloys and these oxides would form in the initial weeks of immersion experiments and would be dissolved and reformed on a weekly basis [12]. However, these effects are not considered in this work due to the limited

experimental dataset that exists on these factors and was beyond the scope of the current study.

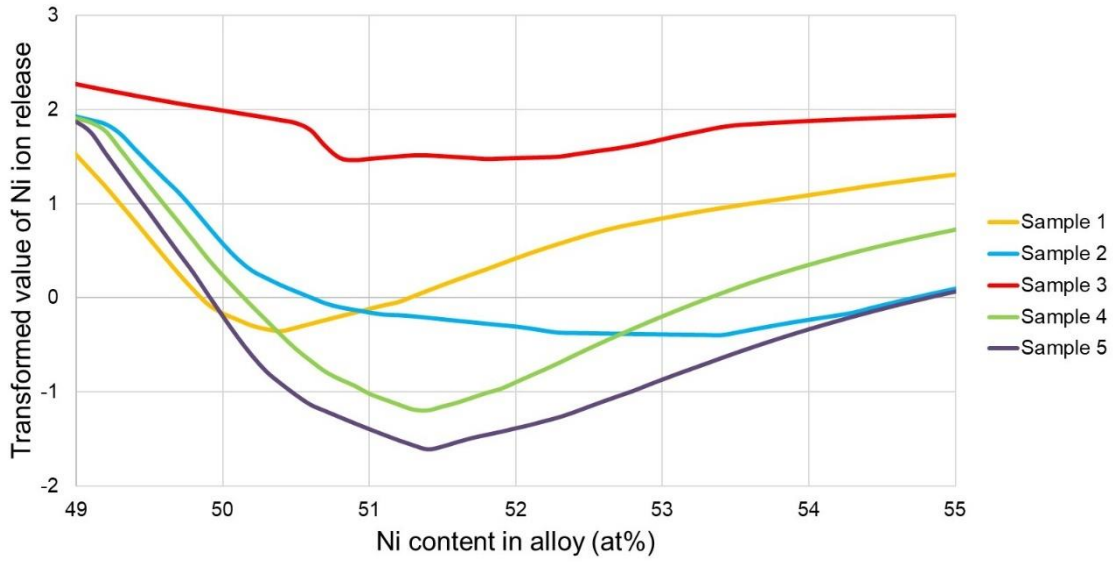

Figure 2.7 Predicted transformed values of Ni ion release for various Ni content (in at.%.) for NiTi alloys. Each "sample" is represented in Table 2.1 and is acquired by considering the best 5 predictions of the model.

Based on the outcome of the Figure 2.7, another synthetic dataset which represented the human oral cavity conditions in case of an infection was created and imported to the model. This condition was selected due to the fact that the pH in the infection condition is lower therefore creating a more aggressive environment. The results of this dataset is presented in the Figure 2.8 and it can be seen that the minimum amount of ion release falls between 51.3-51.5% at.%. Ni in the composition which is also a suitable range in terms of pseudoelasticity and SME.

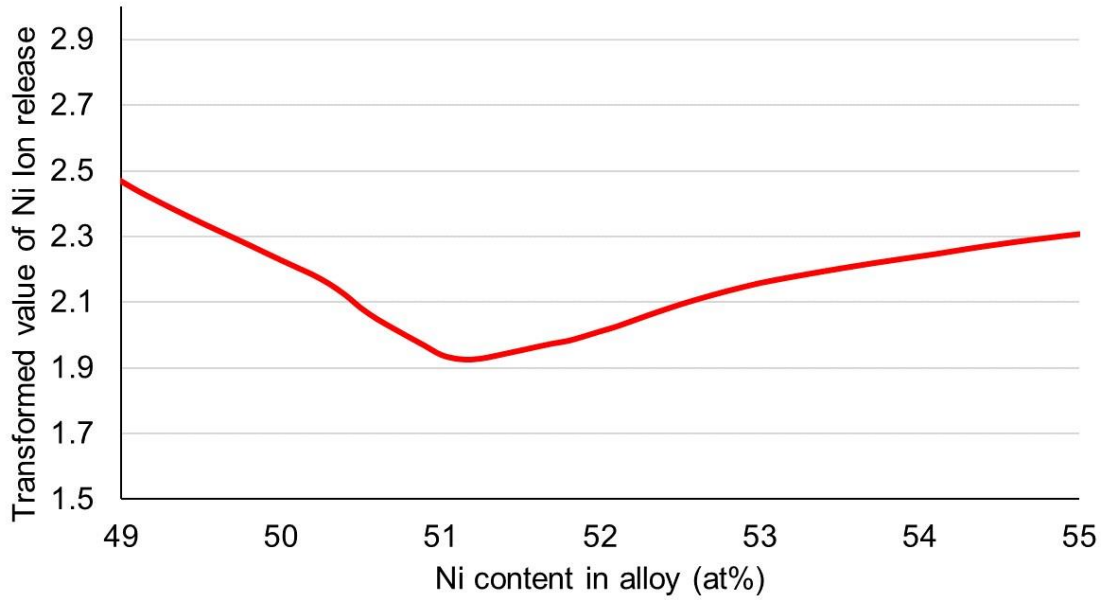

Figure 2.8 Transformed values of Ni ion release predicted by the MLFFNN model for various Ni contents (in at.%) for experimental condition with pH of 2.3 and experiment time of 720 hours (one month).

2.3.2 Validation Experiments

As it is necessary to validate the prediction of computational works, validation experiments were utilized by using commercial NiTi archwires produced by 3M (Unitek Nitinol heat-activated) which contained 51.5% at.%. and balance amount of Ti (which will be referred to as 51.5NiTi from now on). The underlying reason for selecting this material was due to the fact that: a) It was within the range of minimum amount of Ni ion release predicted by the AI framework in this work, and b) This composition has been used extensively in orthodontic archwires due to the pseudoelastic properties it contains. In order to compare the selected composition with the other NiTi alloys, samples with 50.4 and 50.7 at.%. Ni content were produced with surface area of areas of 1.73 and 1.65 cm^2 to be used as the control materials. To make the samples' surface properties similar to the ones that NiTi implants are used in human body, the native oxide layer was not removed from the surface. However, to clean them from the possible contaminations, samples were immersed in ethanol inside an ultrasonic bath and rinsed with water afterwards.

To imitate environment of human oral cavity for immersion experiment, validation samples were immersed in artificial saliva (AS) with the composition presented in the Table 2.2 within a sealed tube with temperature kept at 37 °C via

electronically controlled bath to imitate human body temperatures. After spending the intended time for each sample (1, 7,14 and 30 days), the samples were collected and rinsed with deionized water. Similar procedure was applied to the control materials with the exception that for the sample with 50.7 at.%. Ni was only applied to the 30-day experiment. The pH used in the experiments consisted of 2.3, 4.3 and 5.3 to show different and more aggressive conditions that might happen in oral cavity while an implant is in use including formation of plaques which might be due to unhealthy eating habits [64]. The amount of AS solutions inside the sealed tubes were chosen based on the ASTM G31 standard which is 20 $\frac{ml}{cm^2}$ [65]. To measure the Ni ion released from the collected samples into the immersion solutions, inductively coupled plasma mass spectrometry (ICP-MS) device (Agilent 7700x) method was utilized for each sample's solution.

Results illustrated in Figure 2.9 represents the predicted amount of Ni ion release from the samples with 50.4 and 51.5 at.%. Ni content in an AS immersion solution with pH of 2.3. it is clear that the amount of Ni ion release from the 51.5NiTi is lower than the 50.4 at.%. This result is in reasonable agreement with the experimental results of ICP-MS which is represented in Figure 2.10 showing that the 51.5NiTi releases lower Ni ion in all the experiment duration which validates the model's performance. It is notable that the pH of 2.3 is a quite aggressive environment and it is reasonable to believe that by increase of pH, i.e., increase in the oral cavity health, the Ni ion release would decrease. In order to assess the model's performance and investigate this general claim, a synthetic dataset with various pH of AS solution and 30 days of experiment for the 51.5NiTi was created and imported to the model. The predicted results of the model is presented in the Figure 2.11 shows a good agreement with the aforementioned claim, showing a sharp decrease in ion release from the alloy as the pH increases from 2.3 to 7.0. This claim was also validated through validating immersion experiments which its results are presented in the Table 2.3 as the Ni ion release from the samples to AS solution. In particular, by increase in the pH of the solutions from 2.3 (Validation Sample 1-1) to 3.3 (Validation Sample 1-2) and 4.3

(Validation Sample 1-3), the Ni ion release from the samples decreased from 0.45 to 0.03 and 0.02 $\frac{\mu g}{cm^2}$, respectively, presenting the sharp decrease predicted by the model.

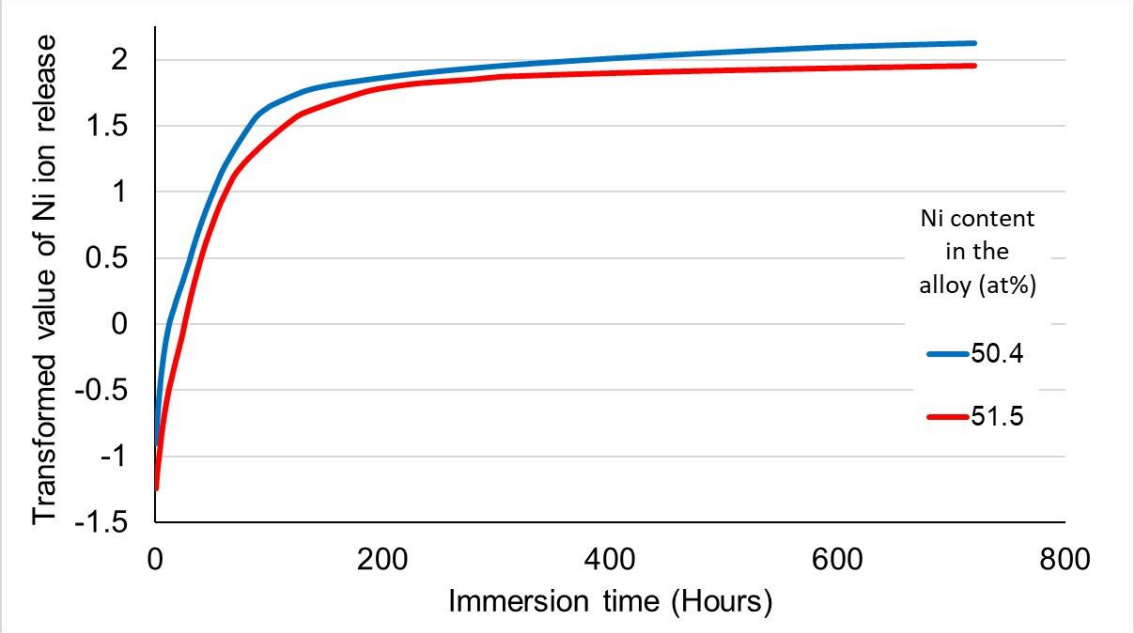

Figure 2.9 Transformed predicted values of Ni ion release for the control and validation NiTi alloy with respective Ni content of 50.4 and 51.5% at.% . The prediction of the model represents the lower amount of ion release for the 51.5 at.% NiTi.

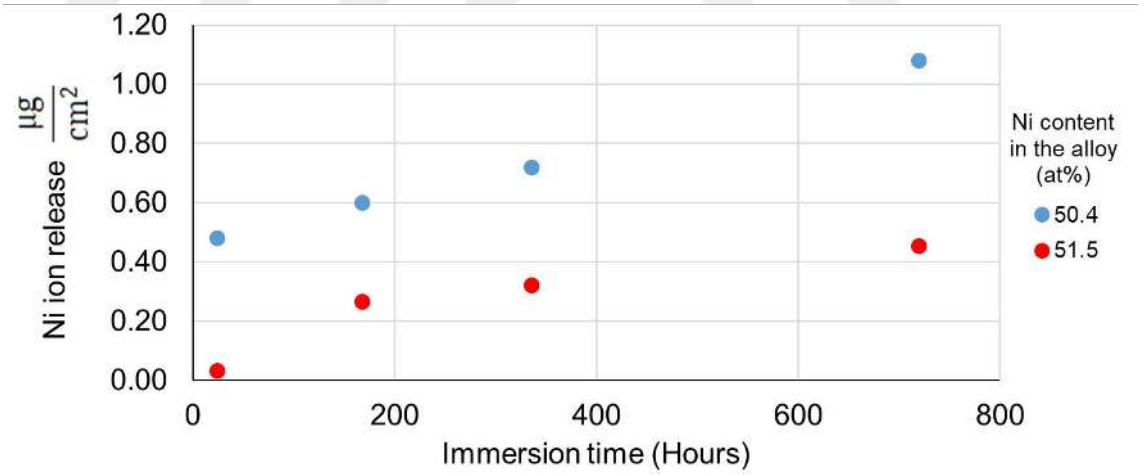

Figure 2.10 The Ni ion release of the validation and control samples with 51.5 and 50.4 at.% Ni content immersed in AS solution with pH of 2.3 and collected after 30 days, representing the lower amount of ion release for the 51.5NiTi.

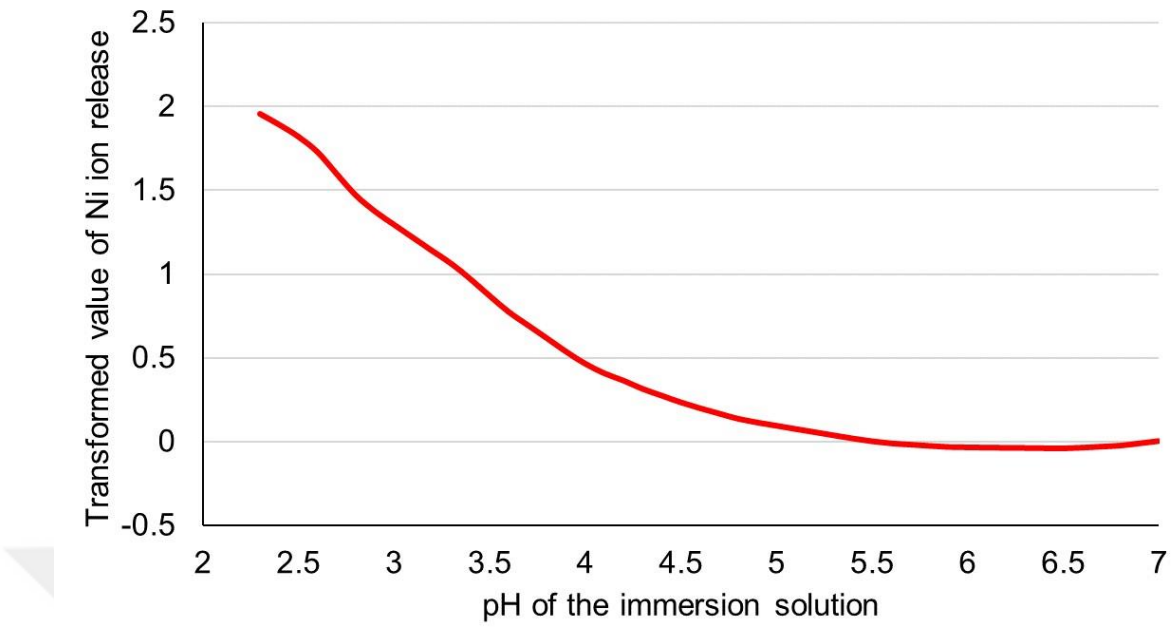

Figure 2.11 Transformed predicted values of Ni ion release for the 51.5NiTi alloy immersed in AS solutions with various pHs for 720 hours (30 days).

In addition, to further assess the performance of 51.5NiTi comparing to the control alloys, the validation samples of 2 and 3 with the specifications provided in the Table 2.3 were used in immersion experiment in AS solution with the 2.3 pH and 30 days of duration. The results of this experiment acquired through ICP-MS shows that the amount of Ni ion release from the 51.5NiTi is the lowest, presenting its ability to be used as the best candidate from NiTi alloys in terms of Ni ion release and biocompatibility in orthodontic applications and dental implants.

Table 2.2 Chemical composition of the AS solution used in immersion experiments for validation.

Ingredients	Amount (g/L)	pH
NaCl	0.4	2.3, 3.3, 4.3 (adjusted
KCl	0.4	by HCl)
$CaCl_2 \cdot 2H_2o$	0.906	
$NaH_2PO_4.2H_2O$	0.69	
$Na_2S.9H_2O$	0.005	
Urea	1	

Table 2.3 Results of validation immersion experiments for 720 hours (30 days) of immersion in AS with various pH.

	Ni %	Shape and dimensions	Surface area	pH	Ni ion release in $\frac{\mu g}{cm^2}$
Validation Sample 1-1	51.5	D = 0.36 mm h = 16.5 cm	1.87	pH= 2.3	0.45
Validation Sample 1-2	51.5	D = 0.36 mm h = 16.5 cm	1.87	pH = 3.3	0.03
Validation Sample 1-3	51.5	D = 0.36 mm h = 16.5 cm	1.87	pH = 4.3	0.02
Validation Sample 2	50.7	D = 3.5 mm h = 1.5 cm	1.65	pH = 2.3	1.20
Validation Sample 3	50.4	D = 2 mm h = 2.75 cm	1.73	pH = 2.3	1.08

As the final comment, the author wants to note that the AI framework presented in this study can be an early "prototype" for a larger AI framework in which biomedical alloys, or alloys of other applications, are designed and manufactured. The selected application studied in this work was within a specific field, but still included variety of parameters. It also worth emphasizing that the NiTi SMA with 51.5 at.%. Ni content has been in use for decades as the material of choice of dental applications, however, the ML model used in this work solely and without any bias predicted this value based on the experimental data available in the literature. From this point of view, the results of the current study present an excellent example of outcomes that can be achieved by use of ML methods in interdisciplinary problems.

2.4 Conclusions

This study represents use of multilayer feedforward neural network (MLFFNN) as a machine learning (ML) method to predict the amount of Ni ion release from NiTi shape memory alloys (SMA) to be used in orthodontic applications. To be more specific, an artificial intelligence (AI) framework was created to utilize already available experimental data including various NiTi composition and experimental conditions of immersion test as the dataset to predict the lowest Ni ion release from the samples. The model's predictions were validated using static immersion experiments inside artificial saliva (AS) solution with different pH and experiment duration to mimic human oral cavity conditions while the release Ni ions were measured using the

inductively coupled plasma mass spectrometer (ICP-MS). Consequently, the results of this work suggested that in the case of NiTi SMAs in orthodontic applications, the lowest amount Ni ion release belongs to the NiTi alloy with 51.5% Ni and balance amount of Ti and this point was validated though immersion experiments. In addition to the fact that the extensive use of this NiTi composition can serve as a separate validation for the current AI framework, it also indicates that the current AI framework can be extended to other biomedical alloying systems for other various applications.

2.5 References

[1] D. Mantovani, Shape memory alloys: Properties and biomedical applications, JOM. 52 (2000) 36–44. https://doi.org/10.1007/s11837-000-0082-4.

[2] T. Duerig, A. Pelton, D. Stöckel, An overview of nitinol medical applications, Mater. Sci. Eng. A. 273–275 (1999) 149–160. https://doi.org/10.1016/S0921-5093(99)00294-4.

[3] K. Otsuka, X. Ren, Recent developments in the research of shape memory alloys, Intermetallics. 7 (1999) 511–528. https://doi.org/10.1016/S0966-9795(98)00070-3.

[4] A. Bansiddhi, T.D. Sargeant, S.I. Stupp, D.C. Dunand, Porous NiTi for bone implants: A review, Acta Biomater. 4 (2008) 773–782. https://doi.org/10.1016/j.actbio.2008.02.009.

[5] G. Mani, M.D. Feldman, D. Patel, C.M. Agrawal, Coronary stents: A materials perspective, Biomaterials. 28 (2007) 1689–1710. https://doi.org/10.1016/j.biomaterials.2006.11.042.

[6] L. Petrini, F. Migliavacca, S. Gialanella, Biomedical Applications of Shape Memory Alloys, J. Metall. 2011 (2011) 15. https://doi.org/10.1155/2011/501483.

[7] R. Käkelä, A. Käkelä, H. Hyvärinen, Effects of nickel chloride on reproduction of the rat and possible antagonistic role of selenium, Comp. Biochem. Physiol. - C Pharmacol. Toxicol. Endocrinol. 123 (1999) 27–37. https://doi.org/10.1016/S0742-8413(99)00006-7.

[8] N. Henrik Nielsen, T. Menné, Nickel sensitization and ear piercing in an unselected Danish population, Contact Dermatitis. 29 (1993) 16–21.

https://doi.org/10.1111/j.1600-0536.1993.tb04530.x.

[9] S.M.M. Toker, D. Canadinc, H.J.J. Maier, O. Birer, Evaluation of passive oxide layer formation–biocompatibility relationship in NiTi shape memory alloys: Geometry and body location dependency, Mater. Sci. Eng. C. 36 (2014) 118–129. https://doi.org/10.1016/j.msec.2013.11.040.

[10] S.M. Toker, G. Gerstein, H.J. Maier, D. Canadinc, Effects of microstructural mechanisms on the localized oxidation behavior of NiTi shape memory alloys in simulated body fluid, J. Mater. Sci. 53 (2018) 948–958. https://doi.org/10.1007/s10853-017-1586-4.

[11] B. Uzer, S.M. Toker, A. Cingoz, T. Bagci-Onder, G. Gerstein, H.J. Maier, D. Canadinc, An exploration of plastic deformation dependence of cell viability and adhesion in metallic implant materials, J. Mech. Behav. Biomed. Mater. 60 (2016) 177–186. https://doi.org/10.1016/j.jmbbm.2016.01.001.

[12] B. Uzer, O. Birer, D. Canadinc, Investigation of the Dissolution–Reformation Cycle of the Passive Oxide Layer on NiTi Orthodontic Archwires, Shape Mem. Superelasticity. 3 (2017) 264–273. https://doi.org/10.1007/s40830-017-0114-3.

[13] B. Uzer, B. Gumus, S. Toker, D. Sahbazoglu, D. Saher, C. Yildirim, S. Polat-Altintas, D. Canadinc, A Critical Approach to the Biocompatibility Testing of Niti Orthodontic Archwires, Int. J. Metall. Met. Phys. 1 (2016) 1–7. https://doi.org/10.35840/2631-5076/9203.

[14] H.C. Man, S. Zhang, F.T. Cheng, X. Guo, In situ formation of a TiN/Ti metal matrix composite gradient coating on NiTi by laser cladding and nitriding, Surf. Coatings Technol. 200 (2006) 4961–4966. https://doi.org/10.1016/j.surfcoat.2005.05.017.

[15] T. Fu, B.G. Liu, Y.M. Zhou, X.M. Wu, Sol-gel titania coating on NiTi alloy with a porous titania film as interlayer, J. Sol-Gel Sci. Technol. 58 (2011) 307–311. https://doi.org/10.1007/s10971-010-2392-5.

[16] J.L. Xu, F. Liu, F.P. Wang, D.Z. Yu, L.C. Zhao, Microstructure and corrosion resistance behavior of ceramic coatings on biomedical NiTi alloy prepared by micro-arc oxidation, Appl. Surf. Sci. 254 (2008) 6642–6647. https://doi.org/10.1016/j.apsusc.2008.04.068.

[17] A.R. Boccaccini, C. Peters, J.A. Roether, D. Eifler, S.K. Misra, E.J. Minay, Electrophoretic deposition of polyetheretherketone (PEEK) and PEEK/Bioglass®

coatings on NiTi shape memory alloy wires, J. Mater. Sci. 41 (2006) 8152–8159. https://doi.org/10.1007/s10853-006-0556-z.

[18] R. Bakhshi, A. Darbyshire, J.E. Evans, Z. You, J. Lu, A.M. Seifalian, Polymeric coating of surface modified nitinol stent with POSS-nanocomposite polymer, Colloids Surfaces B Biointerfaces. 86 (2011) 93–105. https://doi.org/10.1016/j.colsurfb.2011.03.024.

[19] A. Motallebzadeh, M.B. Yagci, E. Bedir, C.B. Aksoy, D. Canadinc, Mechanical Properties of TiTaHfNbZr High-Entropy Alloy Coatings Deposited on NiTi Shape Memory Alloy Substrates, Metall. Mater. Trans. A Phys. Metall. Mater. Sci. 49 (2018) 1992–1997. https://doi.org/10.1007/s11661-018-4605-4.

[20] C.B. Aksoy, D. Canadinc, M.B. Yagci, Assessment of Ni ion release from TiTaHfNbZr high entropy alloy coated NiTi shape memory substrates in artificial saliva and gastric fluid, Mater. Chem. Phys. 236 (2019) 121802. https://doi.org/10.1016/j.matchemphys.2019.121802.

[21] S.F. Kurtoğlu, M.B. Yağcı, A. Uzun, U. Ünal, D. Canadinc, Enhancing biocompatibility of NiTi shape memory alloys by simple NH3 treatments, Appl. Surf. Sci. 525 (2020) 146547. https://doi.org/10.1016/j.apsusc.2020.146547.

[22] M. Es-Souni, M. Es-Souni, H.F. Brandies, On the transformation behaviour, mechanical properties and biocompatibility of two NiTi-based shape memory alloys:: NiTi42 and NiTi42Cu7, Biomaterials. 22 (2001) 2153–2161. https://doi.org/10.1016/S0142-9612(00)00406-3.

[23] P. Tua-Ngam, S. Dechkunakorn, N. Anuwongnukroh, Surface Characteristics, Chemical Composition and Ni Release of NiTi Wire in Different pH, Adv. Mater. Res. 884–885 (2014) 586–592. https://doi.org/10.4028/www.scientific.net/AMR.884-885.586.

[24] X. Jiang, H.-Q. Yin, C. Zhang, R.-J. Zhang, K.-Q. Zhang, Z.-H. Deng, G. Liu, X. Qu, An materials informatics approach to Ni-based single crystal superalloys lattice misfit prediction, Comput. Mater. Sci. 143 (2018) 295–300. https://doi.org/10.1016/J.COMMATSCI.2017.09.061.

[25] D.D. Xue, P. V. Balachandran, J. Hogden, J. Theiler, D.D. Xue, T. Lookman, Accelerated search for materials with targeted properties by adaptive design, Nat. Commun. 7 (2016) 11241. https://doi.org/10.1038/ncomms11241.

[26] J. Ling, E. Antono, S. Bajaj, S. Paradiso, M. Hutchinson, B. Meredig, B.M.

Gibbons, Machine Learning for Alloy Composition and Process Optimization, in: Vol. 6 Ceram. Control. Diagnostics, Instrumentation; Educ. Manuf. Mater. Metall., American Society of Mechanical Engineers, 2018. https://doi.org/10.1115/GT2018-75207.

[27] W. Huang, P. Martin, H.L. Zhuang, Machine-learning phase prediction of high-entropy alloys, Acta Mater. 169 (2019) 225–236. https://doi.org/10.1016/j.actamat.2019.03.012.

[28] D. Xue, D. Xue, R. Yuan, Y. Zhou, P. V. Balachandran, X. Ding, J. Sun, T. Lookman, An informatics approach to transformation temperatures of NiTi-based shape memory alloys, Acta Mater. 125 (2017) 532–541. https://doi.org/10.1016/j.actamat.2016.12.009.

[29] C. Wen, Y. Zhang, C. Wang, D. Xue, Y. Bai, S. Antonov, L. Dai, T. Lookman, Y. Su, Machine learning assisted design of high entropy alloys with desired property, Acta Mater. 170 (2019) 109–117. https://doi.org/10.1016/j.actamat.2019.03.010.

[30] Y. Li, W. Guo, Machine-learning model for predicting phase formations of high-entropy alloys, Phys. Rev. Mater. 3 (2019). https://doi.org/10.1103/PhysRevMaterials.3.095005.

[31] G. Kim, H. Diao, C. Lee, A.T. Samaei, T. Phan, M. de Jong, K. An, D. Ma, P.K. Liaw, W. Chen, First-principles and machine learning predictions of elasticity in severely lattice-distorted high-entropy alloys with experimental validation, Acta Mater. 181 (2019) 124–138. https://doi.org/10.1016/j.actamat.2019.09.026.

[32] N. Islam, W. Huang, H.L. Zhuang, Machine learning for phase selection in multi-principal element alloys, Comput. Mater. Sci. 150 (2018) 230–235. https://doi.org/10.1016/j.commatsci.2018.04.003.

[33] D.C. Pagan, T.Q. Phan, J.S. Weaver, A.R. Benson, A.J. Beaudoin, Unsupervised learning of dislocation motion, Acta Mater. 181 (2019) 510–518. https://doi.org/10.1016/j.actamat.2019.10.011.

[34] E. Alpaydin, Introduction to machine learning, MIT Press Ltd, 2020.

[35] K.P. Murphy, Machine learning: a probabilistic perspective, MIT press, 2012.

[36] S.M. Toker, D. Canadinc, Evaluation of the biocompatibility of NiTi dental wires: A comparison of laboratory experiments and clinical conditions, Mater. Sci. Eng. C. 40 (2014) 142–147. https://doi.org/10.1016/j.msec.2014.03.060.

[37] Anne-Wil Harzing, Publish or Perish, (2007). https://harzing.com/resources/publish-or-perish.

[38] A. Sheibaninia, Effect of Thermocycling on Nickel Release from Orthodontic Arch Wires: an In Vitro Study, Biol. Trace Elem. Res. 162 (2014) 353–359. https://doi.org/10.1007/s12011-014-0136-z.

[39] M. Arndt, A. Brück, T. Scully, A. Jäger, C. Bourauel, Nickel ion release from orthodontic NiTi wires under simulation of realistic in-situ conditions, J. Mater. Sci. 40 (2005) 3659–3667. https://doi.org/10.1007/s10853-005-0448-7.

[40] A. Charles, P. Gangurde, S. Jacob, S. Jatol-Tekade, R. Senkutvan, V. Vadgaonkar, Evaluation of nickel ion release from various orthodontic arch wires: An in vitro study, J. Int. Soc. Prev. Community Dent. 4 (2014) 12. https://doi.org/10.4103/2231-0762.130921.

[41] F.J.J. Gil, E. Espinar, J.M.M. Llamas, J.M.M. Manero, M.P.P. Ginebra, Variation of the superelastic properties and nickel release from original and reused NiTi orthodontic archwires, J. Mech. Behav. Biomed. Mater. 6 (2012) 113–119. https://doi.org/10.1016/j.jmbbm.2011.11.005.

[42] H.H. Huang, Y.H. Chiu, T.H. Lee, S.C. Wu, H.W. Yang, K.H. Su, C.C. Hsu, Ion release from NiTi orthodontic wires in artificial saliva with various acidities, Biomaterials. 24 (2003) 3585–3592. https://doi.org/10.1016/S0142-9612(03)00188-1.

[43] Y.-C. Hu, Multilayer Perceptron for Robust Nonlinear Interval Regression Analysis Using Genetic Algorithms, Sci. World J. 2014 (2014). https://doi.org/10.1155/2014/970931.

[44] F. Pedregosa, G. Varoquaux, A. Gramfort, V. Michel, B. Thirion, O. Grisel, M. Blondel, P. Prettenhofer, R. Weiss, V. Dubourg, Scikit-learn: Machine learning in Python, J. Mach. Learn. Res. 12 (2011) 2825–2830.

[45] I.-K.I. Yeo, R.A. Johnson, A new family of power transformations to improve normality or symmetry, Biometrika. 87 (2000) 954–959. https://doi.org/10.1093/biomet/87.4.954.

[46] Y. Zhang, C. Wen, C. Wang, S. Antonov, D. Xue, Y. Bai, Y. Su, Phase prediction in high entropy alloys with a rational selection of materials descriptors and machine learning models, Acta Mater. 185 (2019) 528–539. https://doi.org/10.1016/j.actamat.2019.11.067.

[47] S. Haykin, Neural Networks and Learning Machines, 2008. https://doi.org/978-0131471399.

[48] C.M. Bishop, Neural networks for pattern recognition, Oxford university press, 1995.

[49] H.B. Barlow, Unsupervised Learning, Neural Comput. 1 (1989) 295–311. https://doi.org/10.1162/neco.1989.1.3.295.

[50] C. Lin, Face detection by color and multilayer feedforward neural network, in: ICIA 2005 - Proc. 2005 Int. Conf. Inf. Acquis., 2005: pp. 518–523. https://doi.org/10.1109/icia.2005.1635143.

[51] D.L. Millar, P.A. Calderbank, On the investigation of a multilayer feedforward neural network model of rock deformability behaviour, in: 8th ISRM Congr., International Society for Rock Mechanics and Rock Engineering, 1995: pp. 933–938.

[52] K. Hornik, M. Stinchcombe, H. White, Multilayer feedforward networks are universal approximators, Neural Networks. 2 (1989) 359–366. https://doi.org/10.1016/0893-6080(89)90020-8.

[53] D. Svozil, V. Kvasnička, J. Pospíchal, Introduction to multi-layer feed-forward neural networks, in: Chemom. Intell. Lab. Syst., Elsevier, 1997: pp. 43–62. https://doi.org/10.1016/S0169-7439(97)00061-0.

[54] V. Nair, G.E. Hinton, Rectified linear units improve restricted boltzmann machines, in: Proc. 27th Int. Conf. Mach. Learn., 2010: pp. 807–814.

[55] S. Theodoridis, Mean-Square Error Linear Estimation, Elsevier, 2015. https://doi.org/10.1016/b978-0-12-801522-3.00004-5.

[56] S.J. Reddi, S. Kale, S. Kumar, On the Convergence of Adam and Beyond, (2019). http://arxiv.org/abs/1904.09237.

[57] P.T. Tran, L.T. Phong, On the Convergence Proof of AMSGrad and a New Version, IEEE Access. 7 (2019) 61706–61716. https://doi.org/10.1109/ACCESS.2019.2916341.

[58] D.P. Kingma, J.L. Ba, Adam: A method for stochastic optimization, in: 3rd Int. Conf. Learn. Represent. ICLR 2015 - Conf. Track Proc., International Conference on Learning Representations, ICLR, 2015. https://arxiv.org/abs/1412.6980v9 (accessed July 20, 2020).

[59] C. Cortes, M. Mohri, A. Rostamizadeh, L2 Regularization for Learning Kernels,

Proc. 25th Conf. Uncertain. Artif. Intell. UAI 2009. (2012) 109–116. http://arxiv.org/abs/1205.2653 (accessed July 22, 2020).

[60] J.D. Hunter, Matplotlib: A 2D Graphics Environment, Comput. Sci. Eng. 9 (2007) 90–95. https://doi.org/10.1109/MCSE.2007.55.

[61] W. McKinney, Data Structures for Statistical Computing in Python, in: 2010: pp. 56–61. https://doi.org/10.25080/Majora-92bf1922-00a.

[62] M. Abadi, A. Agarwal, P. Barham, E. Brevdo, Z. Chen, C. Citro, G.S. Corrado, A. Davis, J. Dean, M. Devin, S. Ghemawat, I. Goodfellow, A. Harp, G. Irving, M. Isard, Y. Jia, R. Jozefowicz, L. Kaiser, M. Kudlur, J. Levenberg, D. Mane, R. Monga, S. Moore, D. Murray, C. Olah, M. Schuster, J. Shlens, B. Steiner, I. Sutskever, K. Talwar, P. Tucker, V. Vanhoucke, V. Vasudevan, F. Viegas, O. Vinyals, P. Warden, M. Wattenberg, M. Wicke, Y. Yu, X. Zheng, M. Rucci, A. Casile, TensorFlow: Large-Scale Machine Learning on Heterogeneous Distributed Systems, ArXiv Prepr. ArXiv1603.04467. 16 (2016) 121–138. https://doi.org/10.1080/09548980500300507.

[63] Y. Bengio, Practical recommendations for gradient-based training of deep architectures, Lect. Notes Comput. Sci. (Including Subser. Lect. Notes Artif. Intell. Lect. Notes Bioinformatics). 7700 LECTU (2012) 437–478. https://doi.org/10.1007/978-3-642-35289-8-26.

[64] R.R. Al-Hity, H.F. Kappert, S. Viennot, F. Dalard, B. Grosgogeat, Corrosion resistance measurements of dental alloys, are they correlated?, Dent. Mater. 23 (2007) 679–687. https://doi.org/10.1016/j.dental.2006.06.008.

[65] ASTM International, ASTM Standard G31-72, 2004, “Standard Practice for Laboratory Immersion Corrosion Testing of Metals,” 2004th ed., ASTM International, West Conshohocken, PA, 2004.

Chapter 3:

DEVELOPMENT OF NOVEL HIGH ENTROPY ALLOYS WITH ULTRAHIGH TEMPERATURE SHAPE MEMORY CAPABILITY

3.1 Introduction

The NiTi shape memory alloys (SMAs) have gained popularity in the materials science field due to their appealing shape memory effect (SME) and pseudoelastic properties arisen from the austenite-to-martensite phase transformation, which helps simplifying the design of devices in various fields such as aerospace or biomedical engineering [1,2]. In particular, the simplified designs utilize Shape memory effect (SME) properties to perform tasks such as causing motion and displacing an object or applying a specific load, instead of the need for sophisticated components in case of using conventional alloys. This simplification, in addition to the possible cost reduction, eliminates the chance of failures in critical components in the aerospace field that rely on oil pressure to function, hence the use of SMAs increase safety measures for these components [3]. However, binary NiTi SMAs show their SME and pseudoelastic properties in rather low temperatures, mostly below 100 °C, therefore constraining the applications of these materials to components functioning in low temperatures [4].

In order to improve the limited thermal working condition of the NiTi alloys and extend their application to higher temperatures, numerous studies were conducted, mainly using two approaches. In one approach, by using various heat treatment and mechanical processes, the microstructures of the alloys were manipulated, and thus the phase transformation temperatures (PTTs) related to austenite-to-martensite and reverse transformations were adjusted [5–7]. Although this approach is seemingly simple, it bears many difficulties finding the optimum procedures, along with the more crucial fact that it cannot increase the working temperature to the sufficient level for many medium or high temperature applications due to the thermodynamic nature of binary NiTi alloys. Therefore, in another approach, a significant number of studies used the addition of various metallic elements to a NiTi base to adjust the PTTs of the NiTi alloys. The outcome of these studies showed that the additional elements can substantially affect the mechanisms of diffusionless martensitic transformations,

therefore varying the PTTs related to such transformations. In particular, these elements would facilitate or hinder the formation of martensite from the parent phase of austenite, therefore changing the thermodynamic equilibrium or kinetics of the transformations, resulting in different responses from the alloy [8–11].

To fully understand the effects of different metallic elements on the PTTs of NiTi based SMAs, numerous studies have been conducted. Several studies showed that the addition of Pt, Hf, Au, Zr and Pd increased the PTTs of the NiTi alloys, therefore increasing their application temperatures [12–20]. On the other hand, several studies showed that the addition of the Fe, Mn, Co, Cr and V decreased the PTTs [21–23]. Therefore, one might conclude that by the addition of the first group of elements to the alloys, the problem of low-temperature PTTs will be solved. However, using these elements increase the thermal hysteresis (TH) and will limit the functionality of the respective alloys. Particularly, the hysteresis shows itself in the form of dissipated heat, Thus, if the heat dispersion time is not enough, it will accumulate in the component, consequently interfering with the phase transformations and the efficiency of the component [24]. Therefore, new methods had to be studied to decrease the TH, and as a response, several studies have shown that the addition of elements such as Cu and Fe to the NiTi base can decrease the TH of the alloys. In particular, it has been shown that a NiTi based alloy with addition of Cu and Pd could make a SMA alloy with near zero TH value without reducing the PTTs to cryogenic temperatures [25,26]. Consequently, it can be concluded that to find a composition that would work properly in high temperatures, it is needed to study the effects of combinations of aforementioned elements to come up with an alloy that has sufficiently high PTTs while owning the least possible TH. Several studies have implemented this method and showed that multi-elemental SMAs can be useful as a tool for achieving desirable properties. As an example, in a series of works, Cu, Fe and Pd were added to a NiTi system to optimize the PTT and TH of the alloys for the applications that demand high PTTs and low hysteresis, and it was shown that such additional elements can enhance the material response for the specific use [27,28]. However, the vast pool of the possible chemical compositions for the alloys requires a costly experimental process, both timewise and financially, to unravel the most suitable compositions, if the conventional methods of trial and error or design of experiments are implemented. Therefore, the need for another approach is indisputable.

An alternative way to the trial and error method in these problems is implementing Machine learning (ML) methods, a data-driven learning tool which gained attention in the last two decades due to its unique abilities that can be used as a complementary method to increase the efficiency of the experimental works [27–38]. In specific, these methods use both computer programming and statistical methods to train a model on a part of a previously prepared dataset, known as "training dataset". Then through optimizing the model by using a performance criterion, which evaluates it by the "test dataset" that the model has not been given before, the ability for prediction of instances with new conditions is created. Additionally, the use of the statistical methods provides the model with the ability to discover both linear and non-linear relationships, therefore, empowering the model to predict highly complex relationships that exist between the parameters of the problem with minimal computational cost [39,40].

The aforementioned potentials of the ML methods can show their value in fields similar to materials science, in which the relations between the parameters of a problem can be highly complex and to unravel these connections, expensive and cumbersome experiments are needed. Therefore, in a trend in recent years, ML methods have started to gain attention in the materials science field. As an example, one recent study investigated the effects of various dopants on the PTTs of NiTi shape memory alloys and provided a ML model to predict the PTTs for several combination of elements. Specifically, using general Landau free energy model, the effect of doping various elements on the point defects of the NiTi alloys were investigated and experimental trends were reproduced via Time dependent Ginzburg-Landau simulations. Consequently, several effective features from these simulations were selected and used as inputs for training a regression ML model, which successfully predicted the PTTs for the doped alloys [41]. In another study, ML methods were used as a tool to minimize the computational efforts to optimize the NiTi chemical composition and microstructure to achieve desired properties via thermodynamically consistent micromechanical simulations. To be more specific, the aforementioned simulations were used to predict the PTTs and TH of the respective alloy and these results were used to train a ML model that circumvented the need for extensive number of simulations for finding these properties for the various compositions of binary NiTi [35]. In addition to these examples, Artificial Neural Networks (ANNs), a commonly used ML method, was used to design a new molybdenum alloy that could simultaneously satisfy the physical and

mechanical needs for refractory applications proving the ability of ANNs as a ML method for optimization problems [42]. These examples, alongside the other existing works, show the great potential of ML methods to be exploited in reducing the costs and enhancing the knowledge acquired through scientific studies, especially for development of novel SMAs. However, most of the published literature focused on changing binary NiTi composition or addition of small amount of alloying elements to the NiTi base, therefore leaving a vast area of possible compositions with promising properties untouched.

The current work's objective is to address the aforementioned issue by establishing an artificial intelligence (AI) framework to find the optimum chemical composition of NiTi alloys with the addition of significant amounts of Cu, Fe, and Pd to achieve the highest PTTs with the lowest possible TH in order to be used in high-temperature applications, such as actuators in aerospace engineering, while the use of ML methods also minimize the experimental efforts of the work to only validation experiments. In particular, Cu and Fe were selected as the alloying elements that have already proven themselves in decreasing the TH of NiTi based SMAs. To increase the PTTs of the combination, Pd was selected from the alloys that increase the PTTs of the composition due to the availability of data in the literature with the aforementioned set of elements comparing to the other elements such as Hf, Au, and Pt. Subsequently, using the vast data available in the published literature about the changes in PTTs and TH of NiTi alloys with the addition of the aforementioned elements, two data pools were formed, and two different models were trained based on each of the datasets to predict the first endothermic peak value as a representative of PTTs and TH value for a specific alloy composition. To implement this, a three-stage process, as shown in Figure 3.1 is implemented. In the first stage, using the previously published literature on the PTTs and TH of the alloys containing Ni, Ti, Cu, Fe, and Pd, two datasets were gathered for PTTs and TH. Consequently, in the second stage using Multilayer Feed-forward Neural Network (MLFFNN), a well-known ML method, predictive models are developed, and the prediction with the most desirable composition was chosen for further investigations.

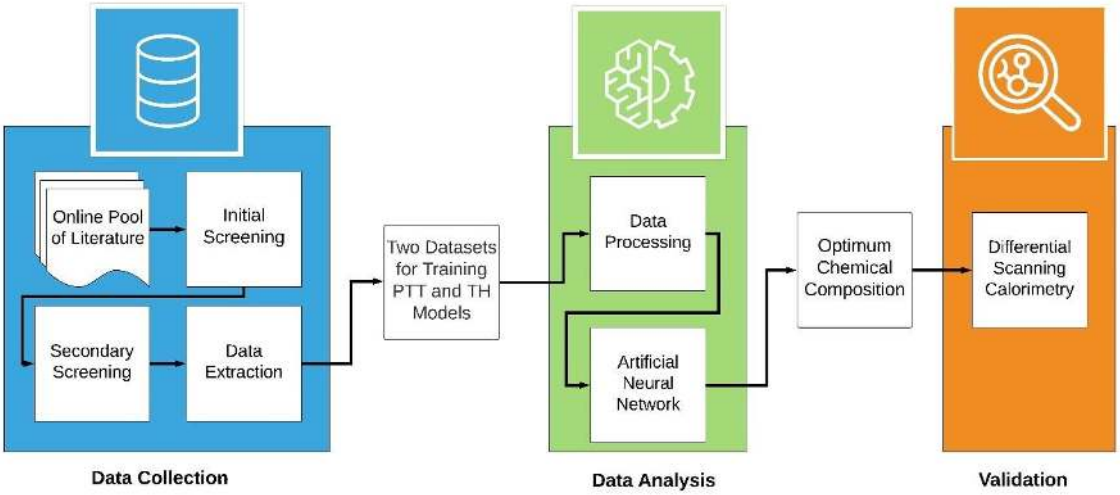

Figure 3.1 Schematics of the optimization process for NiTi based alloy shape memory alloys implemented in this work.

3.2 Computational methods

3.2.1 Dataset

Extracting data from already published literature is proved to be an inexpensive and quick way to provide datasets to train machine learning models [37]. In this work, the scientific publications on the phase transformation temperatures (PTTs) and the thermal hysteresis (TH) of the NiTi based shape memory alloys with the addition of Cu, Fe and Pd were meticulously investigated and the data necessary for the training of ML models were acquired. In particular, two datasets for the training of two different models to predict the PTT and TH of the NiTi based shape memory alloys were gathered by collecting data from already published literature [27,28,43–76]. The dataset collection process is depicted in Figure 3.1. In this process, the scientific literature acquired from online sources were screened firstly to remove the non-English content, then in the second step, the literature that was out of the scope of work was omitted. In the next step, the information related to the chemical compositions (in atomic percentage) of the instances was extracted as the input and the PTT and TH values of them were collected as the output of the datasets. Specifically, the first endothermic peak of the DSC diagrams is chosen to represent the PTT values of the respective alloy (for convenience it is called PTT values from now on) and in the case of the literature only providing the A_s and A_f, the average of these values was assumed to be the endothermic peak value. In addition, for the hysteresis values, the difference of A_f and

M_s were considered. It should be noted that since the processing conditions have a significant impact on both PTT and TH of the alloys, instances with minimum amount of processing were chosen to form a uniform dataset.

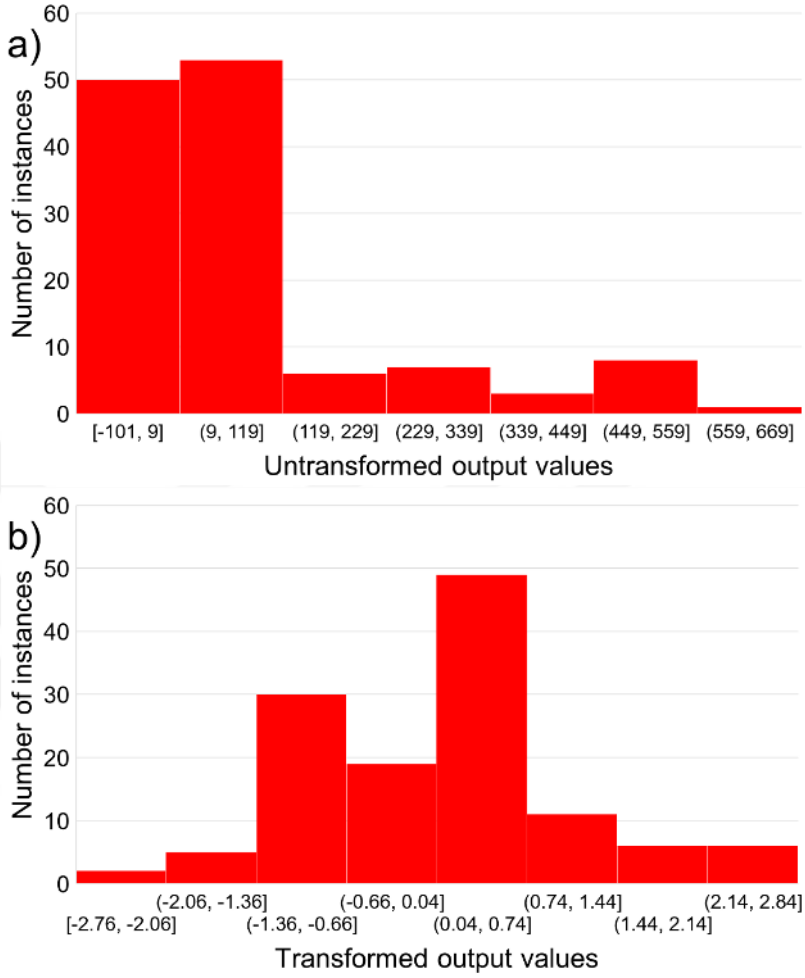

Figure 3.2 (a) Untransformed (b) Transformed distribution of Endothermic peak value used for training of the PTT model.

The addition of externally calculated features to the input features of the datasets has proven to be a useful method to increase the performance of the ML models [27,77]. Therefore, in this work, features of mixing entropy and the concentration of valence electron (cv) were calculated for each instance and were added to the datasets. In particular, the concentration of the valence electrons is shown to have a significant effect on the M_s and A_f of the shape memory alloys with different chemical compositions [78]. In addition, the mixing entropy of the alloys is proved to have a considerable effect on the stability of the alloys [79]. By the addition of these features to the input of both PTT and TH datasets, the input features included 7 features to be used for the training of the models.

3.2.2 Data processing

To prepare the data for training in the ML models and improving the performance of the models for prediction, a data processing step was performed on the datasets. In particular, outlier instances were removed from the dataset and the duplicated ones were replaced by an instance which its output was closer to their average. Finally, since the datasets consisted of instances that did not have a normal distribution, the power transformer function was used to transform these instances into a near normality condition [80]. To be more specific, this function uses a series of subfunctions that map each feature of an instance to a near-normal distribution with the mean of zero [81], and this action is known to improve the performance of the ML models to train on a specific dataset [82]. As an example, the distribution of untransformed and transformed values of the output feature for the PTT dataset is presented in Figure 3.2 (a) and (b), showing the change of the distribution to a near normality distribution.

3.2.3 Artificial Neural networks

Artificial Neural Networks (ANNs) are a group of the ML methods that have gained a great deal of attention in the last two decades due to their exceptional power of modeling they provide for problems with multiple parameters that contain highly complex or nonlinear relationships [31,36–38]. These computational advantages are owing to the fact that the ANNs imitate the human brain functions, giving the ability to use these methods in problems that consist of highly complicated relations between their parameters that are not detectable by human understanding [83,84]. In order to exploit the aforementioned abilities of ANNs, various types of ANNs have been developed which fall into two categories of supervised or unsupervised learning. In supervised learning, the features of a dataset are separated into two groups of input and output features and the input features are used to train the model to predict the output of instances. On the other hand, the unsupervised learning uses the input features of the dataset to predict the relationships existing between the instances on its own. Consequently, to evaluate the prediction power of both of these methods, cross-

validation is used which consists of using an unseen dataset to evaluate the accuracy of a trained model [85].

In this work, an ANN algorithm known as multilayer feedforward neural network (MLFFNN), which in previous studies has proven its ability as a universal tool for approximation and prediction, is utilized to predict the PTT and TH of the NiTi based shape memory alloys [86,87]. In this type of neural network, the architecture includes an input layer where data is imported to the network, which is then passed to the hidden layers undergoing respective calculations. In the last layer, the output layer, the calculated values which are the predicted values are compared to the output values from the dataset and the deviation is used as a criterion to evaluate and improve the model's performance. The data flow in this network is in a way that there is no recurrent or backward flow of data, i.e. the data is only fed in the forward direction through the neurons of each layer. In particular, the input data enters the network through the input layer which has the same number of neurons as the features of the input and is passed to the first hidden layer without any change. In the first hidden layer, the input data undergoes a linear operation with a weight matrix which contains the weights related to each neuron of this layer. The resulted vector is then added a bias vector and is processed by an activation function before passing to the next layer and the same process is done for each layer until the output layer. In the output layer, the last vector which is the predicted value is compared with the real output using a cost function and the error is used in a process known as "back propagation" to optimize the neuron weights via an optimizer function to achieve the lowest error and the highest performance in the model. In this process, in order to avoid the model from overfitting the training data and maintaining its ability to predict unseen information, a regularizer function is used to penalize the high variances in the model's weights [40,88,89]. The aforementioned process demonstrates the importance of the architecture and the functions utilized to achieve the most accurate results. Therefore, in this work, the activation function is selected to be the Rectified Linear Unit (ReLU) activation function which has the advantage of being zero centered as well as not saturating and killing the gradient, which makes it a better choice comparing to earlier functions of sigmoid or Tanh [90]. To calculate the error of the predictions, the "mean squared error" (MSE) function with the formula of $MSE = \frac{1}{n}\sum_{i=1}^{n}(Y_i - \widehat{Y}_i)^2$ is selected due to its ability to help the model to avoid substantial error in predicting the outliers and

compatibility with regression problems [91]. To optimize the weights of the neurons based on the MSE, a recently developed optimizer function known as adaptive moment estimation (ADAM) has been used in this work. This function has the advantage of saving the decaying average of the past squared gradients which can improve the performance of the optimizer [92–94]. In order to control the changes of neurons weights and prevent overfitting, the L2 regularizer function that utilizes the square L2 norm of the weights for regularization has been selected [95].

In order to put the aforementioned functions into a framework to train the MLFFNN model, TensorFlow 2.0, a popular artificial neural network framework is selected for this work and to empower its functionality, libraries such as Keras, Pandas, matplotlib and scikit learn has been imported to this framework [80,96–98]. The next step after setting up the framework is to define the architecture and the hyperparameter which determines the effect of the regularizer and in order to do so, the use of empirical methods is necessary [99]. To be more specific, finding the architecture of the network and the regularizer value need to be done through training the model with various architecture and regularizer values and obtaining the best performance from them by choosing the lowest error achieved. However, this method poses problems in cases that the training and testing datasets do not represent the data features uniformly, making the model's predictions biased, thus decreasing the model's performance. Consequently, in addition to shuffling the dataset, "K-fold cross-validation" was utilized to address this issue. In particular, this method separates each dataset into K subsets and trains the model each time on K-1 of them and validates the model with remaining subset and saves the respective error. This validation process is done over all other subsets which finally gives the average error of the training, as the measure to evaluate the suitability of the architecture and regularization parameter [80]. In this work, in order to find the MLFFNN architecture as well as regularized values, 5-fold cross-validation was used for each of the PTT and TH models and the relative results are presented in the Figure 3.3 (a) and (b). The lowest amount of average MSE for the PTT model was achieved as 0.159 by 5-fold cross-validation and 5 hidden layers with 40 neurons and the regularization value of 0.005. These values for the TH model were 5-fold cross-validations and 6 hidden layers with 40 neurons and 0.03 regularization value which gave 0.344 for the average MSE. Therefore, these values were used in the training of the MLFFNN models.

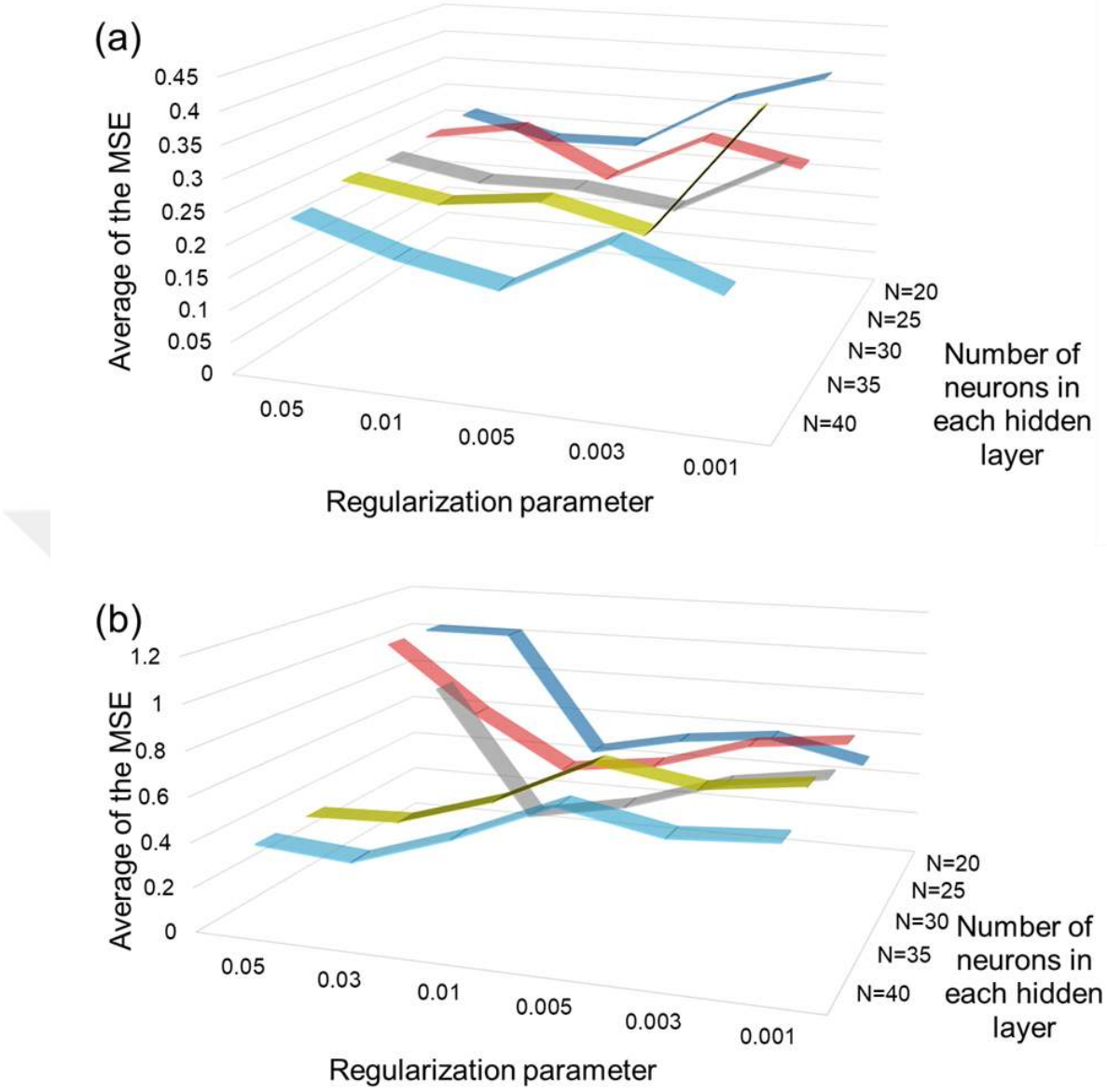

Figure 3.3 Results of 5-fold cross validation for various network size and regularization parameters presenting the average amount of error in terms of MSE for (a) training over PTT dataset (b) training over TH dataset.

3.2.4 Synthetic dataset

In order to find the most suitable chemical composition in terms of high PTTs and low TH response from the alloys, a data pool was constructed as a synthetic dataset with instances made of NiTi-based alloys that their elements range are 44.6 <Ti< 52.1, 0 < Cu < 32, 0 < Fe < 4.6, 0 < Pd < 50 with balance amount of Ni and variation increments of 0.5%. The above ranges were selected to be within the range of the data available inside the training dataset to increase the accuracy. The resulting dataset

included 600,000 instances which then the concentration of valence electrons and mixing entropy were calculated and added for each of the instances as additional features. This synthetic dataset was imported to both PTT and TH model and the predicted values were used for further evaluations.

3.2.5 Desirability approach

In order to find the chemical composition with the highest possible PTT and lowest TH systematically, it is necessary to use a mathematical method to prevent bias and error added to the selection. Therefore, a statistically based approach known as the "Desirability approach" is utilized in this work. This approach is used for optimization problems with multiple responses. In particular, for an input of X_i which undergoes the function of $f(X_i)$ with an output response of Y_i, a "Desirability function" is defined as $d_i(Y_i)$ that represents the closeness of a response to the best possible value. To assess the overall acceptance of instances with multiple responses, a function called overall desirability is defined as $D = (d_1(Y_1)d_2(Y_2) \dots d_i(Y_i))^{1/k}$ which its answer ranges from 0 to 1, respectively for the worst combination of input to the best one [100,101]. In this work, the best results of the desirability approach were chosen for further investigations.

3.3 Results and Discussion

The learning curves resulted from the training of the PTT model on the respective dataset have been provided in Figure 3.4. The training curve in this figure converges to the MSE value of 0.014 which is a sign that the model was able to learn the training data and fit properly to it. In addition, to understand the ability of the model to predict the unseen data, the validation curve is depicted that shows the convergence to the MSE value of 0.081 which is a sign for the ability of the model to be able to predict new instances as well as not overfitting the data. Similar learning curves have been presented in Figure 3.5 for the training of the TH model. In this model, the training curve converged to the MSE value of 0.170 and the validation value converges to 0.175, which shows the model fits the training dataset. Notably, the difference between the MSE values of these two models is coming from the fact that their respective dataset contains different ranges of values as output as well as the possible different quality of

the experimental work. In addition, to visualize the performance of the PTT and TH Model, Figure 3.6 and Figure 3.7 are presented as the performance diagrams of the models. In the performance diagrams, the training and test data are plotted with respect to the vertical axis which represents the predicted values and the horizontal axis which represents the actual experimental values from the dataset. Therefore, if an instance sits on the X=Y line, its predicted value is equal to the experimental value and the deviation from this line presents the error. Figure 3.6 and Figure 3.7 represent the fact that both models converge to the X=Y line. However, to further illustrate the success of the models, 10 instances which had the least absolute error are tabulated in Table 3.1 and Table 3.2 for the PTT and TH model to make the comparison of the actual and predicted values possible.

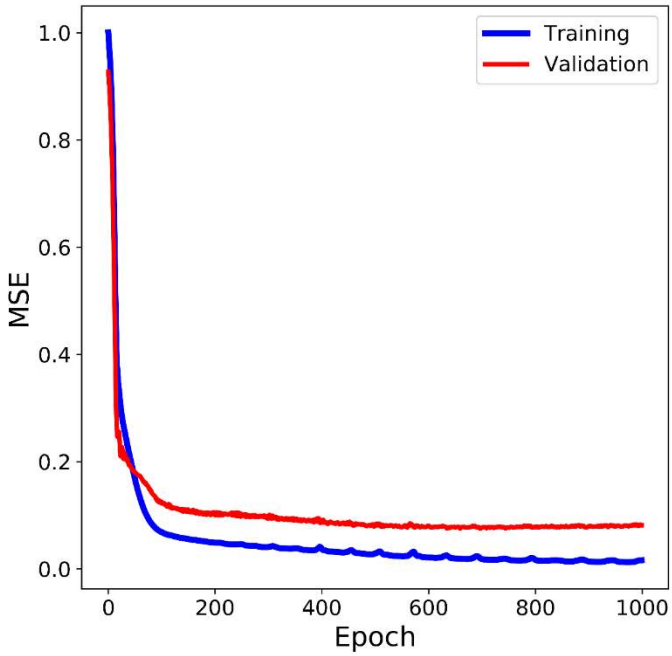

Figure 3.4 Learning Curves for the best PTT model including the training and cross validation curves for 1000 iterations (Epochs).

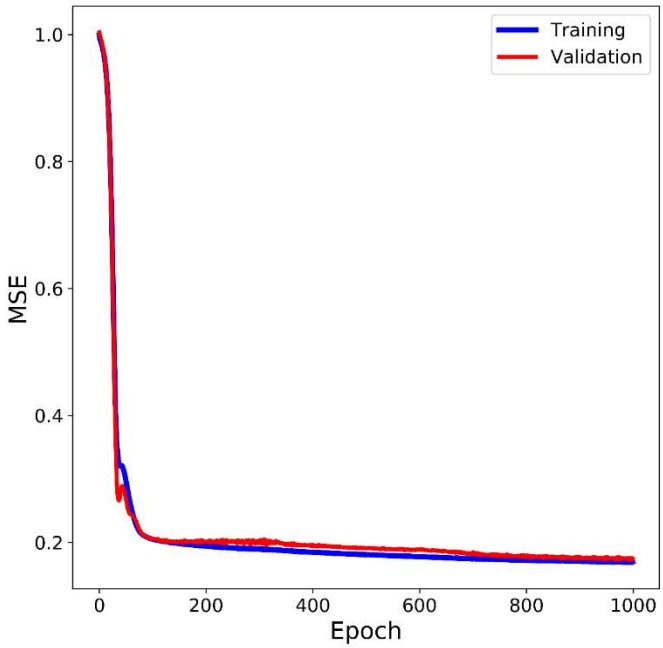

Figure 3.5 Learning Curves for the best TH model including the training and cross validation curves for 1000 iterations (Epochs).

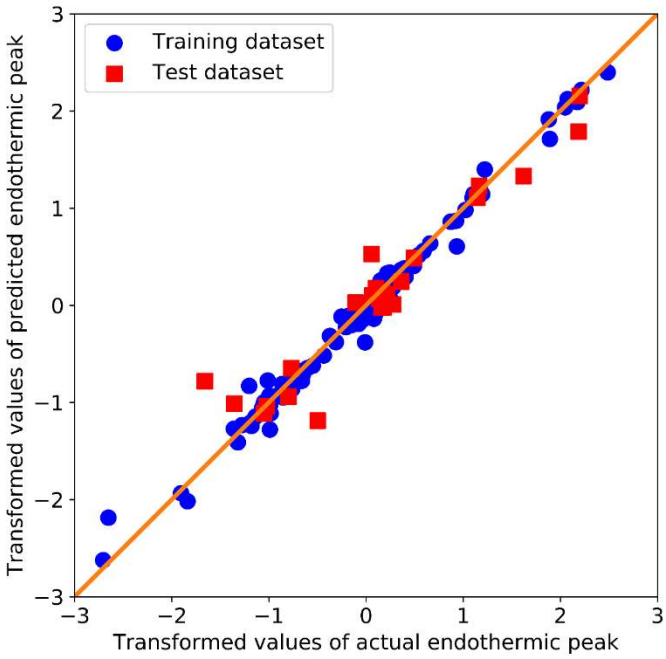

Figure 3.6 Performance diagram of the model presenting the transformed values of predicted endothermic peak in comparison with the actual values reported in the literature.

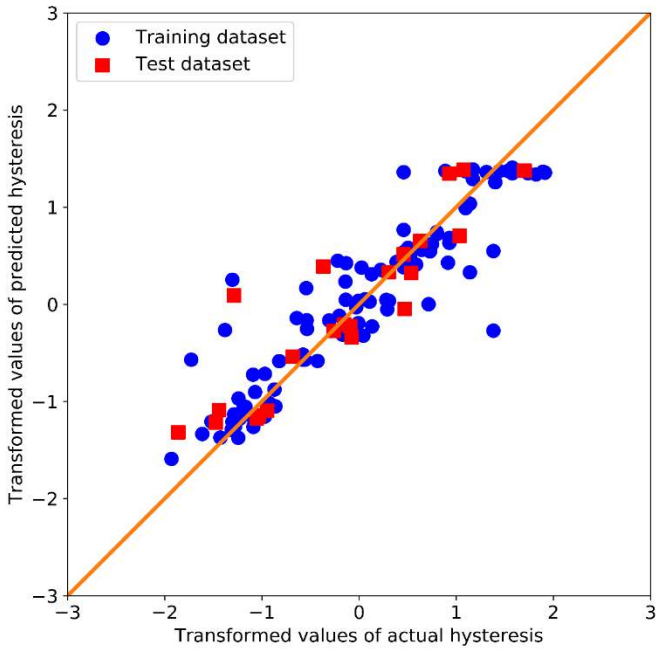

Figure 3.7 Performance diagram of the model presenting the transformed values of thermal hysteresis in comparison with the actual values reported in the literature.

Table 3.1 Comparision of predicted PTT value vs the actual experimental value

Ni	Ti	Cu	Fe	Pd	Entropy	cv	Predicted values	Real Values	MAE
50.3	49.7	0	0	0	0.693129	0.280518	36.41257	53.1	16.68743
43.6	50	3	3.4	0	0.928667	0.278904	-37.0651	-31.27	5.795075
5	50	0	0	45	0.855689	0.21148	493.8547	506	12.14526
33.5	50	12.5	0	4	1.101623	0.275682	28.84954	40.45	11.60046
45	50	5	0	0	0.855689	0.281437	20.28697	64	43.71303
13	51	0	0	36	0.976429	0.220878	287.1169	358.5	71.3831
50.5	49.5	0	0	0	0.693097	0.280863	23.3992	45.47	22.0708
42.8	50	4	3.2	0	0.948688	0.279308	-44.018	-41.59	2.427994
35	50	12	0	3	1.07364	0.277475	15.84401	47.7	31.85599
19.4	50.6	0	0	30	1.024028	0.229351	235.5951	244.6	9.00488

Table 3.2 Comparision of predicted Hysteresis value vs the actual experimental value

Ni	Ti	Cu	Fe	Pd	Entropy	cv	Predicted values	Real Values	MAE
18	52	30	0	0	1.0099	0.2851	7.612029	7.7	0.087971
40	50	10	0	0	0.9433	0.2829	13.24858	13	0.248582
19.4	50.6	0	0	30	1.024	0.2294	18.09843	17.75	0.348433
50	45.8	0	4.2	0	0.8374	0.2848	3.534879	3.92	0.385121
50	43.9	2	4	0.1	0.9219	0.2885	3.437837	3.83	0.392163
19	51	30	0	0	1.0201	0.2868	8.101246	8.5	0.398754
50	46	0	4	0	0.8325	0.2846	3.696513	4.21	0.513487
50	46.8	0.9	2	0.3	0.84	0.284	3.313548	2.64	0.673548
50	34	10	0	6	1.1124	0.297	6.019127	5.32	0.699127
41.4	48.6	10	0	0	0.946	0.2853	15.80433	15	0.804331

In order to utilize the trained models to find the most suitable chemical composition in terms of PTT and TH, the synthetic dataset was imported to these models and the PTT and TH value regarding each instance were predicted, resulting in a dataset with 7 inputs and 2 outputs. To find the optimum value for the highest PTT and lowest TH among the approximately 600,000 possible compositions, the desirability method is implemented on the dataset converting the PTT and TH value to a desirability value for each of the outputs and the overall desirability was calculated from these values for each instance. Finally, the chemical composition with the highest overall desirability was selected as the material of choice for manufacturing and further analysis. This composition includes 17% Ni, 44.5% Ti, 17% Cu, 4.5% Fe and 17% Pd

and the model predicted the PTT as 685.7 C and the TH of 2.26 C. These values could satisfy 0.98 and 0.94 of the desirability of PTT and TH which resulted in overall desirability of 0.97.

3.4 Conclusions

This study represents the application of a multilayer feedforward neural network (MLFFNN) as the ML method to develop two models that predict the phase transformation temperatures (PTTs) and thermal hysteresis (TH) of multicomponent NiTi based shape memory alloys (SMAs). In particular, using two separate datasets acquired from the available literature on the internet, two models were developed to predict a representative PTT value and TH of the NiTi based SMAs with the addition of Cu, Fe, and Pd as alloying elements. Subsequently, the models were used to predict the PTT and TH values for a wide range of synthetic instances. The predicted values for each model were scored using the desirability function to find the optimum chemical composition. The chemical composition with the highest desirability score for both PTTs and TH was selected as the optimum composition for further investigations.

3.5 References

[1] T.W. Duerig, K.N. Melton, Engineering Aspects of Shape Memory Alloys, 1990. https://doi.org/10.1016/c2013-0-04566-5.

[2] E.T.F. Chau, C.M. Friend, D.M. Allen, J. Hora, J.R. Webster, A technical and economic appraisal of shape memory alloys for aerospace applications, Mater. Sci. Eng. A. 438–440 (2006) 589–592. https://doi.org/10.1016/j.msea.2006.02.201.

[3] D.J. Hartl, D.C. Lagoudas, Aerospace applications of shape memory alloys, Proc. Inst. Mech. Eng. Part G J. Aerosp. Eng. 221 (2007) 535–552. https://doi.org/10.1243/09544100JAERO211.

[4] C. Velmurugan, V. Senthilkumar, S. Dinesh, D. Arulkirubakaran, Review on phase transformation behavior of NiTi shape memory alloys, Mater. Today Proc. 5 (2018) 14597–14606. https://doi.org/10.1016/J.MATPR.2018.03.051.

[5] R. Lahoz, L. Gracia-Villa, J.A. Puértolas, Training of the two-way shape memory effect by bending in NiTi alloys, J. Eng. Mater. Technol. Trans. ASME. 124 (2002) 397–401. https://doi.org/10.1115/1.1495001.

[6] Z. Balak, S.M. Abbasi, Influence of the Ti content, training cycles and pre-strain on the two-way shape memory effect in NiTi alloys, Elsevier, 2011. https://doi.org/10.1016/j.matdes.2011.03.036.

[7] K.C. Atli, I. Karaman, R.D. Noebe, D. Gaydosh, The effect of training on two-way shape memory effect of binary NiTi and NiTi based ternary high temperature shape memory alloys, Elsevier, 2013. https://doi.org/10.1016/j.msea.2012.10.009.

[8] S. Sanjabi, Y.Z. Cao, Z.H. Barber, Multi-target sputter deposition of Ni50Ti 50 - XHfx shape memory thin films for high temperature microactuator application, Sensors Actuators, A Phys. 121 (2005) 543–548. https://doi.org/10.1016/j.sna.2005.04.006.

[9] K.-H.H. Wu, Y.Q. Liu, M.J. Maich, ..., H.-K. Tseng, Mechanical properties of a NiTi-Pd high-temperature shape memory alloy, Smart Struct. …. 2189 (1994) 306–313. https://doi.org/10.1117/12.174068.

[10] K.C. Atli, I. Karaman, R.D. Noebe, G. Bigelow, D. Gaydosh, Work production using the two-way shape memory effect in NiTi and a Ni-rich NiTiHf high-temperature shape memory alloy, Smart Mater. Struct. 24 (2015) 125023. https://doi.org/10.1088/0964-1726/24/12/125023.

[11] Z.J. Pu, H.-K. Tseng, K.-H. Wu, Martensite transformation and shape memory effect of NiTi-Zr high-temperature shape memory alloys, in: A.P. Jardine (Ed.), Smart Struct. Mater. 1995 Smart Mater., SPIE, 1995: pp. 171–178. https://doi.org/10.1117/12.209815.

[12] X.B. Ren, K. Otsuka, Why Does the Martensitic Transformation Temperature Strongly Depend on Composition?, Mater. Sci. Forum. 327–328 (2000) 429–432. https://doi.org/10.4028/www.scientific.net/MSF.327-328.429.

[13] K. V. Ramaiah, C.N. Saikrishna, M. Sujata, M. Madan, S.K. Bhaumik, NiTiPt shape memory alloy: microstructure and transformation behaviour, ISSS J. Micro Smart Syst. 8 (2019) 81–88. https://doi.org/10.1007/s41683-019-00039-9.

[14] Y. Yamabe-Mitarai, R. Arockiakumar, A. Wadood, K.S. Suresh, T. Kitashima, T. Hara, M. Shimojo, W. Tasaki, M. Takahashi, S. Takahashi, H. Hosoda, Ti(Pt, Pd, Au) based high temperature shape memory alloys, Mater. Today Proc. 2 (2015) S517–S522. https://doi.org/10.1016/j.matpr.2015.07.338.

[15] P. Olier, J.C. Brachet, J.L. Bechade, C. Foucher, G. Guénin, Investigation of Transformation Temperatures, Microstructure and Shape Memory Properties of NiTi, NiTiZr and NiTiHf Alloys, J. Phys. IV. 05 (1995) C8-741-C8-746.

https://doi.org/10.1051/jp4/199558741.

[16] H. Sehitoglu, Y. Wu, L. Patriarca, G. Li, A. Ojha, S. Zhang, Y. Chumlyakov, M. Nishida, Superelasticity and Shape Memory Behavior of NiTiHf Alloys, Shape Mem. Superelasticity. 3 (2017) 168–187. https://doi.org/10.1007/s40830-017-0108-1.

[17] Y. Zhou, D. Xue, X. Ding, K. Otsuka, J. Sun, X. Ren, High temperature strain glass transition in defect doped Ti-Pd martensitic alloys, Phys. Status Solidi. 251 (2014) 2027–2033. https://doi.org/10.1002/pssb.201350360.

[18] O. Karakoc, C. Hayrettin, A. Evirgen, R. Santamarta, D. Canadinc, R.W. Wheeler, S.J. Wang, D.C. Lagoudas, I. Karaman, Role of microstructure on the actuation fatigue performance of Ni-Rich NiTiHf high temperature shape memory alloys, Acta Mater. 175 (2019) 107–120. https://doi.org/10.1016/j.actamat.2019.05.051.

[19] O. Karakoc, C. Hayrettin, D. Canadinc, I. Karaman, Role of applied stress level on the actuation fatigue behavior of NiTiHf high temperature shape memory alloys, Acta Mater. 153 (2018) 156–168. https://doi.org/10.1016/j.actamat.2018.04.021.

[20] D. Canadinc, W. Trehern, J. Ma, I. Karaman, F. Sun, Z. Chaudhry, Ultra-high temperature multi-component shape memory alloys, Scr. Mater. 158 (2019) 83–87. https://doi.org/10.1016/j.scriptamat.2018.08.019.

[21] H. Zheng, J. Pfetzing, J. Frenzel, G. Eggeler, Nanoindentation of Ti50Ni48Fe2 and Ti 50Ni40Cu10 shape memory alloys, Int. J. Mater. Res. 100 (2009) 594–602. https://doi.org/10.3139/146.110074.

[22] Y. Zhou, D. Xue, X. Ding, Y. Wang, J. Zhang, Z. Zhang, D. Wang, K. Otsuka, J. Sun, X. Ren, Strain glass in doped Ti50(Ni50-xD x) (D = Co, Cr, Mn) alloys: Implication for the generality of strain glass in defect-containing ferroelastic systems, Acta Mater. 58 (2010) 5433–5442. https://doi.org/10.1016/j.actamat.2010.06.019.

[23] J. Frenzel, A. Wieczorek, I. Opahle, B. Maaß, R. Drautz, G. Eggeler, On the effect of alloy composition on martensite start temperatures and latent heats in Ni-Ti-based shape memory alloys, Acta Mater. 90 (2015) 213–231. https://doi.org/10.1016/j.actamat.2015.02.029.

[24] J. Ortín, L. Delaey, Hysteresis in shape-memory alloys, Int. J. Non. Linear. Mech. 37 (2002) 1275–1281. https://doi.org/10.1016/S0020-7462(02)00027-6.

[25] R. Zarnetta, R. Takahashi, M.L. Young, A. Savan, Y. Furuya, S. Thienhaus, B. Maaß, M. Rahim, J. Frenzel, H. Brunken, Y.S. Chu, V. Srivastava, R.D. James, I. Takeuchi, G. Eggeler, A. Ludwig, Identification of quaternary shape memory alloys

with near-zero thermal hysteresis and unprecedented functional stability, Adv. Funct. Mater. 20 (2010) 1917–1923. https://doi.org/10.1002/adfm.200902336.

[26] Y. Wang, D. Wang, S. Hou, Y. Wang, X. Ding, S. Ren, X. Ren, Superelasticity of slim hysteresis over a wide temperature range by nanodomains of martensite, Acta Mater. 66 (2014) 349–359. https://doi.org/10.1016/j.actamat.2013.11.022.

[27] D. Xue, D. Xue, R. Yuan, Y. Zhou, P. V. Balachandran, X. Ding, J. Sun, T. Lookman, An informatics approach to transformation temperatures of NiTi-based shape memory alloys, Acta Mater. 125 (2017) 532–541. https://doi.org/10.1016/j.actamat.2016.12.009.

[28] D.D. Xue, P. V. Balachandran, J. Hogden, J. Theiler, D.D. Xue, T. Lookman, Accelerated search for materials with targeted properties by adaptive design, Nat. Commun. 7 (2016) 11241. https://doi.org/10.1038/ncomms11241.

[29] T. Kostiuchenko, F. Körmann, J. Neugebauer, A. Shapeev, Impact of local lattice relaxations on phase stability and chemical ordering in bcc NbMoTaW high-entropy alloys explored by ab initio based machine-learning potentials, Npj Comput. Mater. (2018) 1–7. https://doi.org/10.1038/s41524-019-0195-y.

[30] Y.J. Chang, C.Y. Jui, W.J. Lee, A.C. Yeh, Prediction of the Composition and Hardness of High-Entropy Alloys by Machine Learning, Jom. 71 (2019) 3433–3442. https://doi.org/10.1007/s11837-019-03704-4.

[31] Y. Zhang, C. Wen, C. Wang, S. Antonov, D. Xue, Y. Bai, Y. Su, Phase prediction in high entropy alloys with a rational selection of materials descriptors and machine learning models, Acta Mater. 185 (2019) 528–539. https://doi.org/10.1016/j.actamat.2019.11.067.

[32] X. Jiang, H.-Q. Yin, C. Zhang, R.-J. Zhang, K.-Q. Zhang, Z.-H. Deng, G. Liu, X. Qu, An materials informatics approach to Ni-based single crystal superalloys lattice misfit prediction, Comput. Mater. Sci. 143 (2018) 295–300. https://doi.org/10.1016/J.COMMATSCI.2017.09.061.

[33] E. Fathalla, Y. Tanaka, K. Maekawa, Remaining fatigue life assessment of in-service road bridge decks based upon artificial neural networks, (2018). https://doi.org/10.1016/j.engstruct.2018.05.122.

[34] Y. Zhang, A. Lunghi, S. Sanvito, Pushing the limits of atomistic simulations towards ultra-high temperature: A machine-learning force field for ZrB2: Machine-learning towards ultra-high temeprature simulation of ZrB2, Acta Mater. 186 (2020)

467–474. https://doi.org/10.1016/j.actamat.2019.12.060.

[35] A. Solomou, G. Zhao, S. Boluki, J.K. Joy, X. Qian, I. Karaman, R. Arróyave, D.C. Lagoudas, Multi-objective Bayesian materials discovery: Application on the discovery of precipitation strengthened NiTi shape memory alloys through micromechanical modeling, Mater. Des. 160 (2018) 810–827. https://doi.org/10.1016/J.MATDES.2018.10.014.

[36] J. Ling, E. Antono, S. Bajaj, S. Paradiso, M. Hutchinson, B. Meredig, B.M. Gibbons, Machine Learning for Alloy Composition and Process Optimization, in: Vol. 6 Ceram. Control. Diagnostics, Instrumentation; Educ. Manuf. Mater. Metall., American Society of Mechanical Engineers, 2018. https://doi.org/10.1115/GT2018-75207.

[37] W. Huang, P. Martin, H.L. Zhuang, Machine-learning phase prediction of high-entropy alloys, Acta Mater. 169 (2019) 225–236. https://doi.org/10.1016/j.actamat.2019.03.012.

[38] C. Wen, Y. Zhang, C. Wang, D. Xue, Y. Bai, S. Antonov, L. Dai, T. Lookman, Y. Su, Machine learning assisted design of high entropy alloys with desired property, Acta Mater. 170 (2019) 109–117. https://doi.org/10.1016/j.actamat.2019.03.010.

[39] K.P. Murphy, Machine learning: a probabilistic perspective, MIT press, 2012.

[40] E. Alpaydin, Introduction to machine learning, MIT Press Ltd, 2020.

[41] Y. Yang, D. Xue, R. Yuan, Y. Zhou, T. Lookman, X. Ding, X. Ren, J. Sun, Doping effects of point defects in shape memory alloys, Acta Mater. 176 (2019) 177–188. https://doi.org/10.1016/j.actamat.2019.06.031.

[42] B.D. Conduit, N.G. Jones, H.J. Stone, G.J. Conduit, Probabilistic design of a molybdenum-base alloy using a neural network, Scr. Mater. 146 (2018) 82–86. https://doi.org/10.1016/j.scriptamat.2017.11.008.

[43] Q. Tian, J. Wu, Tensile behavior of Ti50. 6Pd30Ni19. 4 alloy under different tensile conditions, Mater. Sci. Eng. A. (2002). https://www.sciencedirect.com/science/article/pii/S0921509301014721.

[44] Y. Xu, S. Shimizu, Y. Suzuki, K. Otsuka, T. Ueki, K. Mitose, Recovery and recrystallization processes in Ti-Pd-Ni high-temperature shape memory alloys, Acta Mater. (1997). https://www.sciencedirect.com/science/article/pii/S1359645496002674.

[45] L. Xuemin, T.Y. Hsu, In situ study of phase transformations in a 50.8 at.% Ni-Ti alloy, Metallography. (1987).

https://www.sciencedirect.com/science/article/pii/0026080087900644.

[46] L. Jordan, K. Goubaa, M. Masse, G. Bouquet, Comparative Study Of Mechanical Properties Of Various Ni-Ti Based Shape Memory Alloys In View Of Dental And Medical Applications, Le J. Phys. IV. 01 (1991) C4-139-C4-144. https://doi.org/10.1051/jp4:1991421.

[47] T.H. Nam, T. Saburi, K. Shimizu, Cu-Content Dependence of Shape Memory Characteristics in Ti-Ni-Cu Alloys, Mater. Trans. JIM. 31 (1990) 959–967. https://doi.org/10.2320/matertrans1989.31.959.

[48] S.K. Gong, S. Hu, H. Bin Xu, Recrystallization of $Ti_{51}Ni_{13}Pd_{36}$ High Temperature Shape Memory Alloys, Mater. Sci. Forum. 327–328 (2000) 283–286. https://doi.org/10.4028/www.scientific.net/MSF.327-328.283.

[49] W. Cai, K. Otsuka, M. Asai, Martensite Aging Effect in Ti-Pd and Ti-Pd-Ni High Temperature Shape Memory Alloys, Mater. Trans. JIM. 40 (1999) 895–898. https://doi.org/10.2320/matertrans1989.40.895.

[50] Y.C. Lo, S.K. Wu, H.E. Horng, A study of B2↔B19↔B19′ two-stage martensitic transformation in a Ti50Ni40Cu10 alloy, Acta Metall. Mater. 41 (1993) 747–759. https://doi.org/10.1016/0956-7151(93)90007-F.

[51] J.F. Smith, Q. Jiang, R. Lčk, B. Predel, Cp and fractal phase transformation in the shape memory alloy Ni52Ti, Mater. Sci. Eng. A. 149 (1991) 111–120. https://doi.org/10.1016/0921-5093(91)90792-L.

[52] S. Bakhtiari, NiTi-based Shape Memory Alloys beyond The Shape Memory Effect and Superelasticity, University of Western Australia, 2019.

[53] M.J. Bigeon, M. Morin, Fatigue of the shape memory effect in thin wires-comparison between TiNi and CuZnAL, Le J. Phys. IV. (1995). https://jp4.journaldephysique.org/articles/jp4/abs/1995/02/jp4199505C259/jp4199505C259.html.

[54] H. Li, X. Meng, W. Cai, Shape memory behaviors in a Ti50Ni33.5Cu12.5Pd4 alloy with near-zero thermal hysteresis, J. Alloys Compd. 765 (2018) 166–170. https://doi.org/10.1016/j.jallcom.2018.06.205.

[55] H. Shahmir, M. Nili-Ahmadabadi, C.T. Wang, J.M. Jung, H.S. Kim, T.G. Langdon, Annealing behavior and shape memory effect in NiTi alloy processed by equal-channel angular pressing at room temperature, Mater. Sci. Eng. A. 629 (2015) 16–22. https://doi.org/10.1016/j.msea.2015.01.072.

[56] K. V. Ramaiah, C.N. Saikrishna, Gouthama, S.K. Bhaumik, Microstructure and transformation behavior of Ni24.7Ti50.3Pd25 high temperature shape-memory alloy with Sc micro-addition, Mater. Charact. 106 (2015) 36–43. https://doi.org/10.1016/j.matchar.2015.05.018.

[57] S. Belyaev, N. Resnina, R. Zhuravlev, Work production and variation in shape memory effects during thermal cycling of equiatomic TiNi alloy, in: J. Mater. Eng. Perform., Springer New York LLC, 2014: pp. 2343–2346. https://doi.org/10.1007/s11665-014-0984-x.

[58] Y.W. Kim, H.J. Kim, T.H. Nam, Martensitic transformation behaviors of Ti49+xNi 21-xCu30 (x=0,1,2,3) shape memory alloy strips, in: Phys. Scr. T, 2010: p. 014023. https://doi.org/10.1088/0031-8949/2010/T139/014023.

[59] B. Kockar, K.C. Atli, J. Ma, M. Haouaoui, I. Karaman, M. Nagasako, R. Kainuma, Role of severe plastic deformation on the cyclic reversibility of a Ti 50.3Ni33.7Pd16 high temperature shape memory alloy, Acta Mater. 58 (2010) 6411–6420. https://doi.org/10.1016/j.actamat.2010.08.003.

[60] Y. Chen, H.C. Jiang, S.W. Liu, L.J. Rong, X.Q. Zhao, Damping capacity of TiNi-based shape memory alloys, J. Alloys Compd. 482 (2009) 151–154. https://doi.org/10.1016/j.jallcom.2009.03.148.

[61] X.M. Wang, Z.F. Yue, Experimental and FEM Analysis of the Fracture Behavior in NiTi Shape Memory Alloys, Key Eng. Mater. 324–325 (2006) 919–922. https://doi.org/10.4028/www.scientific.net/kem.324-325.919.

[62] G. Mazzolai, A. Biscarini, B. Coluzzi, F.M. Mazzolai, U. Straube, Diffusion of Hydrogen in the $Ni_{30}Ti_{50}Cu_{20}$ Shape Memory Alloy, Solid State Phenom. 115 (2006) 51–56. https://doi.org/10.4028/www.scientific.net/ssp.115.51.

[63] G. Cheng, Effects of Cu content and heat treatment on the transformation behaviour and shape memory property of Ti-Ni-Cu alloys, Nanyang Technological University, 2006. https://doi.org/10.32657/10356/5087.

[64] Y. Li, Y. Jin, R. Yu, Empirical Relationship Between Recoverable Strain Energy and Temperature for TiNi and TiNiCu Alloys, Acta Metall. Sin. (1992).

[65] F.S. Liu, Y. Qian, H. Bin Xu, The Dynamic Impact Behavior of $Ti_{50}Ni_{47}Fe_3$ Shape Memory Alloys, Mater. Sci. Forum. 475–479 (2005) 1969–1972. https://doi.org/10.4028/www.scientific.net/msf.475-479.1969.

[66] H. Miyamoto, T. Taniwaki, T. Ohba, K. Otsuka, S. Nishigori, K. Kato, Two-

stage B2-B19-B19′ martensitic transformation in a Ti 50Ni30Cu20 alloy observed by synchrotron radiation, Scr. Mater. 53 (2005) 171–175. https://doi.org/10.1016/j.scriptamat.2005.03.044.

[67] M. Hosogi, N. Okabe, T. Sakuma, S. Miyazaki, Effects of Cold Working and Heat Treatment on Transformation Temperature of Ti-41.7Ni-8.5Cu (at%) Shape Memory Alloy and Its Probabilistic Prediction, 2003.

[68] Q. Tian, J. Wu, Characterisation of phase transformation in Ti50+xPd30Ni20-x alloys, Intermetallics. 10 (2002) 675–682. https://doi.org/10.1016/S0966-9795(02)00048-1.

[69] P. Bassani, S. Besseghini, NiTiCu shape memory alloy : Superplastic elongation during thermal cycling, Le J. Phys. IV. 11 (2001) Pr8-381-Pr8-386. https://doi.org/10.1051/jp4:2001864.

[70] W. Cai, S. Tanaka, K. Otsuka, Thermal Cyclic Characteristics under Load in a $Ti_{50.6}Pd_{30}Ni_{19.4}$ Alloy, Mater. Sci. Forum. 327–328 (2000) 279–282. https://doi.org/10.4028/www.scientific.net/msf.327-328.279.

[71] Y. Shirakawa, Y. Morizono, M. Nishida, New Precipitate Phase in Pd and Ni Rich Ti-Pd-Ni Shape Memory Alloys, Mater. Sci. Forum. 327–328 (2000) 171–174. https://doi.org/10.4028/www.scientific.net/MSF.327-328.171.

[72] A. Biscarini, B. Coluzzi, G. Mazzolai, A. Tuissi, ..., Extraordinary high damping of hydrogen-doped NiTi and NiTiCu shape memory alloys, J. Alloy. …. (2003). https://www.sciencedirect.com/science/article/pii/S0925838803002676.

[73] L. Sun, K.-H. Wu, Two-way memory effect (TWME) in NiTi-Pd high-temperature shape memory alloys, in: V.K. Varadan (Ed.), Smart Struct. Mater., spiedigitallibrary.org, 1994: pp. 298–305. https://doi.org/10.1117/12.174067.

[74] D.B. Chernov, Y.U.I. Paskal, V.E. Gyunter, L. Monasevich, Structure Transformation Diagrams of Alloys Based on Titanium Nickelide and the Effects of Shape Memory, Izv. VUZ Fiz. (1981).

[75] D. Vokoun, P. Šittner, R. Stalmans, Study of the effect of curing treatment in fabrication of SMA/polymer composites on deformational behavior of NiTi–5at.% Cu SMA wires, Scr. Mater. (2003). https://www.sciencedirect.com/science/article/pii/S1359646202004633.

[76] V.A. Antonov, Y.A.. . Sykovsky, A.I. Larkin, A. V. Shelyakov, Elements Of Optical Processors Based On Shape Memory Effect, in: Y.N. Denisyuk, T.H. Jeong

(Eds.), Hologr. …, spiedigitallibrary.org, 1990: p. 20. https://doi.org/10.1117/12.963791.

[77] N. Islam, W. Huang, H.L. Zhuang, Machine learning for phase selection in multi-principal element alloys, Comput. Mater. Sci. 150 (2018) 230–235. https://doi.org/10.1016/j.commatsci.2018.04.003.

[78] M. Zarinejad, Y. Liu, Dependence of Transformation Temperatures of NiTi-based Shape-Memory Alloys on the Number and Concentration of Valence Electrons, Adv. Funct. Mater. 18 (2008) 2789–2794. https://doi.org/10.1002/adfm.200701423.

[79] D.B. Miracle, O.N. Senkov, A critical review of high entropy alloys and related concepts, Acta Mater. 122 (2017) 448–511. https://doi.org/10.1016/j.actamat.2016.08.081.

[80] F. Pedregosa, G. Varoquaux, A. Gramfort, V. Michel, B. Thirion, O. Grisel, M. Blondel, P. Prettenhofer, R. Weiss, V. Dubourg, Scikit-learn: Machine learning in Python, J. Mach. Learn. Res. 12 (2011) 2825–2830.

[81] I.-K.I. Yeo, R.A. Johnson, A new family of power transformations to improve normality or symmetry, Biometrika. 87 (2000) 954–959. https://doi.org/10.1093/biomet/87.4.954.

[82] W.A. Yousef, Prudence when assuming normality: An advice for machine learning practitioners, Pattern Recognit. Lett. 138 (2020) 44–50. https://doi.org/10.1016/j.patrec.2020.06.026.

[83] S. Haykin, Neural Networks and Learning Machines, 2008. https://doi.org/978-0131471399.

[84] C.M. Bishop, Neural networks for pattern recognition, Oxford university press, 1995.

[85] H.B. Barlow, Unsupervised Learning, Neural Comput. 1 (1989) 295–311. https://doi.org/10.1162/neco.1989.1.3.295.

[86] C. Lin, Face detection by color and multilayer feedforward neural network, in: ICIA 2005 - Proc. 2005 Int. Conf. Inf. Acquis., 2005: pp. 518–523. https://doi.org/10.1109/icia.2005.1635143.

[87] D.L. Millar, P.A. Calderbank, On the investigation of a multilayer feedforward neural network model of rock deformability behaviour, in: 8th ISRM Congr., International Society for Rock Mechanics and Rock Engineering, 1995: pp. 933–938.

[88] K. Hornik, M. Stinchcombe, H. White, Multilayer feedforward networks are

universal approximators, Neural Networks. 2 (1989) 359–366. https://doi.org/10.1016/0893-6080(89)90020-8.

[89] D. Svozil, V. Kvasnička, J. Pospíchal, Introduction to multi-layer feed-forward neural networks, in: Chemom. Intell. Lab. Syst., Elsevier, 1997: pp. 43–62. https://doi.org/10.1016/S0169-7439(97)00061-0.

[90] A.F. Agarap, Deep Learning using Rectified Linear Units (ReLU), ArXiv Prepr. ArXiv1803.08375. (2018). http://arxiv.org/abs/1803.08375.

[91] S. Theodoridis, Mean-Square Error Linear Estimation, Elsevier, 2015. https://doi.org/10.1016/b978-0-12-801522-3.00004-5.

[92] S.J. Reddi, S. Kale, S. Kumar, On the Convergence of Adam and Beyond, (2019). http://arxiv.org/abs/1904.09237.

[93] P.T. Tran, L.T. Phong, On the Convergence Proof of AMSGrad and a New Version, IEEE Access. 7 (2019) 61706–61716. https://doi.org/10.1109/ACCESS.2019.2916341.

[94] D.P. Kingma, J.L. Ba, Adam: A method for stochastic optimization, in: 3rd Int. Conf. Learn. Represent. ICLR 2015 - Conf. Track Proc., International Conference on Learning Representations, ICLR, 2015. https://arxiv.org/abs/1412.6980v9 (accessed July 20, 2020).

[95] C. Cortes, M. Mohri, A. Rostamizadeh, L2 Regularization for Learning Kernels, Proc. 25th Conf. Uncertain. Artif. Intell. UAI 2009. (2012) 109–116. http://arxiv.org/abs/1205.2653 (accessed July 22, 2020).

[96] J.D. Hunter, Matplotlib: A 2D Graphics Environment, Comput. Sci. Eng. 9 (2007) 90–95. https://doi.org/10.1109/MCSE.2007.55.

[97] W. McKinney, Data Structures for Statistical Computing in Python, in: 2010: pp. 56–61. https://doi.org/10.25080/Majora-92bf1922-00a.

[98] M. Abadi, A. Agarwal, P. Barham, E. Brevdo, Z. Chen, C. Citro, G.S. Corrado, A. Davis, J. Dean, M. Devin, S. Ghemawat, I. Goodfellow, A. Harp, G. Irving, M. Isard, Y. Jia, R. Jozefowicz, L. Kaiser, M. Kudlur, J. Levenberg, D. Mane, R. Monga, S. Moore, D. Murray, C. Olah, M. Schuster, J. Shlens, B. Steiner, I. Sutskever, K. Talwar, P. Tucker, V. Vanhoucke, V. Vasudevan, F. Viegas, O. Vinyals, P. Warden, M. Wattenberg, M. Wicke, Y. Yu, X. Zheng, M. Rucci, A. Casile, TensorFlow: Large-Scale Machine Learning on Heterogeneous Distributed Systems, ArXiv Prepr. ArXiv1603.04467. 16 (2016) 121–138. https://doi.org/10.1080/09548980500300507.

[99] Y. Bengio, Practical recommendations for gradient-based training of deep architectures, Lect. Notes Comput. Sci. (Including Subser. Lect. Notes Artif. Intell. Lect. Notes Bioinformatics). 7700 LECTU (2012) 437–478. https://doi.org/10.1007/978-3-642-35289-8-26.

[100] N.R. Costa, J. Lourenço, Z.L. Pereira, Desirability function approach: A review and performance evaluation in adverse conditions, Chemom. Intell. Lab. Syst. 107 (2011) 234–244. https://doi.org/10.1016/j.chemolab.2011.04.004.

[101] I.J. Jeong, K.J. Kim, An interactive desirability function method to multiresponse optimization, Eur. J. Oper. Res. 195 (2009) 412–426. https://doi.org/10.1016/j.ejor.2008.02.018.

Chapter 4:
CONCLUSIONS AND FUTURE WORK

Artificial intelligence and machine learning methods have been widely used in various scientific fields to improve the outcome of the studies, in addition to increasing the efficiency of experimental and computational works. In the materials science field, use of machine learning method has helped to enhance the understanding of the relations existing within parameters of a problem as well as increasing the efficiency of experimental works. Therefore, in this work, the machine learning methods were used to solve the problems of Ni ion release for biomedical applications of NiTi shape memory alloys as well as increasing the functionality of multi component shape memory alloy of NiTi to be used in aerospace applications.

This study firstly focuses on the implementation of machine learning method in biomedical applications of NiTi. To be more specific, In the second chapter, using the available data on the Ni ion release of NiTi alloys, a dataset was developed and was used in a Multi Layer Feed Forward Neural Network (MLFFNN) model to predict the most biocompatible chemical composition of NiTi alloys. Subsequently, using immersion experiments, these results were validated and the most bio compatible chemical composition of NiTi alloys with 51.5 at.% was proposed for further investigation.

In the third chapter, the machine learning was implemented to expand the applications of NiTi based shape memory alloys with addition of Cu, Fe and Pd, to more sophisticated and demanding working conditions. In particular, using the prediction ability of the artificial neural networks as the machine learning method, two MLFFNN models were developed and two separate datasets were extracted from literatures were fed into them. As a result, the first endothermic peak value of the alloys as the representative of the phase transformation temperature was predicted by one model and the thermal hysteresis of the alloys were predicted by the other one. Finally, the optimum chemical composition of the NiTi based alloys were selected using the desirability method and the chemical composition with 17% Ni, 44.5% Ti, 17% Cu, 4.5% Fe and 17% Pd was selected for further investigation.

Considering the results of the aforementioned study, promising outcomes are possible for future works. In particular, machine learning methods can be used as a tool

to find the relationship of the physical properties such as valence electron concentration and electronegativity to the phase transformation temperatures and thermal hysteresis of shape memory alloys, as well as providing the ability to find other affecting parameters that are currently unknown without conducting costly experiments. Therefore, giving the chance to create a general model to predict the phase transformation temperatures and thermal hysteresis for other alloying systems.

In conclusion, this work has proven that the implementation of artificial intelligence in materials science can open a new door for the studies that demand an extensive amount of experimental work for their success by decreasing the associated experimental cost. Specifically, by effectively implementing artificial intelligence frameworks to predict the optimum chemical composition for binary NiTi used in orthodontics and multi-component NiTi-based alloys utilized in high-temperature applications, the validity of this approach was proved.

Appendix A: Training Dataset for development of ANN model in the second chapter Ni ion release

Nickel at.%	Titanium at.%	Other elements	Wire Surface area cm2	Solution's pH	Solution amount ml	Time hours	Results ug/cm2
50.05	49.95	0	0.2553	2.5	2	24	4.28
50.05	49.95	0	0.2553	3.75	2	24	3.16
50.05	49.95	0	0.2553	5	2	24	1.32
50.05	49.95	0	0.2553	6.25	2	24	0.56
50.05	49.95	0	0.2553	2.5	2	72	14.45
50.05	49.95	0	0.2553	3.75	2	72	3.51
50.05	49.95	0	0.2553	5	2	72	2.02
50.05	49.95	0	0.2553	6.25	2	72	1.97
50.05	49.95	0	0.2553	2.5	2	168	21.23
50.05	49.95	0	0.2553	3.75	2	168	4.02
50.05	49.95	0	0.2553	5	2	168	2.33
50.05	49.95	0	0.2553	6.25	2	168	2.45
50.05	49.95	0	0.2553	2.5	2	336	38.79
50.05	49.95	0	0.2553	3.75	2	336	6.33
50.05	49.95	0	0.2553	5	2	336	3.02
50.05	49.95	0	0.2553	6.25	2	336	2.63
50.05	49.95	0	0.2553	2.5	2	672	58.11
50.05	49.95	0	0.2553	3.75	2	672	9.84
50.05	49.95	0	0.2553	5	2	672	4.3
50.05	49.95	0	0.2553	6.25	2	672	3.07
50.1	49.9	0	2.413	6.75	100	168	3.04185
50.1	49.9	0	2.413	6.75	100	336	2.7973
50.1	49.9	0	2.413	6.75	100	504	2.2254
50.93	49.07	0	0.2553	2.5	2	24	1.32
50.93	49.07	0	0.2553	3.75	2	24	0.57
50.93	49.07	0	0.2553	5	2	24	0.29
50.93	49.07	0	0.2553	6.25	2	24	0.11
50.93	49.07	0	0.2553	2.5	2	72	6.04
50.93	49.07	0	0.2553	3.75	2	72	0.69
50.93	49.07	0	0.2553	5	2	72	0.64
50.93	49.07	0	0.2553	6.25	2	72	0.4
50.93	49.07	0	0.2553	2.5	2	168	11.79
50.93	49.07	0	0.2553	3.75	2	168	0.71
50.93	49.07	0	0.2553	5	2	168	0.7
50.93	49.07	0	0.2553	6.25	2	168	0.4
50.93	49.07	0	0.2553	2.5	2	336	23.89
50.93	49.07	0	0.2553	3.75	2	336	0.8
50.93	49.07	0	0.2553	5	2	336	0.77
50.93	49.07	0	0.2553	6.25	2	336	0.47

50.93	49.07	0	0.2553	2.5	2	672	24.77
50.93	49.07	0	0.2553	3.75	2	672	1
50.93	49.07	0	0.2553	5	2	672	1
50.93	49.07	0	0.2553	6.25	2	672	0.57
51	49	0	0.4826	5	5.489362	168	1.93
51	49	0	0.4826	5	5.489362	168	0.43
51.95	48.05	0	0.2553	2.5	2	24	1.47
51.95	48.05	0	0.2553	3.75	2	24	0.66
51.95	48.05	0	0.2553	5	2	24	0.39
51.95	48.05	0	0.2553	6.25	2	24	0.07
51.95	48.05	0	0.2553	2.5	2	72	6.19
51.95	48.05	0	0.2553	3.75	2	72	0.6
51.95	48.05	0	0.2553	5	2	72	0.72
51.95	48.05	0	0.2553	6.25	2	72	0.63
51.95	48.05	0	0.2553	2.5	2	168	12.83
51.95	48.05	0	0.2553	3.75	2	168	1.61
51.95	48.05	0	0.2553	5	2	168	0.92
51.95	48.05	0	0.2553	6.25	2	168	0.87
51.95	48.05	0	0.2553	2.5	2	336	16.81
51.95	48.05	0	0.2553	3.75	2	336	2.12
51.95	48.05	0	0.2553	5	2	336	2.07
51.95	48.05	0	0.2553	6.25	2	336	1.65
51.95	48.05	0	0.2553	2.5	2	672	25.07
51.95	48.05	0	0.2553	3.75	2	672	5.43
51.95	48.05	0	0.2553	5	2	672	3.6
51.95	48.05	0	0.2553	6.25	2	672	1.74
52	45	3	0.4826	5	5.489362	168	0.09
52.03	47.01	0.96	0.2553	2.5	2	24	3.69
52.03	47.01	0.96	0.2553	3.75	2	24	1.35
52.03	47.01	0.96	0.2553	5	2	24	1.09
52.03	47.01	0.96	0.2553	6.25	2	24	0.07
52.03	47.01	0.96	0.2553	2.5	2	72	5.6
52.03	47.01	0.96	0.2553	3.75	2	72	1.81
52.03	47.01	0.96	0.2553	5	2	72	1.21
52.03	47.01	0.96	0.2553	6.25	2	72	1.5
52.03	47.01	0.96	0.2553	2.5	2	168	7.22
52.03	47.01	0.96	0.2553	3.75	2	168	2.18
52.03	47.01	0.96	0.2553	5	2	168	1.57
52.03	47.01	0.96	0.2553	6.25	2	168	1.88
52.03	47.01	0.96	0.2553	2.5	2	336	11.5
52.03	47.01	0.96	0.2553	3.75	2	336	2.24
52.03	47.01	0.96	0.2553	5	2	336	1.92
52.03	47.01	0.96	0.2553	6.25	2	336	2.04
52.03	47.01	0.96	0.2553	2.5	2	672	12.38
52.03	47.01	0.96	0.2553	3.75	2	672	2.44
52.03	47.01	0.96	0.2553	5	2	672	3.6

52.03	47.01	0.96	0.2553	6.25	2	672	2.63
53	47	0	0.4826	5	5.489362	168	0.21
53	47	0	0.4826	5	5.489362	168	0.03
57.37	42.63	0	0.6503	7.4	6	1	0.552668
57.37	42.63	0	0.6503	7.4	6	5	1.659849
57.37	42.63	0	0.6503	7.4	6	24	2.997693
57.37	42.63	0	0.6503	7.4	6	120	4.473935
57.37	42.63	0	0.6503	7.4	6	360	6.134707

Appendix B: Training Dataset for development of ANN model in the third chapter (PTTs)

Ni	Ti	Cu	Fe	Pd	entropy	cv	Endothermic peak value
55.38	44.62	0	0	0	0.687347	0.289178	50.13
51.24	48.76	0	0	0	0.69284	0.282136	-20.5
51	49	0	0	0	0.692947	0.281724	-64.5
51	49	10	0	0	0.923206	0.291845	42.5
50.8	49.2	0	0	0	0.693019	0.28138	-47.5
50.7	49.3	0	0	0	0.693049	0.281208	17.56
50.5	49.5	0	0	0	0.693097	0.280863	45.47
50.5	49.5	0	0	0	0.693097	0.280863	31
50.3	49.7	0	0	0	0.693129	0.280518	53.1
50.3	49.7	0	0	0	0.693129	0.280518	38
50	50	0	0	0	0.693147	0.28	79.99
50	49	0	1	0	0.742167	0.28115	34.63
50	48	0	2	0	0.777119	0.282297	-18.12
50	47	0	3	0	0.806631	0.283439	-73.43
49.8	50.2	0	0	0	0.693139	0.279654	78.1
49	50	0	0.2	0.8	0.747171	0.278282	85.36
48.6	50	0	0.9	0.5	0.766132	0.278478	59.01
48.3	50	0	1.6	0.1	0.771142	0.278876	29.43
48.2	50	0.6	0.9	0.3	0.788861	0.279051	47.19
48.1	50	0.2	1.5	0.2	0.786466	0.278791	28.71
48	52	0	0	0	0.692347	0.276527	113.98
48	50	2	0	0	0.777119	0.280576	63
47.91	52.09	0	0	0	0.692273	0.27637	105
47	50	0	3	0	0.806631	0.278268	-99.2
46.8	50	0.9	2	0.3	0.839983	0.278504	16.8
46.7	50	0.8	2.3	0.2	0.839977	0.278502	8.62
46.5	50	1.1	2.2	0.2	0.848638	0.278647	10.64
46.24	49.54	4.21	0	0	0.837985	0.281993	27.5
46	50	0	4	0	0.832532	0.277689	-39.1
46	50	1.1	2.8	0.1	0.860408	0.278501	-12.22
45.8	50	0	4.2	0	0.837363	0.277573	-38.83
45.7	50	0	4.3	0	0.839739	0.277515	-42.17
45.7	50	1.2	3	0.1	0.869616	0.278414	-9.08
45.2	48.8	6	0	0	0.877836	0.283782	57.5
45.2	50	1	3.8	0	0.875813	0.278094	-25.44
45.1	50	1.4	3.5	0	0.882795	0.278384	-25.31
45	50	5	0	0	0.855689	0.281437	64
44.6	50	1.9	3.4	0.1	0.903868	0.278385	-23.08
44.5	50	1.5	3	1	0.921126	0.276706	-50.27
44.5	50	2.1	3.4	0	0.902977	0.278644	-25.11

44.5	50	1.7	3.7	0.1	0.90504	0.278154	-28.04
44.5	50	1.9	3.4	0.2	0.909581	0.278185	-30.05
44.5	50	1.6	3.7	0.2	0.907456	0.277925	-28.87
44.4	50	2	3.6	0	0.904984	0.278499	-33.92
44.2	50	1.9	3.8	0.1	0.91392	0.278154	-29.72
44.2	50	1.9	3.9	0	0.909269	0.278297	-31.29
44	50	1	1	4	0.928663	0.271879	-34.13
44	50	2	4	0	0.914801	0.278268	-53.33
44	50	2.3	3.6	0.1	0.921147	0.278385	-32.05
44	50	2.3	3.7	0	0.91655	0.278528	-39.36
43.9	50	2.1	4	0	0.917866	0.278297	-40.34
43.9	50	1.5	4.6	0	0.912618	0.277776	-44.91
43.9	50	2	4	0.1	0.921886	0.278067	-41.48
43.8	50	2.6	3.6	0	0.922722	0.278673	-33.57
43.8	50	2	4.1	0.1	0.924268	0.278009	-42.23
43.6	50	3	3.4	0	0.928667	0.278904	-31.27
43.5	50	2	4.5	0	0.926461	0.277978	-46.68
42.8	50	4	3.2	0	0.948688	0.279308	-41.59
42.8	50	3.6	2.8	0.8	0.968203	0.277822	-39.05
42.5	50	7.5	0	0	0.904502	0.282154	-6
42	50	8	0	0	0.912982	0.282297	27.74
42	50	5	3	0	0.965907	0.279712	-46.59
41.8	48.2	10	0	0	0.946638	0.285941	-101
41.7	49.8	8.5	0	0	0.921454	0.282783	62.75
41.6	48.4	10	0	0	0.946344	0.285601	-71
41.4	48.6	10	0	0	0.946032	0.28526	-52
41.2	48.8	10	0	0	0.945703	0.28492	-32
41.2	50	6	2.8	0	0.980827	0.280115	-53.5
40.8	49.2	10	0	0	0.94499	0.284237	5
40.6	49.4	10	0	0	0.944606	0.283896	22
40.4	49.6	10	0	0	0.944205	0.283554	32.5
40.4	50	4.6	1	4	1.029181	0.272897	-3.33
40.2	49.8	10	0	0	0.943786	0.283211	44
40	50	10	0	0	0.943348	0.282869	33.55
40	50	0	0	10	0.943348	0.261194	5.77
39.6	50	8	2.4	0	1.004976	0.28092	-15.3
38	50	10	2	0	1.022754	0.281724	0.68
37.5	50	12.5	0	0	0.974315	0.283582	-40
36.4	50	12	1.6	0	1.035027	0.282526	13.24
36	48	0	0	16	1.013313	0.254286	503.56
35	50	0	0	15	0.998579	0.252708	88.2
35	50	15	0	0	0.998579	0.284294	31
35	50	12	0	3	1.07364	0.277475	47.7
34.8	50	14	1.2	0	1.042236	0.283325	-1.59
34.5	50.5	0	0	15	0.996735	0.251897	79
34	50	13	0	3	1.083794	0.277756	25.9

34	50	10	0	6	1.112432	0.271199	30.2
34	50	12	0	4	1.096556	0.275542	37.6
34	50	14	0	2	1.066865	0.28	45.65
34	50	16	0	0	1.006582	0.284579	60.1
34	50	0	0	16	1.006582	0.251076	58.18
33.7	50.3	0	0	16	1.005403	0.250592	104.5
33.5	50	12.5	0	4	1.101623	0.275682	40.45
33	50	17	0	0	1.013665	0.284863	46.38
30	50	20	0	0	1.029653	0.285714	50.66
30	50	0	0	20	1.029653	0.244755	124.45
30	50	20	0	0	1.029653	0.285714	45.85
29.5	50.5	0	0	20	1.027032	0.243962	138
26	48	0	0	26	1.052784	0.238926	499.77
25	50	25	0	0	1.039721	0.287129	53.62
25	50	0	0	25	1.039721	0.237288	182.9
24.7	50.3	25	0	0	1.037614	0.28662	197
24.5	50.5	0	0	25	1.03618	0.236512	195
24	48	0	0	28	1.051244	0.236074	498.45
22	50	28	0	0	1.036112	0.287975	42.12
21	48	0	0	31	1.043108	0.231922	472.83
21	49	30	0	0	1.038469	0.290221	64.1
20	50	30	0	0	1.029653	0.288538	34.89
20	50	0	0	20	0.990349	0.232558	262
20	50	0	0	30	1.029653	0.230263	256.1
20	50	30	0	0	1.029653	0.288538	59.8
20	50	0	0	30	1.029653	0.230263	235.5
19.8	50.2	0	0	30	1.027806	0.229959	248.97
19.5	50.5	0	0	30	1.024984	0.229503	251.5
19.4	50.6	0	0	30	1.024028	0.229351	244.6
19.4	50.6	0	0	30	1.024028	0.229351	233
19	51	0	0	30	1.020136	0.228741	216.57
19	51	30	0	0	1.020136	0.286846	77.8
18	50	32	0	0	1.019856	0.2891	34.56
18	52	30	0	0	1.009897	0.285147	82.3
16	48	0	0	36	1.013313	0.225316	475.51
15	50	0	0	35	0.998579	0.223642	426
13	51	0	0	36	0.976429	0.220878	358.5
11	48	0	0	41	0.960661	0.219077	466.85
10	50	0	0	40	0.943348	0.217391	423
5	50	0	0	45	0.855689	0.21148	506
3.5	50.5	0	0	46	0.819552	0.209624	511
0	50	0	0	50	0.693147	0.205882	583

Appendix C: Training Dataset for development of ANN model in the third chapter (TH)

Ni	Ti	Cu	Fe	Pd	entropy	cv	DeltaT
55.38	44.62	0	0	0	0.687347	0.289178	1.72
51.24	48.76	0	0	0	0.69284	0.282136	66
51	49	0	0	0	0.692947	0.281724	74
51	49	10	0	0	0.923206	0.291845	20
50.8	49.2	0	0	0	0.693019	0.28138	15
50.7	49.3	0	0	0	0.693049	0.281208	36.16
50.5	49.5	0	0	0	0.693097	0.280863	72
50.42	49.58	0	0	0	0.693112	0.280725	30
50.3	49.7	0	0	0	0.693129	0.280518	28.59
50	50	0	0	0	0.693147	0.28	42
50	49	0	1	0	0.742167	0.28115	39.15
50	48	0	2	0	0.777119	0.282297	39.14
50	49	0	0.2	0.8	0.747171	0.28	28.61
50	49	0	0.4	0.6	0.748897	0.280286	26.82
50	48.6	0	0.9	0.5	0.766132	0.280887	19.29
50	39.6	8	2.4	0	1.004976	0.29841	12.66
50	48.2	0.6	0.9	0.3	0.788861	0.282147	11.05
50	34.8	14	1.2	0	1.042236	0.308437	10.79
50	38	10	2	0	1.022754	0.301784	10.34
50	41.2	6	2.8	0	0.980827	0.295002	10.16
50	40.4	4.6	1	4	1.029181	0.288808	9.1
50	36.4	12	1.6	0	1.035027	0.305127	8.62
50	34	0	0	16	1.006582	0.276006	8.53
50	44	1	1	4	0.928663	0.281933	8.36
50	34	16	0	0	1.006582	0.310873	7.4
50	34	14	0	2	1.066865	0.306122	6.65
50	40	0	0	10	0.943348	0.277372	6.04
50	35	12	0	3	1.07364	0.301958	5.93
50	42	5	3	0	0.965907	0.293286	5.83
50	34	12	0	4	1.096556	0.301493	5.8
50	34	10	0	6	1.112432	0.296979	5.32
50	34	13	0	3	1.083794	0.303793	4.7
50	43.9	2.1	4	0	0.917866	0.288734	4.54
50	44	2.3	3.7	0	0.91655	0.288791	4.31
50	44.5	1.5	3	1	0.921126	0.286079	4.26
50	46	0	4	0	0.832532	0.284579	4.21
50	42.8	3.6	2.8	0.8	0.968203	0.29003	4.13
50	43.9	1.5	4.6	0	0.912618	0.288228	4.13
50	45.8	0	4.2	0	0.837363	0.284806	3.92
50	45.7	0	4.3	0	0.839739	0.28492	3.89
50	43.9	2	4	0.1	0.921886	0.288501	3.83

50	43.6	3	3.4	0	0.928667	0.289829	3.78
50	43.8	2	4.1	0.1	0.924268	0.288613	3.73
50	44.5	1.7	3.7	0.1	0.90504	0.287573	3.72
50	42.8	4	3.2	0	0.948688	0.291562	3.71
50	43.5	2	4.5	0	0.926461	0.2891	3.46
50	44.4	2	3.6	0	0.904984	0.288087	3.4
50	45.1	1.4	3.5	0	0.882795	0.28679	3.29
50	43.8	2.6	3.6	0	0.922722	0.289268	3.25
50	46	1.1	2.8	0.1	0.860408	0.285369	3.24
50	45.2	1	3.8	0	0.875813	0.286337	3.15
50	44.5	1.9	3.4	0.2	0.909581	0.287593	3.15
50	48.6	0	0.8	0.6	0.766568	0.280744	3.12
50	46.1	1.2	2.7	0	0.854148	0.285487	3.12
50	44.6	1.9	3.4	0.1	0.903868	0.287629	3.07
50	48.7	0	1.3	0	0.753422	0.281494	3.07
50	44.5	1.6	3.7	0.2	0.907456	0.28734	3.05
50	48.3	0	1.6	0.1	0.771142	0.281808	2.87
50	45.7	1.2	3	0.1	0.869616	0.285794	2.75
50	44.2	1.9	3.9	0	0.909269	0.288228	2.72
50	46.8	0.9	2	0.3	0.839983	0.283998	2.64
50	44.2	1.9	3.8	0.1	0.91392	0.288079	2.53
50	46.5	1.1	2.2	0.2	0.848638	0.284655	2.32
50	48.1	0.2	1.5	0.2	0.786466	0.282064	2.09
50	46.7	0.8	2.3	0.2	0.839977	0.284172	1.84
49.8	50.2	0	0	0	0.693139	0.279654	46.57
49.72	50.28	0	0	0	0.693132	0.279516	57
49.41	50.59	0	0	0	0.693078	0.278979	56.7
48	52	0	0	0	0.692347	0.276527	31
48	50	2	0	0	0.777119	0.280576	31
47	50	0	3	0	0.806631	0.278268	59.6
46.79	50.01	3.2	0	0	0.812058	0.280903	30
46.24	49.54	4.21	0	0	0.837985	0.281993	15
45.2	48.8	6	0	0	0.877836	0.283782	24
45	50	5	0	0	0.855689	0.281437	21
44.68	49.19	4.21	1.92	0	0.91821	0.281503	49
42.5	50	7.5	0	0	0.904502	0.282154	8
42	50	8	0	0	0.912982	0.282297	8.65
41.8	48.2	10	0	0	0.946638	0.285941	18
41.7	49.8	8.5	0	0	0.921454	0.282783	23.65
41.6	48.4	10	0	0	0.946344	0.285601	15
41.4	48.6	10	0	0	0.946032	0.28526	15
41.2	48.8	10	0	0	0.945703	0.28492	16
41	49	10	0	0	0.945355	0.284579	16
40.8	49.2	10	0	0	0.94499	0.284237	14
40.6	49.4	10	0	0	0.944606	0.283896	17
40.4	49.6	10	0	0	0.944205	0.283554	15

40.2	49.8	10	0	0	0.943786	0.283211	12
40	50	10	0	0	0.943348	0.282869	30
40	50	10	0	0	0.943348	0.282869	13
37.5	50	12.5	0	0	0.974315	0.283582	6
35	50	15	0	0	0.998579	0.284294	13
35	50	15	0	0	0.998579	0.284294	9.7
34.5	50.5	0	0	15	0.996735	0.251897	10
33.7	50.3	0	0	16	1.005403	0.250592	16.2
33.5	50	12.5	0	4	1.101623	0.275682	4.5
33	50	17	0	0	1.013665	0.284863	15.15
30	50	0	0	20	1.029653	0.244755	8.6
30	50	20	0	0	1.029653	0.285714	5.5
29.5	50.5	0	0	20	1.027032	0.243962	11
25	50	25	0	0	1.039721	0.287129	9.7
24.7	50.3	25	0	0	1.037614	0.28662	9
24.5	50.5	0	0	25	1.03618	0.236512	7
22	50	28	0	0	1.036112	0.287975	6.02
21	49	30	0	0	1.038469	0.290221	9.5
20	50	0	0	30	1.029653	0.230263	19.6
20	50	30	0	0	1.029653	0.288538	8.12
19.8	50.2	0	0	30	1.027806	0.229959	15.68
19.5	50.5	0	0	30	1.024984	0.229503	24
19.4	50.6	0	0	30	1.024028	0.229351	17.75
19	51	0	0	30	1.020136	0.228741	21.08
19	51	30	0	0	1.020136	0.286846	8.5
18	50	32	0	0	1.019856	0.2891	12.78
18	52	30	0	0	1.009897	0.285147	7.7
13	51	0	0	36	0.976429	0.220878	40
10	50	0	0	40	0.943348	0.217391	24
5	50	0	0	45	0.855689	0.21148	23
3.5	50.5	0	0	46	0.819552	0.209624	28
0	50	0	0	50	0.693147	0.205882	49